Final Report of the International Nuclear Energy Research Initiative OSMOSE Project (FY01-FY04)

Nuclear Engineering
Argonne National Laboratory

About Argonne National Laboratory
Argonne is operated by The University of Chicago for the U.S. Department of Energy Office of
Science, under contract W-31-109-Eng-38. The Laboratory's main facility is outside Chicago,
at 9700 South Cass Avenue, Argonne, Illinois 60439. For information about Argonne and its
pioneering science and technology programs, see www.anl.gov.

Final Report of the International Nuclear Energy Research Initiative OSMOSE Project (FY01-FY04)

R. T. Klann[1], JP. Hudelot[2], G. Perret[1], N. Drin[3], J. Lee[4], Y. Cao[4]

[1]Argonne National Laboratory
9700 South Cass Ave.
Argonne, IL 60439
US

[2]Commissariat à l'Energie Atomique
Cadarache
13109 St Paul lez Durance
France

[3]Commissariat à l'Energie Atomique
Valrho
Pierrelatte - BP 171
30207 Bagnols-sur-Cèze cedex
France

[4]University of Michigan
Ann Arbor, MI 48109
US

December 17, 2004

I-NERI Annual Technical Progress Report
December 31, 2004

Project Title: OSMOSE – An Experimental Program for Improving Neutronic Predictions of Advanced Nuclear Fuels

Lead US Investigating Organization: Argonne National Laboratory
US Principal Investigator: Raymond T. Klann

Lead Collaborating Investigating Organization: CEA-Cadarache
Lead Collaborating Principal Investigator: Jean-Pascal Hudelot

Other Collaborating Organizations: University of Michigan

EXECUTIVE SUMMARY

The design of nuclear systems has shifted over the years from a "test and build" approach to a much more analytical methodology based on the many advances in computational techniques and nuclear data. To a large extent current reactors can be calculated almost as well as they can be measured. This is due in particular to the high quality nuclear data available for the few major isotopes which dominate the neutronics of these systems. Nevertheless, most of the future nuclear systems concepts and advanced fuels development programs currently underway use significant quantities of minor actinides to address modern day issues such as proliferation resistance and low cost. The need for better nuclear data have been stressed by various organizations throughout the world, and results of studies have been published which demonstrate that current data are inadequate for designing the projects under consideration [1] [2]. In particular, a Working Party of the OECD has been concerned with identifying these needs [3] and has produced a detailed High Priority Request List for Nuclear Data.

The first step in obtaining better nuclear data consists of measuring accurate integral data and comparing it to integrated energy dependent data: this comparison provides a direct assessment of the effect of deficiencies in the differential data. Several US and international programs have indicated a strong desire to obtain accurate integral reaction rate data for improving the major and minor actinide cross sections. Specifically, these include: ^{232}Th, ^{233}U, ^{234}U, ^{235}U, ^{236}U, ^{238}U, ^{237}Np, ^{238}Pu, ^{239}Pu, ^{240}Pu, ^{241}Pu, ^{242}Pu, ^{241}Am, ^{242}Am, ^{243}Am, ^{242}Cm, ^{243}Cm, ^{244}Cm, ^{245}Cm, ^{246}Cm, and ^{247}Cm. Data on the major actinides (i.e. ^{235}U, ^{236}U, ^{238}U, ^{239}Pu, ^{240}Pu, ^{241}Pu, ^{242}Pu, and ^{241}Am) are reasonably well-known and available in the Evaluated Nuclear Data Files - (JEF, JENDL, ENDF-B). However, information on the minor actinides (i.e.^{232}Th, ^{233}U, ^{237}Np, ^{238}Pu, ^{242}Am, ^{243}Am, ^{242}Cm, ^{243}Cm, ^{244}Cm, ^{245}Cm, ^{246}Cm, and ^{247}Cm) is less well-known and considered to be relatively poor in some cases, having to rely on models and extrapolation of few data points. This is mainly due to the difficulty of obtaining relatively pure samples of sufficient quantity (up to about one gram) to perform reliable reaction rate measurements.

A large and exhaustive experimental program has been planned in the MINERVE reactor facility at CEA-Cadarache. One of the programs – OSMOSE (Oscillation in Minerve of Isotopes in Eupraxic Spectra) – aims at obtaining in different experimental lattices an accurate experimental database for separated heavy nuclides.

DOE is collaborating with CEA on the OSMOSE program through the International Nuclear Energy Research Initiative. ANL is serving as the U.S. lead laboratory and the University of Michigan is providing technical support. The INERI project is focused on supporting the measurements to be conducted at CEA-Cadarache (through experimental support for conducting the measurements, pre-analysis and planning, and post-measurement data analysis activities). The DOE/CEA collaboration on the OSMOSE program includes the supply of separated ^{240}Pu, ^{241}Pu, ^{242}Pu and ^{243}Am from DOE, the participation of DOE in the conduct of the experiments, and the development and comparison of analytic tools and models of CEA and DOE based on Monte Carlo and deterministic methods.

The objective of this collaborative program between the U.S. DOE and the French CEA is to measure very accurate integral reaction rates in representative spectra for the actinides important

to future nuclear system designs, and to provide the experimental data for improving the basic nuclear data files. The main outcome of the OSMOSE measurement program will be an experimental database of reactivity-worth measurements in different neutron spectra for the heavy nuclides. This database can then be used as a benchmark to verify and validate reactor analysis codes. The OSMOSE program aims at improving neutronic predictions of advanced nuclear fuels through measurements in the MINERVE facility on samples containing the following separated actinides : ^{232}Th, ^{233}U, ^{234}U, ^{235}U, ^{236}U, ^{238}U, ^{237}Np, ^{238}Pu, ^{239}Pu, ^{240}Pu, ^{241}Pu, ^{242}Pu, ^{241}Am, ^{243}Am, ^{244}Cm and ^{245}Cm.

The OSMOSE program began in 2001 and will continue through 2013 with the following timeline:

2002 – reactor modifications, reactor modeling and pre-analysis, isotopic separations
2003 – fabrication of initial samples, characterization of the reactor and pilot rod
2004 – fabrication of additional samples, reactor characterization measurements
2005 – measurements of separated actinides and absorbers in UO_2-dominated spectra
2006 – measurements of separated actinides and absorbers in MOX-dominated spectra
2007 – measurements of separated actinides and absorbers in epithermal spectra
2008 – reactor upgrades, data analysis for UO_2 and MOX spectra
2009 – measurements in different epithermal spectra
2010 – measurements in fast spectra
2011 – measurements in fast spectra
2012 – measurements in harder fast spectra and project close-out

This report highlights activities that have been performed within the original DOE International Nuclear Energy Research Initiative program and covers progress on the OSMOSE program for fiscal years 2001-2004.

The collaborative project is defined by five major tasks – reactor modifications, reactor modeling, sample fabrication, experiments, and data analysis.

Reactor modifications to the MINERVE facility were completed in 2002 and included upgrading the reactor control console, control room, and renewal of the pilot rod.

As part of the effort to characterize the reactor and core configurations, an extensive effort was undertaken to describe all of the geometry and material specifications for the MINERVE reactor. This led to the issuing of the Material Specification Report in English and French. As the first two core configurations to be loaded include the R1-UO2 and R1-MOX configurations, these were the focus of the reactor modeling and characterization analyses. The analytic effort has been performed using separate suites of reactor analysis codes in the U.S. and in France. The effort has included creating models of the reactor based on Monte Carlo and deterministic techniques.

The Monte Carlo models use the MCNP-4C code system with the continuous energy cross sections of the ENDFB-VI library and fully describes the neutronic region of interest of the MINERVE reactor.

The deterministic models are based on the REBUS code system. The models use an XYZ geometry with approximately 200×200×100 mesh cells. The self-shielded cross sections are provided by the one-dimensional-transport-code-system WIMS-ANL 5.07 and collapsed to 7 groups.

CEA used the MCNP-4C and TRIPOLI-4 Monte Carlo codes and the APOLLO-2 deterministic code.

The Monte Carlo and deterministic models have been used to calculate control rod reactivity worths, axial and radial power profiles, spectral indices, and ^{238}U modified conversion ratio for the R1-UO2 and R1-MOX configurations. The deterministic model is also used to calculate the reactivity worth of UO$_2$ and borated calibration samples in the R1-UO2 and R1-MOX configurations.

The OSMOSE program requires the fabrication of 21 oxide samples containing separated actinides (^{232}Th, ^{233}U, ^{234}U, ^{235}U, ^{236}U, ^{238}U, ^{237}Np, ^{238}Pu, ^{239}Pu, ^{240}Pu, ^{241}Pu, ^{242}Pu, ^{241}Am, ^{243}Am and ^{244}Cm, ^{245}Cm). The samples consist of assembled fuel pellets containing the isotopes of interest and a double zircaloy cladding.

To support the project, DOE supplied CEA with samples of seperated ^{240}Pu, ^{241}Pu, ^{242}Pu and ^{243}Am in 2003. CEA installed an oven in one of their hot cells at the Marcoulle facility. To date, CEA has produced pellets for 5 of the samples and has performed purification and analysis on the other isotope stock materials.

The objective of the measurements is to characterize the neutron flux, spectrum, and power distribution of the reactor to qualify the computational models and neutron cross-sections. The goal of the calibration measurements is to demonstrate the oscillation technique on known and calibrated samples, and to support the development of the analytic technique for reactivity-worth measurements. All of the reactor characterization and safety measurements have been completed for the R1-UO2 and R1-MOX configurations.

In addition, calibration samples have been oscillated in both reactor configurations and calibration curves have been created for both configurations. The reactivity worth of the calibration samples have been calculated with REBUS. The UO$_2$ samples are very well predicted by the calculations for both configurations, whereas the borated calibration samples are not as well predicted. The poor agreement between the experimental signal issued from the oscillations of the borated calibration samples and their calculated reactivity is thought to come from uncertainties in the composition of the borated samples and a possible migration of the boron to the periphery of the sample during the sintering of the fabrication process inducing self shielding effects. New borated calibration samples with a well known composition are being fabricated and will permit to confirm these conclusions.

Data analysis tasks addressed the analysis and reduction of data for each series of measurements, and the comparison with calculated results for the R1-UO2 and R1-MOX core configurations. Spectral indices measurements (^{239}Pu/^{235}U, ^{241}Pu/^{239}Pu and ^{237}Np/^{239}Pu), performed in the central

oscillation channel, agree within 1% with the calculated values using MCNP and the ENDFB-VI data library except for the ^{237}Np/^{239}Pu spectral index in the R1-UO2 configuration which agrees within two standard deviations.

^{238}U modified conversion ratios have been calculated with MCNP for the R1-MOX configuration. The measured and calculated modified conversion ratios agree within two standard deviations.

Axial fission rate distributions have been calculated using the REBUS and MCNP models. The axial bucklings are estimated on a region carefully based on parametric studies. For the R1-UO2 configuration, the axial bucklings calculated with REBUS and MCNP agree with the experimental values within one standard deviation except for the ^{237}Np profile. For the R1-MOX configuration, calculated and experimental values agree within two standard deviations except for the ^{237}Np profile.

Radial fission rate distributions have been calculated using the REBUS and MCNP code systems and compared with experimental values for the R1-MOX configuration. The MCNP model predicts the experimental values well for the pins away from the MOX/UOX interface. The REBUS models underestimated the power in the UOX pins and overestimated the power in the MOX pins.

TABLE OF CONTENTS

INTRODUCTION

The design of nuclear systems has shifted over the years from a "test and build" approach to a much more analytical methodology based on the many advances in computational techniques and nuclear data. To a large extent current reactors can be calculated almost as well as they can be measured. This is due in particular to the high quality nuclear data available for the few major isotopes which dominate the neutronics of these systems. Nevertheless, most of the future nuclear systems concepts and advanced fuels development programs currently underway use significant quantities of minor actinides to address modern day issues such as proliferation resistance and low cost. For example, high burnup fuels contain large quantities of americium and curium. Systems designed for plutonium and minor actinide burning are very sensitive to uncertainties in americium and curium data. There are also several other programs where the minor actinide data are essential. These include the Accelerator Transmutation of Waste concepts, Generation-IV concepts, and Burnup Credit programs.

The need for better nuclear data have been stressed by various organizations throughout the world, and results of studies have been published which demonstrate that current data are inadequate for designing the projects under consideration [1] [2]. In particular, a Working Party of the OECD has been concerned with identifying these needs [3] and has produced a detailed High Priority Request List for Nuclear Data. The first step in obtaining better nuclear data consists of measuring accurate integral data and comparing it to integrated energy dependent data: this comparison provides a direct assessment of the effect of deficiencies in the differential data. Several US and international programs have indicated a strong desire to obtain accurate integral reaction rate data for improving the major and minor actinide cross sections. Specifically, these include: ^{232}Th, ^{233}U, ^{234}U, ^{235}U, ^{236}U, ^{238}U, ^{237}Np, ^{238}Pu, ^{239}Pu, ^{240}Pu, ^{241}Pu, ^{242}Pu, ^{241}Am, ^{242}Am, ^{243}Am, ^{242}Cm, ^{243}Cm, ^{244}Cm, ^{245}Cm, ^{246}Cm, and ^{247}Cm. Data on the major actinides (i.e. ^{235}U, ^{236}U, ^{238}U, ^{239}Pu, ^{240}Pu, ^{241}Pu, ^{242}Pu, and ^{241}Am) are reasonably well-known and available in the Evaluated Nuclear Data Files - (JEF, JENDL, ENDF-B). However, information on the minor actinides (i.e.^{232}Th, ^{233}U, ^{237}Np, ^{238}Pu, ^{242}Am, ^{243}Am, ^{242}Cm, ^{243}Cm, ^{244}Cm, ^{245}Cm, ^{246}Cm, and ^{247}Cm) is less well-known and considered to be relatively poor in some cases, having to rely on models and extrapolation of few data points. This is mainly due to the difficulty of obtaining relatively pure samples of sufficient quantity (up to about one gram) to perform reliable reaction rate measurements.

A large and exhaustive experimental program has been planned in the MINERVE reactor facility at CEA-Cadarache. One of the programs – OSMOSE (Oscillation in Minerve of Isotopes in Eupraxic Spectra) – aims at obtaining in different experimental lattices a single and accurate experimental database for separated heavy nuclides.

The objective of the OSMOSE program is to measure very accurate integral reaction rates in representative spectra for the actinides important to future nuclear system designs and to provide the experimental data for improving the basic nuclear data files. These data will support advanced reactors designed for transmutation of waste or plutonium burning, sub-critical systems such as found in advanced accelerator applications, and waste disposal and treatment programs in the area of criticality safety. The OSMOSE program is very generic, in the sense that it will measure these reaction rates over a broad range of isotopes and spectra and will be used to provide guidance to

all nuclear data programs in the world. The data will provide information valuable to a large number of projects as noted above.

The OSMOSE program [4] will provide precise experimental data (integral absorption cross-sections) for a majority of the heavy nuclides important to reactor and nuclear fuel cycle physics - ^{232}Th, ^{233}U, ^{234}U, ^{235}U, ^{236}U, ^{238}U, ^{237}Np, ^{238}Pu, ^{239}Pu, ^{240}Pu, ^{241}Pu, ^{242}Pu, ^{241}Am, ^{243}Am, ^{244}Cm, and ^{245}Cm. Table 1 shows the isotopes of interest in the OSMOSE program and highlights which isotopes are critical for the various programs. Table 2 shows the target improvements in the quality of the nuclear data for the listed actinide isotopes. The study of these nuclides is performed on a large range of neutron spectra corresponding to specific experimental lattices (thermal, epithermal, moderated/fast, and fast spectra).

The OSMOSE experimental program will produce very accurate sample worth measurements for a series of actinides in various spectra, from over-moderated thermal spectra to fast spectra. The objective of the analytical program is to make use of this experimental data to establish deficiencies in the basic nuclear data libraries, identify their origins, and propose paths towards correcting them, in coordination with international nuclear data programs.

Table 1:OSMOSE Program – Isotopes of Interest								
	JEFF3 validation	Criticality Burn-up credit	Pu recycling	Transmutation and incineration	Decay Heat power	Subsurface long-term Storage	Reactivity loss per cycle	Thorium cycle
^{232}Th	⊗							⊗
^{233}U	⊗							⊗
^{234}U	⊗	⊗					⊗	
^{235}U	⊗	⊗				⊗	⊗	
^{236}U	⊗	⊗					⊗	
^{238}U	⊗	⊗					⊗	
^{237}Np	⊗	⊗		⊗		⊗	⊗	
^{238}Pu	⊗	⊗	⊗	⊗	⊗	⊗	⊗	
^{239}Pu	⊗	⊗	⊗	⊗	⊗	⊗	⊗	
^{240}Pu	⊗	⊗	⊗	⊗	⊗	⊗	⊗	
^{241}Pu	⊗	⊗	⊗	⊗	⊗	⊗	⊗	
^{242}Pu	⊗	⊗	⊗	⊗	⊗	⊗	⊗	
^{241}Am	⊗	⊗	⊗	⊗	⊗	⊗	⊗	
^{243}Am	⊗	⊗	⊗	⊗	⊗	⊗	⊗	
^{244}Cm	⊗	⊗	⊗	⊗	⊗	⊗	⊗	
^{245}Cm	⊗	⊗		⊗	⊗	⊗	⊗	

Table 2:Target Improvements in Nuclear Data for the OSMOSE Program			
Actinide	Parameter	Current Uncertainty (at 1σ)	Target Uncertainty (at 1σ)
^{233}U	η_{therm} $\eta_{epitherm}$	± 2500 pcm ± 4000 pcm	± 1500 pcm ± 2500 pcm
^{234}U	I_r σ_i^{th}	± 10 % ± 2 %	± 3 % ± 1.5 %
^{236}U	I_r	± 5 %	± 3 %
^{237}Np	$I_{r\,th}$ σ_i^{th}	± 7 % ± 3 %	± 2 % ± 1.5 %
^{238}Pu	$I_{r\,th}$ σ_i^{th}	± 9 % ± 2 %	± 4 % ± 1.5 %
^{239}Pu	η_{therm} $\eta_{epitherm}$	± 3000 pcm ± 4000 pcm	± 2000 pcm ± 2000 pcm
^{240}Pu	I_r	± 3 %	± 1.5 %
^{242}Pu	I_r	± 4 %	± 2 %
^{241}Am	$I_{r\,th}$ σ_i^{th}	± 7 % ± 3 %	± 2 % ± 1.5 %
^{243}Am	I_r	± 5 %	± 3 %
^{244}Cm	I_r	± 5 %	± 3 %
^{245}Cm	η_{therm}	± 4000 pcm	± 1500 pcm
^{232}Th	I_r	± 4 %	± 2 %

Ir = resonance integral, σ_i^{th}= microscopic capture cross section, η = reproduction factor

The measurement program is utilizing the MINERVE reactor at CEA-Cadarache, which is a low-power uranium fueled pool reactor. The normal accuracy for small-worth samples in this reactor is on the order of 1% for relative reactivity-worth measurements and 2% for absolute reactivity-worth measurements. The total uncertainty in the OSMOSE samples is estimated to be about 3% including the uncertainty in the isotopic composition. Reactivity effects of less than 10 pcm (0.0001 or approximately 1.5 cents) will be measured and compared with calibrations to determine the differential reactivity-worth of the sample. Accuracies in small reactivity effects this low are only achieved through oscillation techniques.

Seven different neutron spectra will be created in the MINERVE facility: over-moderated UO_2 (representative of a fuel processing plant or flooded storage cask), UO_2 matrix in water (representative of LWRs), mixed oxide fuel matrix (representative of cores containing MOX fuels), two thermal/epithermal spectra (representative of under-moderated reactors), moderated fast spectrum (representative of fast reactors which have some slowing down due to moderators such as lead-bismuth or sodium), and a very hard spectrum (representative of fast reactors with little moderation from reactor coolant). The different spectra are achieved by changing the lattice within the MINERVE reactor.

The OSMOSE program began in 2001 with the preparation of samples. Reactor modifications were completed in 2003. The measurement program at MINERVE began in 2003 with the qualification of the MINERVE reactor and will continue through 2013.

The following timeline is established for the OSMOSE program:

2002 – reactor modifications, reactor modeling and pre-analysis, isotopic separations
2003 – fabrication of initial samples, characterization of the reactor and pilot rod
2004 – fabrication of additional samples, reactor characterization measurements
2005 – measurements of separated actinides and absorbers in UO_2-dominated spectra
2006 – measurements of separated actinides and absorbers in MOX-dominated spectra
2007 – measurements of separated actinides and absorbers in epithermal spectra
2008 – reactor upgrades, data analysis for UO_2 and MOX spectra
2009 – measurements in different epithermal spectra
2010 – measurements in fast spectra
2011 – measurements in fast spectra
2012 – measurements in harder fast spectra and project close-out

DOE is collaborating with CEA on the OSMOSE program through this project within the International Nuclear Energy Research Initiative. ANL is serving as the lead laboratory and the University of Michigan is providing technical support. The INERI project is focused on supporting the measurements to be conducted at CEA-Cadarache (through experimental support for conducting the measurements, pre-analysis and planning, and post-measurement data analysis activities). The DOE/CEA collaboration on the OSMOSE program includes the supply of separated ^{240}Pu, ^{241}Pu, ^{242}Pu and ^{243}Am from DOE, the participation of DOE in the conduct of the experiments, and the development and comparison of analytic tools and models of CEA and DOE based on Monte Carlo and deterministic methods.

The INERI project has been divided into 5 distinct tasks – reactor modifications, reactor modeling, sample fabrication, experimental measurements, and data analysis. Within these high level tasks, there are numerous sub-tasks such as reactor modeling of different core configurations and calculations for different core parameters. A lead laboratory has been identified for each high-level task and other supporting laboratory efforts are also noted. The roles and responsibilities for the tasks associated with the OSMOSE project are shown in Table 3.

Table 3:Roles and responsibilities for each organization		
Task Description	Lead	Support
Task 1: Reactor Modifications	CEA-Cadarache	ANL
Task 2: Reactor Modeling	ANL	CEA-Cadarache, U of M
Task 3: Sample Fabrication	CEA-Valrho	CEA-Cadarache, ANL
Task 4: Experiments	CEA-Cadarache	ANL
Task 5: Data Analysis	ANL	CEA-Cadarache, U of M

1 REACTOR MODIFICATIONS

1.1 Renewal of the control room and the control system of the reactor

Before restarting the MINERVE reactor, the entire control system was upgraded and extensive maintenance was completed on several other systems.

The upgrade of the control system of the reactor and the control room was completed in December, 2002. The new SIREX control system demonstrates better performance than the previous system. In addition, the system includes digital systems for data acquisition, online monitoring of power, and display systems for operators. Figure 1 shows the new control room.

The control system is now in accordance with recommendations from safety authorities and is consistent with existing control systems at other French facilities.

Figure 1: Photo of the new control room

1.2 Renewal of the control system of the pilot rod and the pilot rod

Maintenance of the control rods, safety rods, and the pilot rod was performed in 2002. The maintenance of the pilot rod and the improvement of its ball bearings improved the accuracy of the reactivity worth measurements performed by the oscillation technique. The control rods, safety rods, and pilot rod were re-installed inside the MINERVE reactor in September 2002.

1.3 Renewal of the oscillation system

The oscillator device that vertically positions the measured samples was also updated. The mechanical components and motors were not changed, but the electronics and positioning detectors were upgraded. The goal was to improve the accuracy on the positioning of the oscillation sample inside the reactor core and the reproducibility of the positioning during all the cycles of a measurement. The new oscillating system was validated in September 2002 and successfully tested in association with the data acquisition system in December 2002.

New software associated with the numerical recording and clock systems were installed and showed a much improved reproducibility (see Table 4 and Figure 2) on the position of the oscillator (better than 0.5 mm between cycles).

Table 4: Reproducibility of the position of the oscillator

cycle number	mean value in upper position (Volts (angle of rotation))	s.d.	mean value in lower position (Volts (angle of rotation))	s.d.
1	2.68	0.006	0.32	0.005
2	2.68	0.006	0.32	0.005
3	2.68	0.007	0.32	0.006
4	2.68	0.007	0.32	0.006
5	2.68	0.007	0.32	0.005
6	2.68	0.007	0.32	0.005
7	2.68	0.006	0.32	0.005
8	2.67	0.037	0.33	0.036
9	2.68	0.008	0.32	0.006
10	2.68	0.007	0.32	0.006
11	2.68	0.007	0.32	0.006
12	2.68	0.007	0.32	0.005
13	2.67	0.038	0.33	0.037
14	2.68	0.006	0.32	0.005
15	2.68	0.008	0.32	0.007
16	2.68	0.007	0.32	0.006
17	2.68	0.007	0.32	0.006
18	2.68	0.007	0.32	0.006
19	2.68	0.006	0.32	0.005
20	2.68	0.006	0.32	0.005
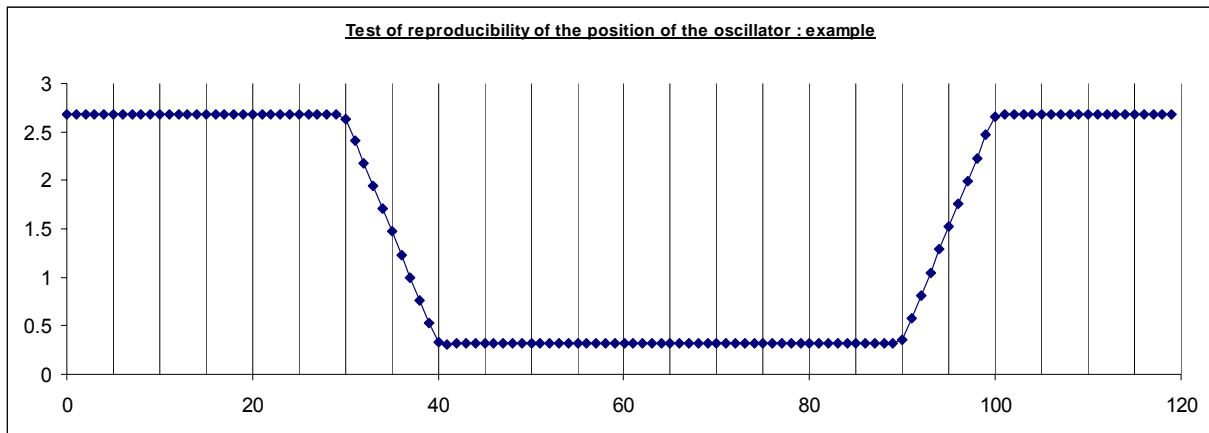
Figure 2: Example of signal of position of the oscillator during one cycle

1.4 Fabrication of a linear positioner

A new system for measurement of the fission rate axial profile was developed and qualified. It is based on a computer-driven system allowing accuracy better than 1 mm on the position of the measured miniature fission chamber. This system is called POLINE, for LINEar POsitioner.

2 REACTOR MODELING

Monte Carlo and deterministic models of the MINERVE facility in the R1-UO2 and R1-MOX configurations were developed to assess core and safety parameters. The deterministic model is also used to calculate the reactivity worth of oscillation samples in the central channel of the core. The models are based on the composition and geometry specifications identified in the Material Specification Report for the MINERVE reactor [5].

2.1 Monte Carlo model

The MCNP-4C code system [6] with the continuous energy cross sections of the ENDFB-VI library was used to create a model of the MINERVE reactor. This model fully describes the neutronic region of interest of the MINERVE reactor by avoiding any unnecessary homogenization. It is extensively based on the Material Specification Report [5] and is fully described in reference [7].

The MCNP model describes the MINERVE core surrounded by at least 30 cm of water and/or structural material, resulting in a 271.5 cm by 271.5 cm by 220 cm region. The core can be schematically described as an experimental zone surrounded by a driver zone (in 4 quadrants). Fuel pins in the experimental zone are used to generate the appropriate flux spectrum in the center and the driver zone feeds the experimental zone with neutrons. The experimental fuel pin lattice is surrounded by an aluminum buffer within a chimney. The driver zone is located outside the chimney and graphite is used as reflector around it. Figure 3 and Figure 4 show radial and axial views of the complete MCNP geometry.
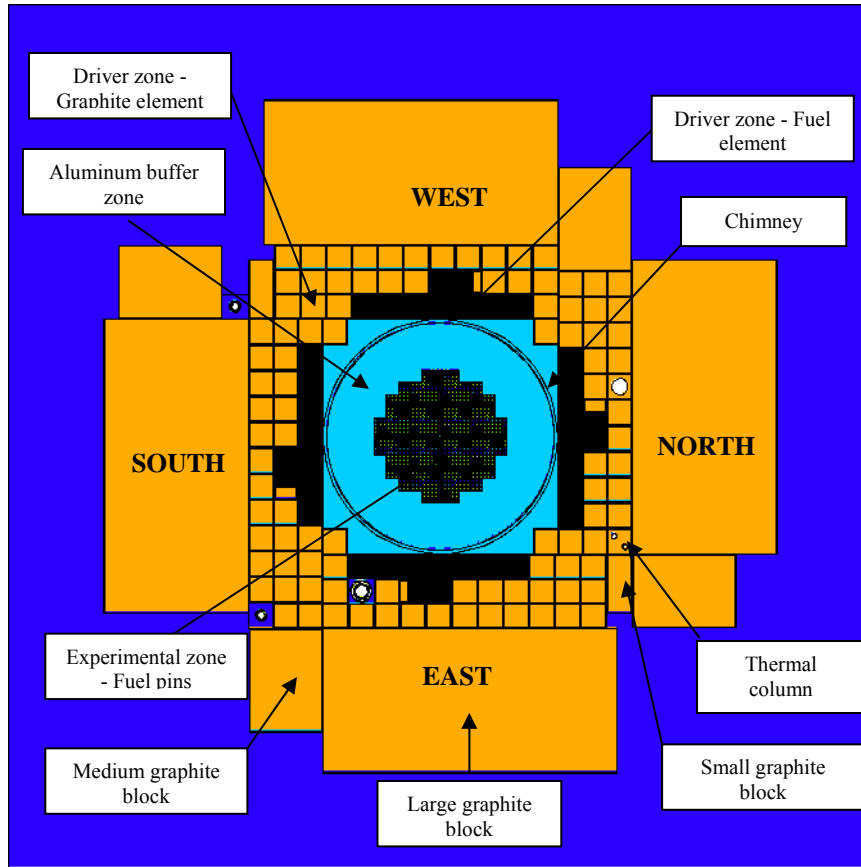
Figure 3: Radial view of the MCNP model in the R1-UO2 configuration
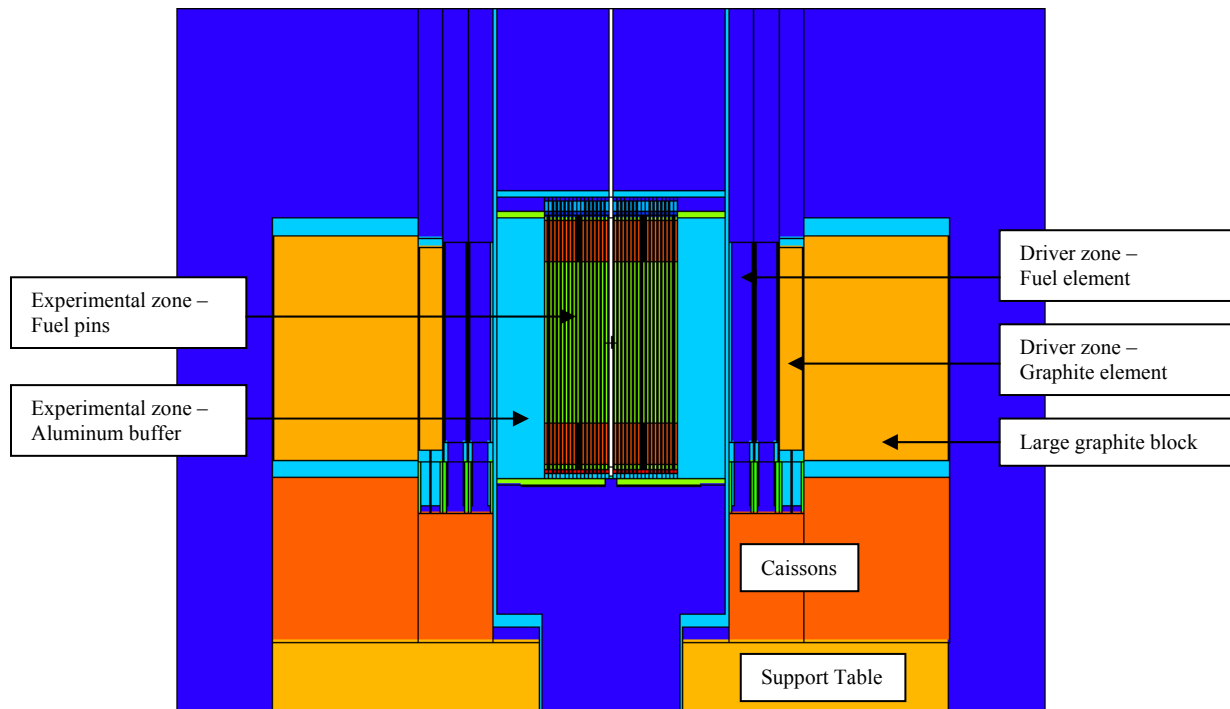
Figure 4: Axial view of the MCNP model in the R1-UO2 configuration

2.2   Deterministic model

The deterministic model is based on the REBUS code system [8]. REBUS has been used to solve the diffusion equation in XYZ geometry with the finite difference method. The self-shielded cross sections used in REBUS are provided by the one-dimensional-transport-code-system WIMS-ANL 5.07 [9]. The WIMS and REBUS models are fully described in [7].

The physical size of the REBUS and MCNP model are the same. Figure 5 and Figure 6 show a radial and an axial view of the complete geometry for the REBUS model.

The number of mesh used in the R1-UO2 and R1-MOX configurations is 190×190×116 and 202×202×116, respectively. In the XY plan, one mesh is used for each cell of the experimental fuel pin lattice (every 1.26 cm) and the mesh size is roughly the same in all the driver elements. The graphite blocks (large and medium) are mapped using a mesh every 2 cm in the X and Y dimension and an approximate 5cm-mesh-size is used for the surrounding water in the XY plan. Axially, the mesh size is defined by the fuel elements and pins of the geometry. The surrounding water is mapped with a 10 cm mesh size, the structural material around the fuel (grid plate of the driver regions, lower and upper end plug and stainless steel spacers) is mapped using a 1-2 cm mesh size, and the fuel and the Plexiglas spacers of the experimental zone are mapped with a 1 cm mesh size.

Microscopic cross sections for the different homogenized regions have been calculated using the one-dimensional-transport-code-system WIMS-ANL 5.07. The starting 69 group structure of the ENDFB-VI library was collapsed to 7 groups (Table 5).

Table 5: REBUS group structure	
Group	Energy
1	500 keV – 10 MeV
2	9.118 keV – 500 keV
3	1.123 eV – 9.118 keV
4	0.4 eV – 1.123 eV
5	0.14 eV – 0.4 eV
6	0.05 eV – 0.4 eV
7	0 - 0.05 eV

10
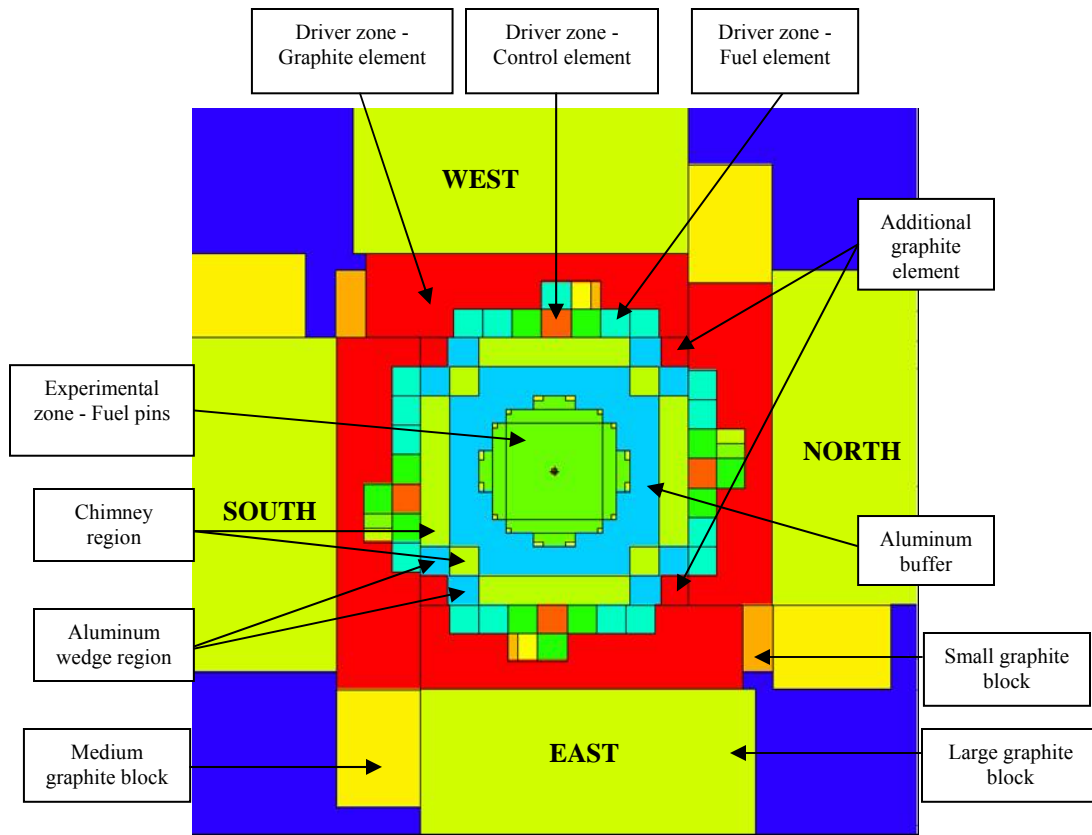
Figure 5: Radial view of the REBUS model in the R1-UO2 configuration
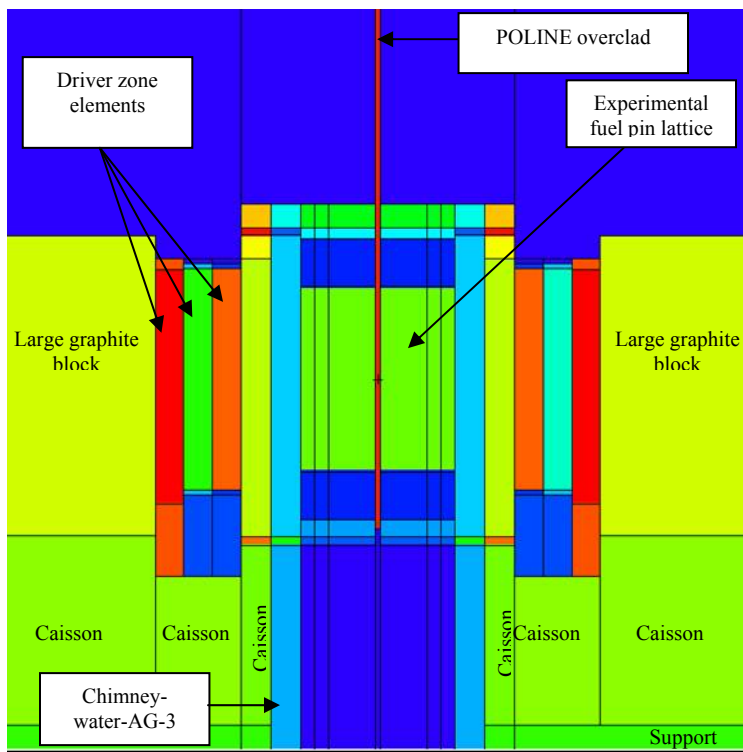
Figure 6: Axial view of the REBUS model in the R1-UO2 configuration

11

3 SAMPLE FABRICATION

3.1 Objective

The OSMOSE program requires the fabrication of 21 oxide samples containing separated actinides (^{232}Th, ^{233}U, ^{234}U, ^{235}U, ^{236}U, ^{238}U, ^{237}Np, ^{238}Pu, ^{239}Pu, ^{240}Pu, ^{241}Pu, ^{242}Pu, $^{241,\ 243}$Am and ^{244}Cm, ^{245}Cm).

The samples consist of assembled fuel pellets containing the isotopes of interest and a double zircaloy cladding. Specifications for the samples include: the pellet size, the pellet density, the homogeneity of the distribution of the actinides inside the UO2 matrix, and the minimization of contamination during the fabrication process.

3.2 Supply of isotopes

Most of the isotopes were available in the Atalante facilities of CEA Marcoule. ^{240}Pu, ^{241}Pu, ^{242}Pu and ^{243}Am were supplied by DOE through the I-NERI collaboration.

The contract between DOE and CEA for the supply of isotopes was signed (following several legal reviews) in February 2003 by CEA. Because of the war in Iraq, it was difficult to find a company willing to ship the isotopes abroad. The shipping was completed in August 2003. Figure 7 shows these isotopes stocked in a hot cell at CEA Marcoule.

Figure 7: ^{243}Am, ^{240}Pu, ^{241}Pu and ^{242}Pu from DOE stocked in a hot cell in Marcoule

The current inventory of ^{241}Pu is only 0.3 g. This means that only one sample containing ^{241}Pu can be manufactured instead of two. This translates to an experimental uncertainty in epithermal and fast spectra for this isotope that will not be as good as originally previewed.

As for ^{236}U, it was impossible to find sufficient mass necessary for the experiment (0.6 g). It was thus replaced by URT which is reprocessed fuel containing 1% of ^{236}U and 4% of ^{235}U. These samples should allow the effect from ^{236}U to be determined from the ^{235}U signal. The final uncertainties may be higher than originally anticipated but it should still be an improvement over existing data. URT fuel was provided by COGEMA in 2003.

Table 6 summarizes the status of the isotope supply.

Table 6: Status of the isotope supplies, quantity, purification need and supplier			
	Quantity (g)	Purification	Supply
^{232}Th	48 2	N	CEA
^{233}U	0.5	Y	CEA
^{234}U	0.3	Y	CEA
URT	0.6	N	COGEMA
^{238}U	48	N	CEA
^{237}Np	0.1 0.6	Y	CEA
^{238}Pu	0.4	Y	CEA
^{239}Pu	0.6	Y	CEA
^{240}Pu	0.15	N	DOE
^{241}Pu	0.3	Y	DOE
^{242}Pu	0.5	N	DOE
^{241}Am	0.06 0.2	Y	CEA
^{243}Am	0.1 0.5	N	DOE
^{244}Cm	2	N	CHEMOTRADE
$^{244+245}$Cm	1	N	CHEMOTRADE

Many of the isotopes have to be purified and converted into oxide to match the chemicals and powder process specifications. This long and accurate procedure requires several operations like dissolution, valence adjustment, chromatographic refinement, intermediate compound synthesis and final calcinations to form the actinide oxide. Step by step analyses demonstrate the validity of the purification process followed by the study of the X-ray diffraction pattern of the material.

For this work several purification routes have been undertaken:
- purification of ^{241}Am by oxalic precipitation,
- preparation of ^{239}Pu from metal standard MP2 (Metallic Plutonium #2),
- purification of ^{234}U from ^{238}Pu (Figure 8).

After the preparation of the ^{234}U sample material, the main effort was the purification of the ^{239}Pu material. The French MP2 standard was used but an oxide conversion of the metal had to be performed before mixing with UO_2.

The usual chemical process is Ag^{2+} dissolution followed by a purification to remove the silver. The final steps are oxalic precipitation and calcination. These operations were completed without problems and the chemical analysis confirmed the success of the preparation.
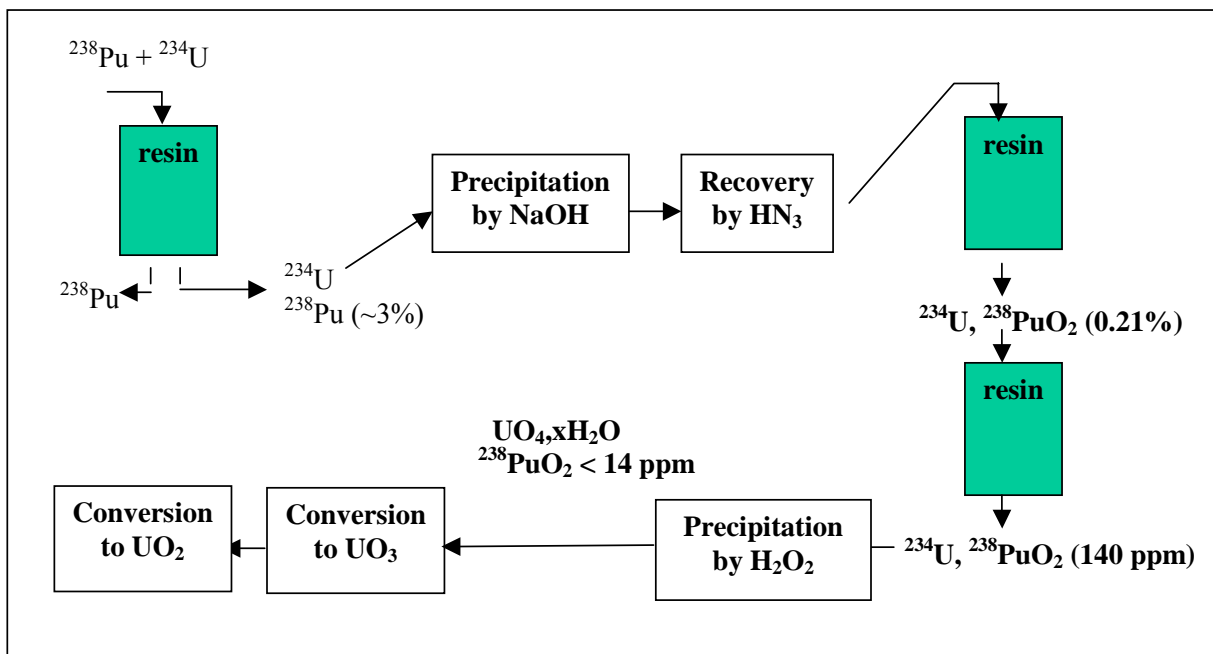
Figure 8: Purification of ^{234}U from ^{238}Pu

3.3   Research and development of the process

Research and development on the manufacturing process began in the middle of 2001 and was completed by the end of 2002. R&D efforts occurred in several phases, including the sintering process, actinide mixing and homogeneity, process contamination control, on the welding process, and the design of a new sintering oven.

The goal of the R&D phase on actinide mixing and homogeneity was to check that the distribution of the actinides are homogeneous inside each pellet, and are reproducible between pellets. Cerium was chosen to simulate the actinide. Pellets of mixed UO_2 and CeO_2 were fabricated. The maximum concentration of 1.1% in Cerium inside the UO_2 matrix corresponds to the maximum concentration of actinides in the OSMOSE samples. Results show an excellent

homogeneity of the distribution of Uranium and Cerium inside the pellets with a high reproducibility. Figure 9 shows the two distributions.

The sintering process was tested for both uranium and thorium oxides. In both cases, the ratio of the density to the theoretical density was better than 95 % of the target value. Dimensions of the fuel pellets were within the specified values. UO_2 pellets were pressed at 300 MPa and sintered at 1700°C for 4 hours in Ar/H2 atmosphere. ThO_2 pellets were pressed at 300 MPa and sintered at 1680°C for 7 hours in Ar/H2 atmosphere. The Thorium oxide required additional front end crushing in order to increase the specific surface area. Figure 10 shows a magnification of a UO_2 fuel pellet with no porosity.

The sintering phase was performed in an adapted dilatometer oven that allows the fabrication of only one pellet at a time. The oven operates in a glove box as it is not compatible with remote hot cell operations. Contamination control on the fabrication process was studied and developed during 2002. The contamination control of the process was demonstrated by quality assurance tests on the fabricated UO_2 and ThO_2 pellets during 2003.
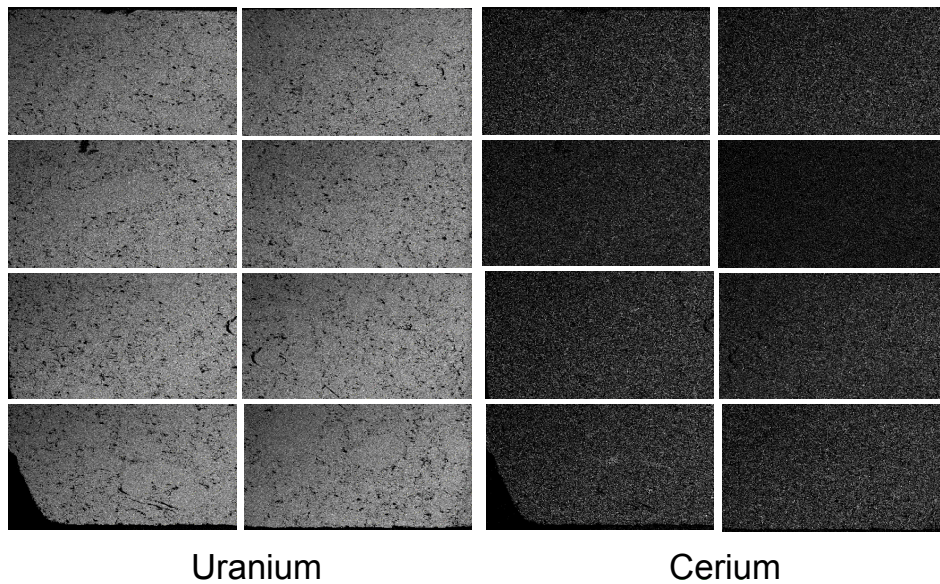
Uranium   Cerium

Figure 9: Homogeneity of Uranium and Cerium distribution in a UO_2 + 1.1 % Ce pellet
(Electronic microscope with magnification x50)
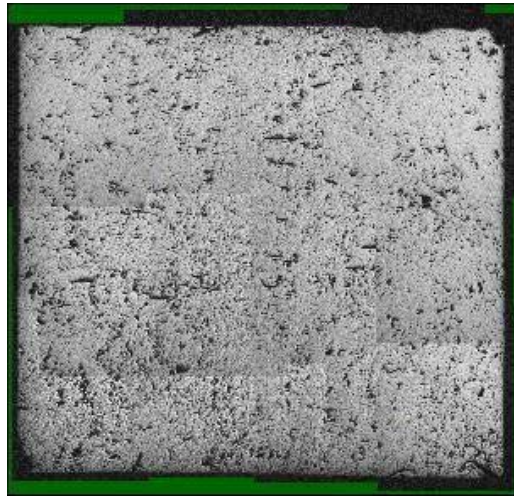
Figure 10: UO_2 pellet with optical microscope (x50)

The effect of the high concentration of the isotopic materials inside the UO_2 matrix was also studied.

This study was necessary because of the high ratio of ^{232}Th (4%) and its effect on the sintering process. Five pellets were sintered with the dilatometer having this ratio of ^{232}Th inside UO_2. This was performed by a student in CEA Marcoule in the first half of 2003. The main conclusions of the study are that a density higher than 95% TD can be achieved, and that the kinetics on the sintering process depend on the isotopic ratio mixed with the UO_2.

A low ratio will increase the kinetics where as high ratios will reduce it. Note that after electronic microscope examination, neither porosity nor cracks were observed inside $UThO_2$ (4%) pellets, which qualifies the modified MIMAS process developed by CEA Marcoule. Examples of preliminary sample pellets are shown in Figure 11.

UO_2 fuel pellets $(UO_2 + 4\% ThO_2)$ fuel pellet
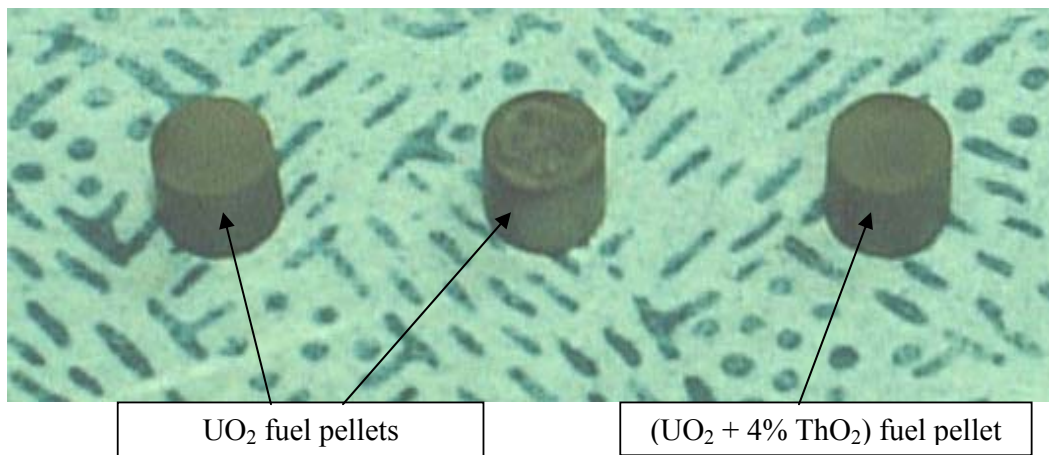
Figure 11: Sample UO_2 and $(UO_2 + 4\% ThO_2)$ fuel pellets

3.4   Technical Aspect

An oven was specially designed for OSMOSE sample fabrication in 2002. The oven was fabricated, and installed at CEA Marcoule in 2003.

The OSMOSE oven is shown in Figure 12. The primary design criteria for the new oven included: the ability to reach temperatures of 2000°C in an Argon atmosphere and 1750°C in O_2 atmosphere, the ability to be remotely operated inside a shielded hot cell, physical dimensions not to exceed 40 cm of height and 24 cm of diameter, and the ability to sinter 40 pellets at the same time.

After completion of tests in the mockup shop and modifications to the hot cell, the OSMOSE oven was inserted into the hot cell and installed.
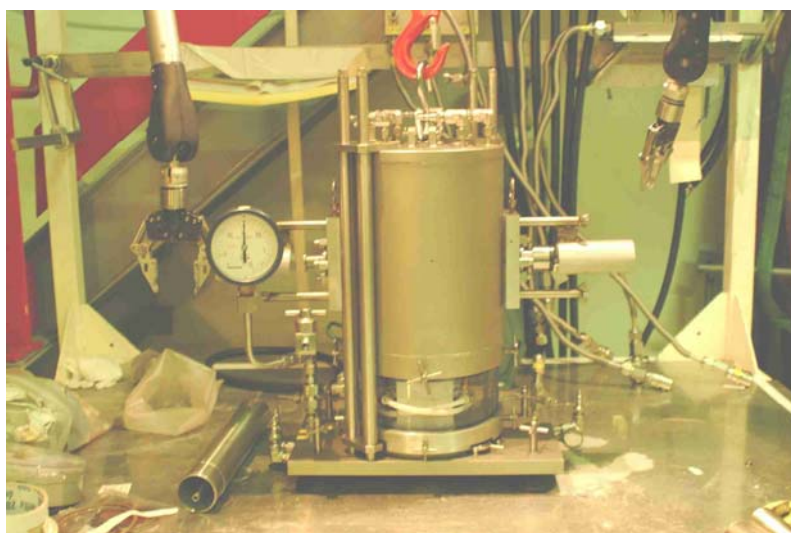
Figure 12: Dedicated OSMOSE oven on test outside the shielded cell

The oven installation and checkout was completed in early January 2004. The safety authority of the Atalante facility gave the final authorization in middle of January 2004 to operate the OSMOSE oven. During several months, the oven has been operating normally except for some minor problems with the water cooling. Figure 13 shows the oven during the last long time run in the hot cell (the red notice informs to avoid any remote operation during the test).

In July 2004, a problem occurred as a result of the power supply connectors which pass through the shielding of the hot cell. Due to the thermal effect of the high current (300 A) the connection unit caused a small leak through the shielded cell which caused the pressure in the hot cell to fall outside of the acceptable range for operation. Therefore the connection unit was removed for safety reasons. The supplier had to prepare a new connection unit with an improved design. The unit was installed and tested during summer. The furnace is now operating properly and the pellet fabrication began in August 2004.
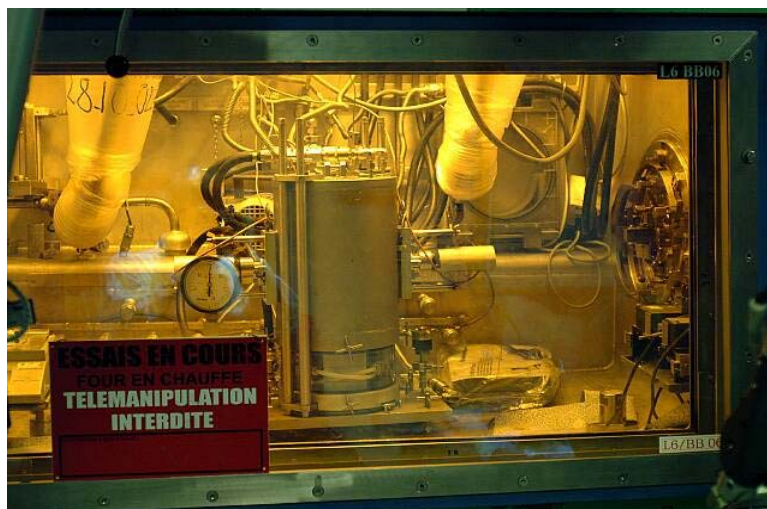
Figure 13: OSMOSE oven installed in the hot cell

3.5 Pellet fabrication

In parallel to the OSMOSE oven installation, sintering of individual pellets was performed in a dilatometer on 23 UO_2 pellets. 20 pellets were acceptable, with a density greater than 95 % of theoretical density, with a mean of 95.9 %TD, and within tolerances on the dimensions and reproducibility of the dimensions.

With the new oven and operating conditions, further improvements on the densification and on the homogeneity of the pellets were achieved.

Parametric studies were carried out to optimize the sintering process. A temperature of 1750°C under Ar/H2 atmosphere gave the best results for the pellet density and uniformity among pellets.

Pellets were fabricated for 5 sets of samples: $UnatO_2$, UO_2+ThO_2, $UO_2 + ^{234}UO_2$, and $UO_2 + ^{237}NpO_2$ (2 samples). Table 7 lists the values of the density for the manufactured pellets. The pellets show mean densities better than the specification of 95% of the theoretical density. Figure 14 shows one of the pellets of $UO_2 + ^{234}UO_2$.

Table 7: Results of pellets manufactured in OSMOSE Oven			
Sample	Mean density (% of T.D.)	Minimum density (% of T.D.)	Maximum density (% of T.D.)
U nat	96.02	95.05	97.85
Unat+^{232}Th	95.08	94.34	96.28
Unat+^{234}U	95.63	93.75	96.62
Unat+^{237}Np (0.21%)	95.56	94.48	97.40
Unat+^{237}Np (1.25%)	96.10	95.92	96.27

Figure 14: $UO_2 + {}^{234}U$ pellet

The first $UreO_2$ pellets have been prepared and after sintering the density achieved a value of 96.24% of the theoretical density.

Fabrication tests were undertaken with ${}^{239}Pu$. A few pellets have been made to adjust the dimension of the press.

The acceptance procedure for the already manufactured set of pellets ($UnatO_2$, $UO_2 + ThO_2$, $UO_2 + {}^{234}UO_2$, $UO_2 + {}^{237}NpO_2$ (x2)) was conducted by CEA and the pellets were accepted.

3.6 Welding

A laser welding technique was developed in the first half of 2002 and gave excellent results. The technique requires adaptation for operation inside a remote hot cell. The laser welding technique produced acceptable welds on Zircaloy claddings (thickness of 0.5 and 0.2 mm). The welding process has not been officially qualified by the Welding Institute as of October, 2004.

The delay in qualification has allowed time to improve the design of the cap and to complete the new specification of the pins.

Other equipment for pellet fabrication and cladding was also tested. The helium filling equipment is now ready. It will be used to check the quality of the welding of the OSMOSE pins (He leak-free test). During these studies, the dimensional characteristics of the welding cap required modification. The change in these specifications has been reviewed by CEA and the acceptance is now given.

It is expected to finish the qualification during November 2004. The welding operation is not on the critical path and does not impact the schedule for pellet fabrication. (The first pins are scheduled at the end of June 2005).

3.7 Analysis

The analysis should assure that the 14 different separated isotopes mixed with the natural UO_2 matrix are consistent with the specifications (isotopic composition and atom ratio). The mass of the separated isotope included inside each sample must be known with a target total uncertainty of 5%. This requires an uncertainty on the analysis better than 2% because there is a 3% uncertainty in the sample from the manufacturing process.

Preliminary tests were performed in April and May 2003 on a mix of ^{237}Np and of natural UO_2 and results were within specifications.

A broad range of equipment and techniques for sample analysis are required because of the diversity of sample isotopes and the low quantities of isotopes in the samples. R&D is being performed to study and improve the analysis techniques, specifically, TIMS, ICP/MS, ICP/AES and alpha and gamma spectroscopy techniques.

The isotopic and chemical characterization of the actinides have been determined for the ^{237}Np, ^{238}Pu, ^{239}Pu, ^{240}Pu, ^{242}Pu, ^{241}Am and ^{234}U samples using mainly mass spectrometry techniques. The ^{241}Am level (<500 ppm) has also been checked by alpha spectroscopy in all of the samples.

Except the analysis work for the control of the isotopes, two others tasks have been performed:
- The first task was to follow the development of the purification process by checking the several samples,
- The second task was the supply of the missing spikes for the isotopic determination by TIMS. The ^{241}Am is now available following the high level grade alpha counting performed in CEA Saclay. With this new spike, the ^{243}Am standard has been qualified.

A new standard for mass spectrometer analysis was also created. The standard is a ^{242}Pu spike and was used for the isotopic dilution analysis of the ^{239}Pu. The latter being the main spike for the other plutonium isotopes.

4 TASK 4: EXPERIMENTS

4.1 Oscillation measurements

This section details the oscillation measurements performed. The calibration of the pilot rod and the oscillation measurements of the calibration samples are reported for the R1-UO2 and R1-MOX configurations.

4.1.1 Calibration of the pilot rod for the R1-UO2 and R1-MOX configurations

To calibrate the pilot rod it is necessary to determine the reactivity of the core for each rotor angle (reactivity curve), and the variation of the reactivity induced by a small variation of rotor angle (differential efficiency curve) [10].

4.1.1.1 Reactivity curve of the pilot rod

The reactivity curve provides the relation between the pilot rod voltage (proportional to the rotor angle) and the reactivity of the core. The experimental technique used to determine this curve is fully described in references [10] and [11].

The reactivity curves obtained in the R1-UO2 and R1-MOX core configurations [5] are shown in Figure 15 and Figure 16.
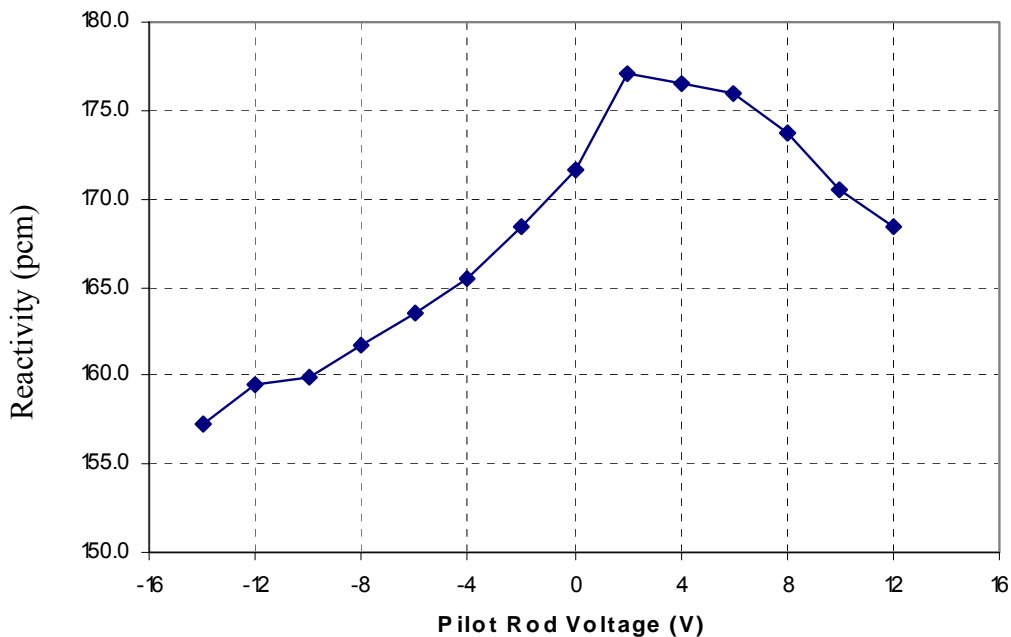
Figure 15: Reactivity Curve of the Pilot Rod in the R1-UO2 configuration
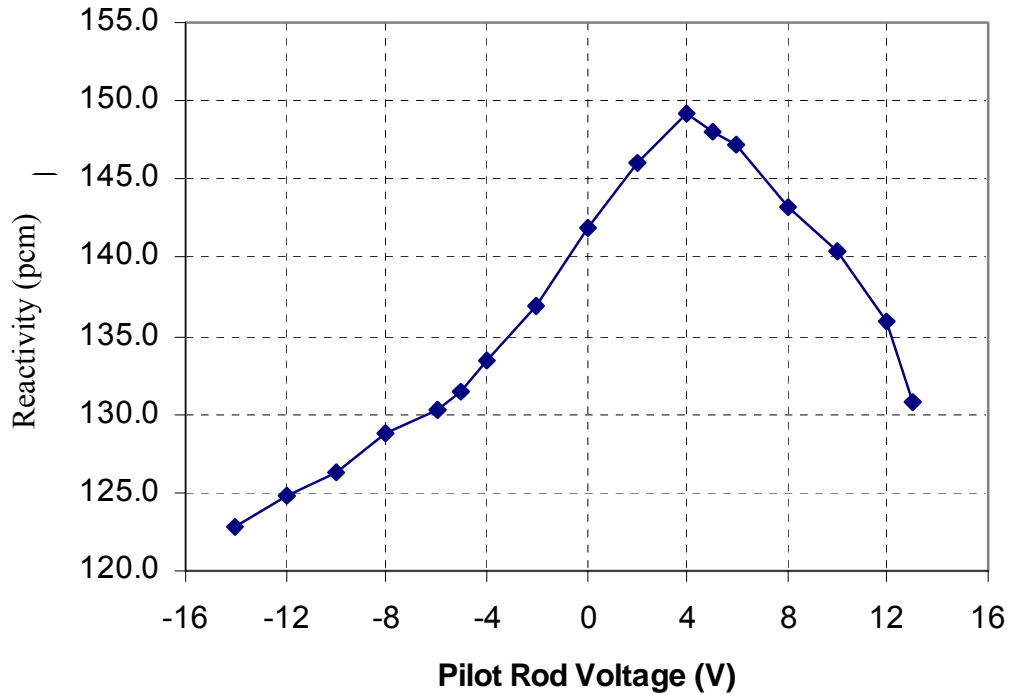
Figure 16: Reactivity Curve of the Pilot Rod in the R1-MOX configuration

For the R1-UO2 and R1-MOX configurations, the pilot rod is able to compensate for a variation of reactivity of ± 10 pcm. Samples are designed so that the maximum variation of reactivity between the studied sample and the reference sample during oscillation experiments is less than 10 pcm.

4.1.1.2 Differential efficiency curve of the pilot rod

The differential efficiency curve is the variation of the pilot rod angle ($\Delta\theta$) induced by a fixed small variation of reactivity ($\Delta\rho$) around the pilot rod angle θ. It is expressed by $f(\theta)=\Delta\rho/\Delta\theta$. The differential efficiency curves of the pilot rod for the R1-UO2 configuration and for the R1-MOX configuration are shown in Figure 17 and Figure 18.

On an appropriate pilot rod angle range, the differential efficiency curve is linear and can be recast as $f(\theta) = f(\theta_0) \times (1 + K \times (\theta - \theta_0))$ where θ_0 is a reference mean angle (chosen in the middle of the linear part of the differential efficiency curve) and K depends on the slope of $f(\theta)$ and on θ_0 [10] [11]. The angle of the pilot rod is measured in arbitrary pilot units. Assuming a reference mean angle θ_0 = -700000 pilot units, the constants K deduced from Figure 17 and Figure 18 are K = -8.6416.10^{-7} for the R1-UO2 configuration, and K = -8.584.10^{-7} for the R1-MOX configuration.

During an oscillation, the variation of pilot rod angle $\Delta\theta$ around the mean pilot rod angle θ is multiplied by $f(\theta)$ to obtain a variation of reactivity.

Figure 17: Differential efficiency curve of the pilot rod in the R1-UO2 configuration
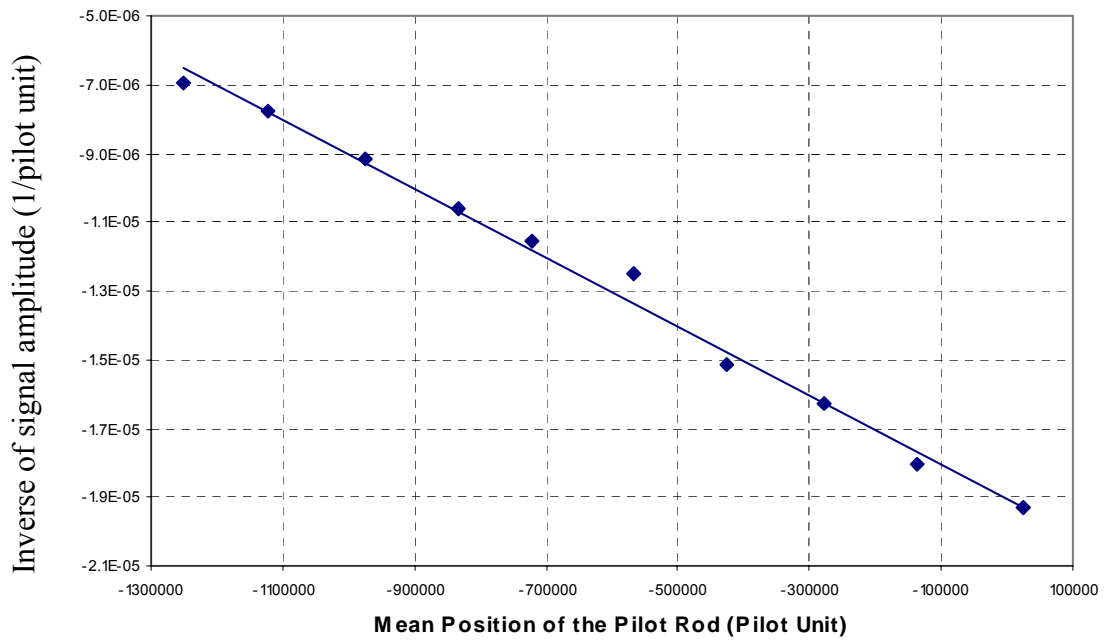
Figure 18: Differential efficiency curve of the pilot rod in the R1-MOX configuration

4.1.2 Calibration measurements for the R1-UO2 and R1-MOX configurations

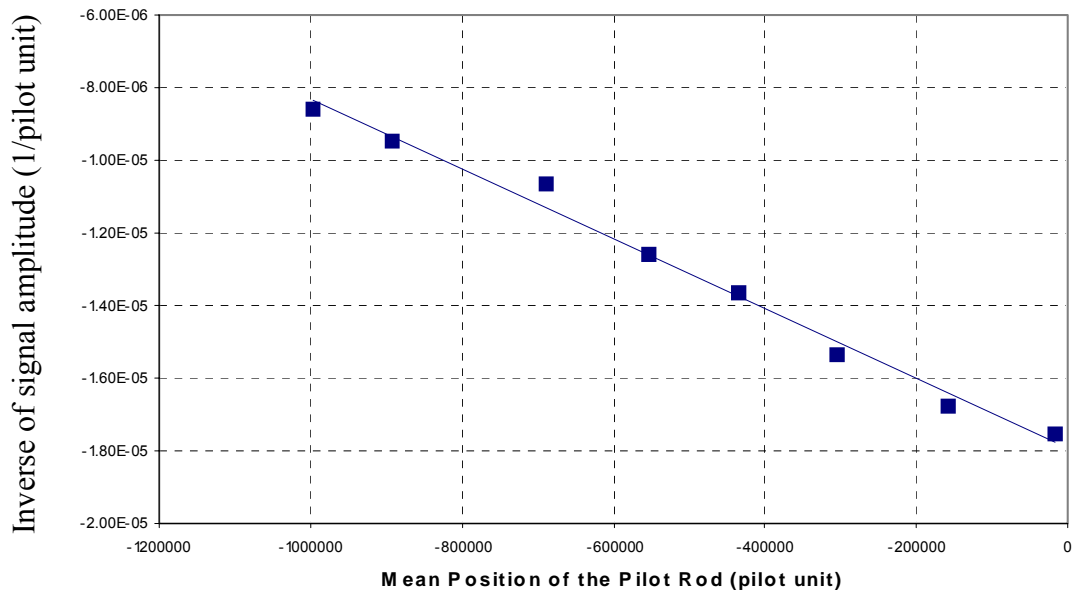The calibration measurements were performed for the R1-UO2 and R1-MOX configurations. The characteristics of the ^{235}U and borated calibration samples are listed in Table 8.

Table 8: Characteristics of the calibration samples					
Type	Name	Clad imprinting	Fissile mass (g)	^{235}U enrichment (wt. %)	Boron (ppm)
^{235}U	01-UO2-0.25%	H1	50.6	0.2512 ± 0.0005	0
	01-UO2-0.50%	H2	50.7	0.4945 ± 0.001	0
	01-UO2-0.71%	H3	50.9	0.7104 ± 0.0014	0
	01-UO2-1%	H4	51.5	1.0022 ± 0.002	0
	01-UO2-2%	H5	51.5	2.0061 ± 0.004	0
	01-UO2-3%	H6	51.5	3.0079 ± 0.006	0
	01-UO2-4%	H7	51.5	3.9977 ± 0.008	0
	01-UO2-4.95%	H8	51.7	4.9317 ± 0.0099	0
B	UO2 BORE 0 ppm	7	48.94	0.25	0
	UO2 BORE 60 ppm	8	48.95	0.25	60
	UO2 BORE 150 ppm	9	48.95	0.25	150
	UO2 BORE 419 ppm	10	48.79	0.25	419
	UO2 BORE 0 ppm	32	51.92	0.53	0
	UO2 BORE 333 ppm	33	51.50	0.53	333
	UO2 BORE 1062 ppm	34	51.06	0.53	1062
	UO2 BORE 2360 ppm	35	49.54	0.53	2360

The mean value of the pilot rod signal is averaged over 5 measurements for each calibration sample and listed in Table 9 and Table 10 for the R1-UO2 and R1-MOX configurations. The uncertainty is deduced from comparison of the standard deviation of each measurement with the dispersion of the 5 measurements by using the Pearson law. The borated samples #34 and #35 could not be measured in the R1-UO2 configuration because the signals were outside of the linear portion of the differential efficiency curve.

Table 9: Calibration Measurements with ^{235}U and borated samples in the R1-UO2 configuration		
Sample	Mean experimental value (pilot unit)	Experimental uncertainty (pilot unit)
H1 (0.25% ^{235}U)	11528	2153
H2 (0.5% ^{235}U)	42000	2153
H3 (0.71% ^{235}U)	73467	2153
H4 (1% ^{235}U)	104953	2153
H5 (2% ^{235}U)	219321	2153
H6 (3% ^{235}U)	313875	4734
H7 (4% ^{235}U)	403243	2153
H8 (4.955% ^{235}U)	475926	2153
7 (0.25 % ^{235}U. 0 ppm)	22299	3757
9 (0.25 % ^{235}U. 150 ppm)	-124638	4417
10 (0.25 % ^{235}U. 419 ppm)	-428772	2153
32 (0.53 % ^{235}U. 0 ppm)	34973	2153
33 (0.53 % ^{235}U. 333 ppm)	-316500	2153

Table 10: Calibration Measurements with ^{235}U and borated samples in the R1-MOX configuration		
Sample	Mean experimental value (pilot unit)	Experimental uncertainty (pilot unit)
H1 (0.25% ^{235}U)	-11907	5027
H2 (0.5% ^{235}U	-5157	1552
H3 (0.71% ^{235}U)	-67	1700
H4 (1% ^{235}U)	6856	1267
H5 (2% ^{235}U)	36727	2349
H6 (3% ^{235}U)	61321	3768
H7 (4% ^{235}U)	85974	3152
H8 (4.955% ^{235}U))	104687	4720
7 (0.25 % ^{235}U. 0 ppm)	-10964	1343
9 (0.25 % ^{235}U. 150 ppm)	-41613	5013
10 (0.25 % ^{235}U. 419 ppm)	-104193	3232
32 (0.53 % ^{235}U. 0 ppm)	-7551	1551
33 (0.53 % ^{235}U. 333 ppm)	-72967	3844
34 (0.53 % ^{235}U. 1062 ppm)	-216175	1699
35 (0.53 % ^{235}U. 2360 ppm)	-389847	1699

The calibration measurements of the [235]U and borated samples are shown in Figure 19 and Figure 20 for the R1-UO2 configuration. The signal of the [235]U samples is normalized to the [235]U sample with a 0.25% enrichment (H1) and the signal of the borated samples are normalized to the borated samples free of boron (#7 and #32). Figure 21 and Figure 22 show the results of the calibration measurements in the R1-MOX configuration.
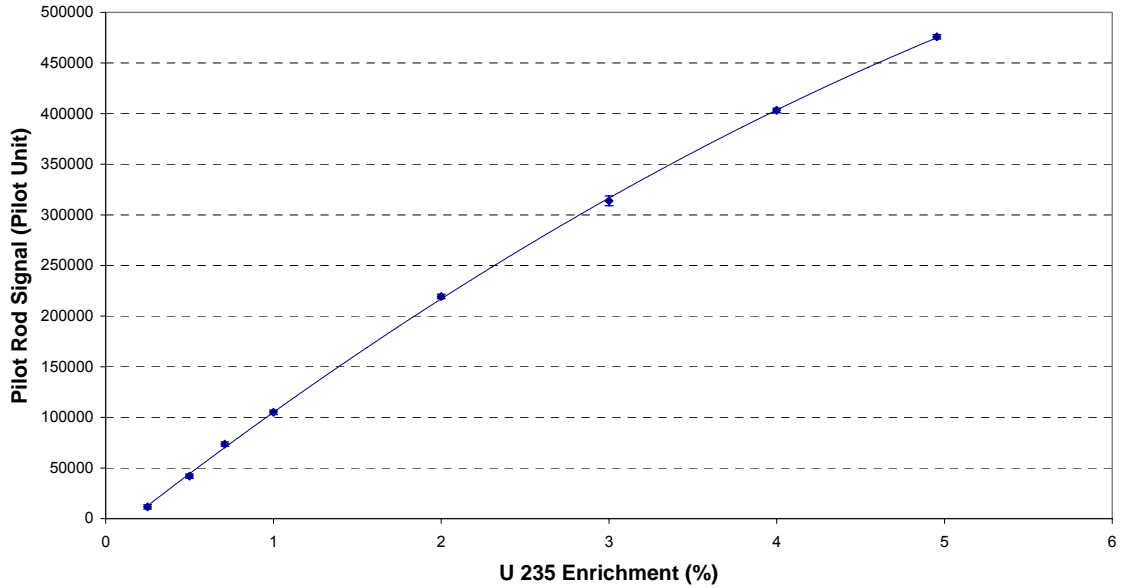
Figure 19: Calibration curve of the [235]U calibration samples for the R1-UO2 configuration
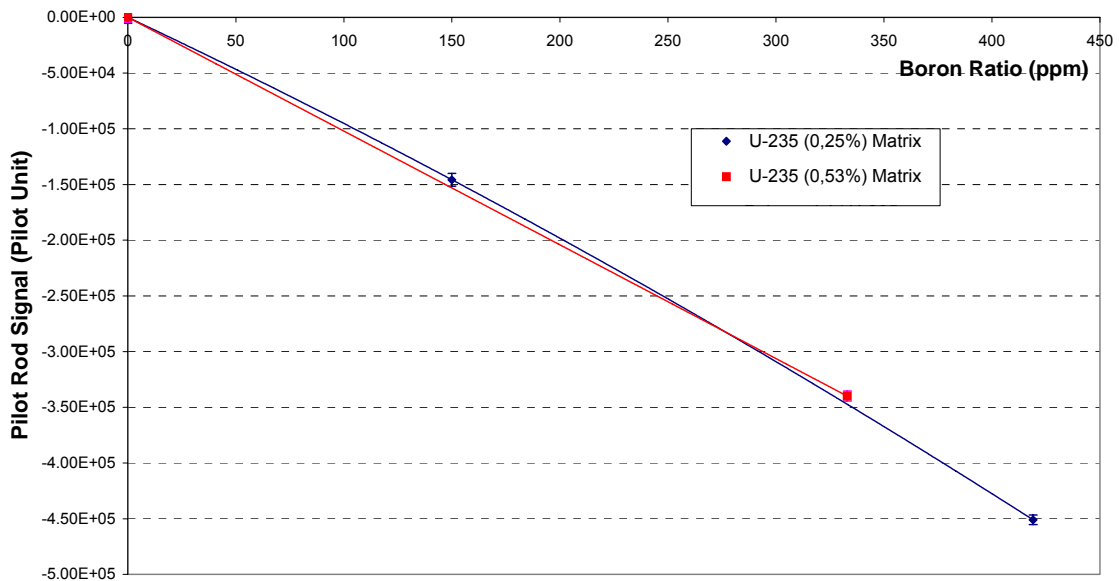
Figure 20: Calibration curve of the borated calibration samples for the R1-UO2 configuration

26

Figure 21: Calibration curve of the ^{235}U calibration samples for the R1-MOX configuration
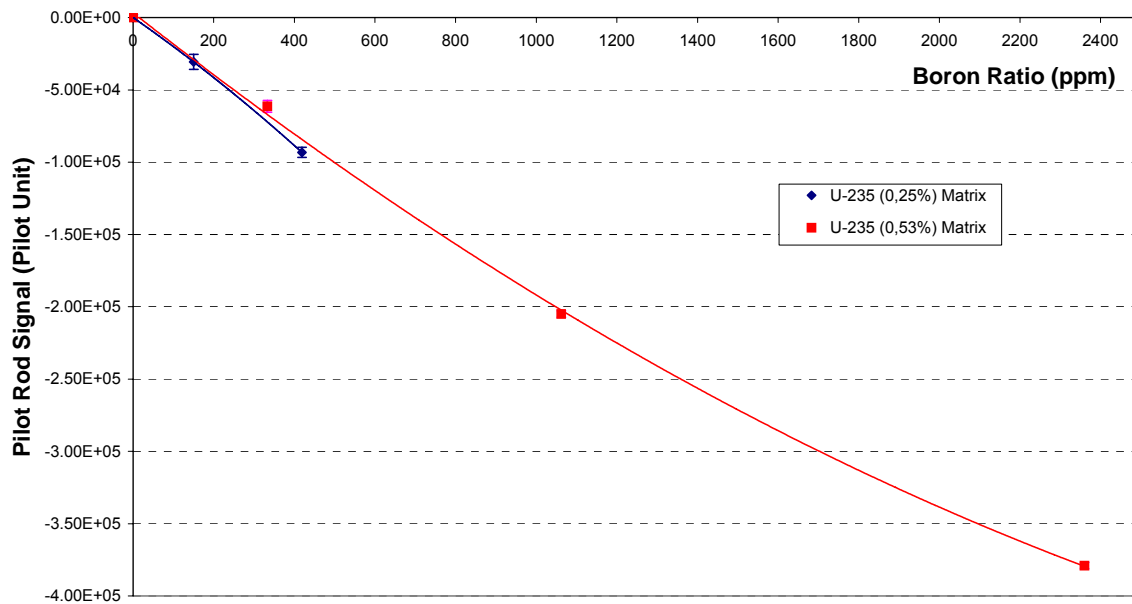
Figure 22: Calibration curve of the borated calibration samples for the R1-MOX configuration

4.1.3 Complementary oscillation procedure tests

The current oscillation procedure is comprised of 10 square oscillations with a 120s period [10]. During the oscillation, the pilot rod compensates for the flux variation from the sample to hold the reactor critical.

The same 10 square oscillations with a 120s period have been used without pilot rod compensation and compared with the current procedure. Measurements were performed for the oscillation cane loaded with the boron sample #8 in one case, and the UO_2 sample H4 in the other (Table 8).

The time dependence of the flux is recorded during the oscillation without compensation, and the reactivity change is deduced using the inversion of the point kinetics equation. The reactivity variation derived without pilot rod compensation is compared with the measurement using pilot rod compensation. Figure 23 shows the signals issued from the oscillation of the UO_2 sample H4. A y-axis is used for each measurement. The reactivity signal issued from the oscillation procedure with pilot rod compensation is more stable than without feedback.
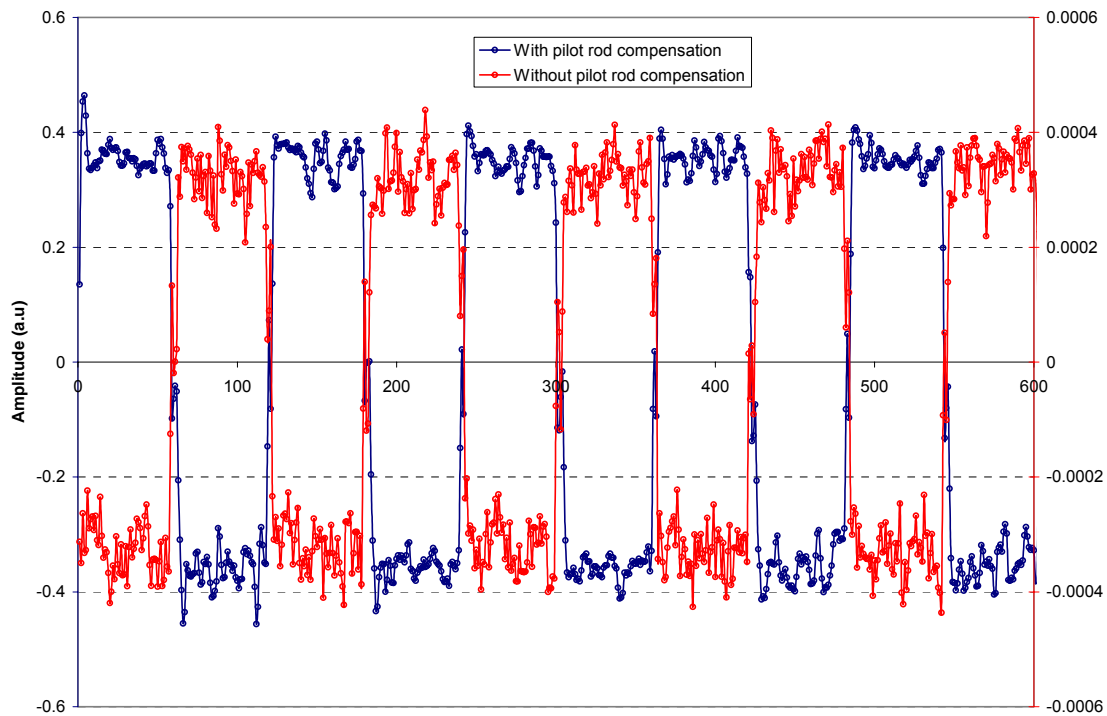
Figure 23: Reactivity deduced from oscillation of the H4 UO_2 sample with and without pilot rod compensation.

To compare the amplitude of the variation of the reactivity signals with and without pilot rod compensation, we use the ratio of reactivity variation amplitude $\Delta\rho$ for the H4 and #8 samples. A simple mean value on each relevant cycle has been used and the ratios are: $\Delta\rho_{H4}/ \Delta\rho_{\#8} = 0.62$ and $\Delta\rho_{H4}/ \Delta\rho_{\#8} = 0.57$ with and without pilot rod compensation, respectively. The measurements differed by about 8% which is good for this simple test.

28

4.2 Measurements for the characterization of the neutron spectrum

Spectral indices and modified conversion ratio measurements [10] [12] [13] have been performed to characterize the neutron spectrum for the R1-UO2 and R1-MOX configurations.

4.2.1 Spectral indices measurements

The spectral indices are measured using ^{235}U, ^{241}Pu, ^{239}Pu and ^{237}Np miniature fission chambers [14] [15] located in the central oscillation channel at the fuel mid-plane. The measured spectral indices are listed in Table 11 for the R1-UO2 and R1-MOX configurations.

Table 11: Measured spectral indices				
	R1-UO2		R1-MOX	
Ratio	Spectral Index	s.d.(%)	Spectral Index	s.d. (%)
^{239}Pu/^{235}U	1.913	1.2 %	1.941	1.2 %
^{241}Pu/^{239}Pu	1.133	1.3 %	1.158	1.3 %
^{237}Np/^{239}Pu	0.00383	3.6 %	0.00742	3.6 %

The fission of ^{237}Np is a threshold reaction (~1MeV). The ^{237}Np/^{239}Pu spectral index is a measure of the fast neutrons and is an indicator of the "hardness" of the neutron spectrum. The ^{237}Np/^{239}Pu ratio doubles from the R1-UO2 to the R1-MOX configuration because of the harder neutron spectrum in the R1-MOX configuration.

4.2.2 Modified conversion ratio measurements

The modified conversion ratio of ^{238}U is defined as the ratio of the ^{238}U capture rate to the total fission rate. The modified conversion ratio was measured using single peak gamma-spectroscopy measurements on irradiated fuel pins. The experimental technique is fully detailed in references [10], [12] and [13]. The modified conversion ratio is [10]:

$$\frac{C8}{F} = \frac{\lambda_{U9} - \lambda_{Np}}{\lambda_{FP}} \frac{\lambda_{Np}}{\lambda_{U9}} \frac{N_{Np}}{N_{FP}} Y_{FP} \frac{g_{FP}}{g_{Np}} \frac{\eta_{FP}}{\eta_{Np}} \frac{f_{FP}}{f_{Np}} \frac{\left(1 - e^{-\lambda_{FP} t_e}\right) e^{-\lambda_{FP} t_c} \left(1 - e^{-\lambda_{FP} tm}\right)}{\left(1 - e^{-\lambda_{Np} t_e}\right) e^{-\lambda_{Np} t_c} \left(1 - e^{-\lambda Np tm}\right)}$$

Equation 1

where C8 is the ^{238}U capture rate, F is the total fission rate, λ_i is the decay constant of nuclide i, N_i is the integral count of the photopeak for nuclide i, η_i is the detection efficiency for the gamma ray of nuclide i, g_i is the gamma-ray emission probability for nuclide i, Y_{FP} is the effective fission yield of fission product FP, f_i is the gamma-ray shielding factor of nuclide i (or the probability for the gamma rays of nuclide i to escape from the fuel to the detector without any interaction), and t_e, t_c, t_m, t_a are respectively the irradiation, cooling, real measurement, and net measurement times.

For the R1-MOX configuration, the conversion ratio has been measured on the UO$_2$ (3% wt. in U-235) fuel pins UOX7 and UOX10 (Figure 24). The UO$_2$ (3%) pins UOX0, UOX1 and UOX4 (Figure 25) have been used for the R1-UO2 configuration.
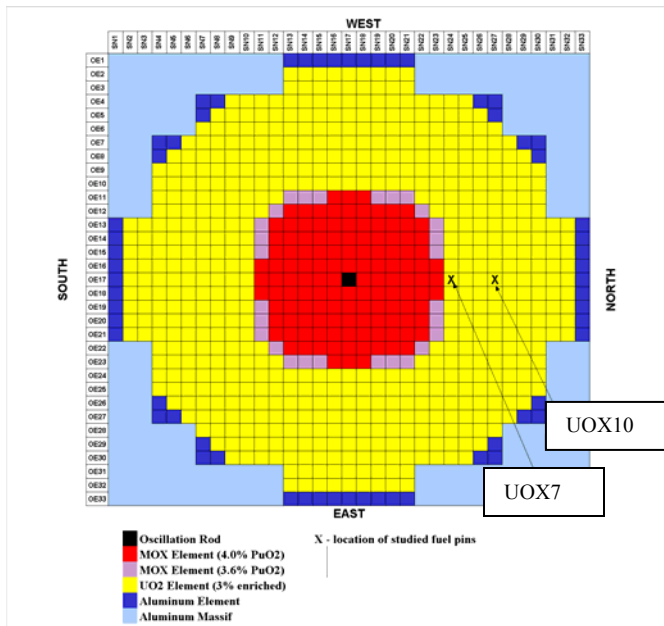
Figure 24: Locations of the studied fuel pins in the R1-MOX configuration
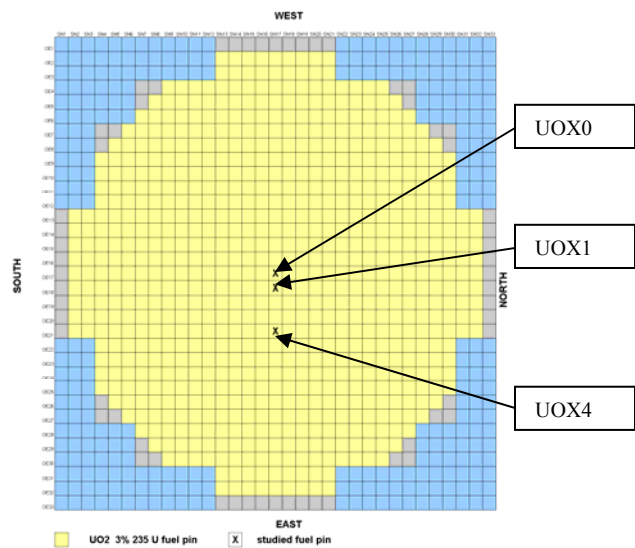
Figure 25: Locations of the studied fuel pins in the R1-UO2 configuration

The gamma-ray shielding factors (f_i) and the effective fission yields (Y_{FP}) are computed using MCNP [10] [12]. Calculations of the reaction rates inside the fuel pin are necessary to determine the gamma-ray shielding factors and the effective fission yield. The fuel pellet is divided into 8 concentric layers of equal volume, in which the total fission rate and the ^{238}U capture rate are calculated. The total thermal and fast fission rates and the ^{238}U capture rate are also calculated for the entire fuel pin. The distribution of the total fission rate and the ^{238}U capture rate are shown in Figure 26. The neutron self-shielding effect is very important mostly for the ^{238}U capture rate, with a ratio of approximately 2 between the outer layer and the central layer.

The gamma-ray shielding factors, calculated with the Monte Carlo code MCNP-4C2, are listed in Table 12. The results are the same using either the JEF2.2 or the ENDF-B6.8 data libraries.

The effective fission yields calculated with MCNP-4C2 and the ENDF-B6.8 and JEF2.2 data libraries are listed in Table 13. The results obtained with ENDF-B6.8 and JEF2.2 are consistent but the uncertainties are larger with JEF2.2 (~6.6%) than with ENDF-B6.8 (~ 1.3%). This is due to a larger uncertainty on the thermal fission yield of U-235 in JEF2.2 than in ENDF-B6.8.
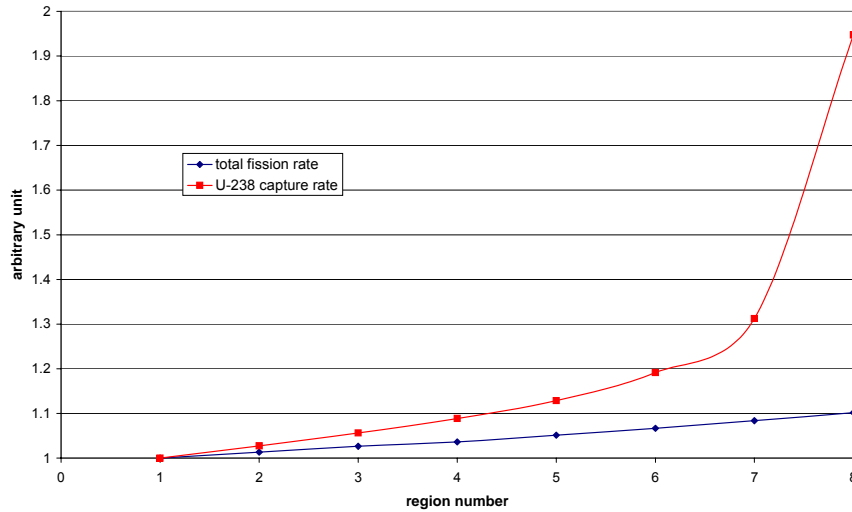
Figure 26: Distribution of the U-238 capture rate and the total fission rate of the UOX10 fuel pin for the R1-MOX configuration

Table 12: Gamma-ray shielding factors					
		Ce-143		Np-239	
Configuration	Fuel pin	f	s.d. (%)	f	s.d. (%)
R1-UO2	UOX0	0.3138	0.35 %	0.3068	0.41 %
	UOX1	0.3138	0.41 %	0.3071	0.41 %
	UOX4	0.3138	0.41 %	0.3069	0.41 %
R1-MOX	UOX7	0.3141	0.65 %	0.3069	1.26 %
	UOX10	0.3141	0.60 %	0.3056	1.20 %

Table 13: Effective fission yields of the Ce-143					
		ENDF-B6.8		JEF2.2	
Configuration	Fuel Pin	Effective Fission Yield (%)	s.d. (%)	Effective Fission Yield (%)	s.d. (%)
R1-UO2	UOX0	5.870	1.29 %	-	-
	UOX1	5.864	1.28 %	-	-
	UOX4	5.870	1.29 %	-	-
R1-MOX	UOX7	5.860	1.27 %	5.863	6.65 %
	UOX10	5.877	1.29 %	5.877	6.67 %

Figure 27 and Figure 28 show examples of gamma-ray spectrum and [143]Ce and [239]Np photopeaks.
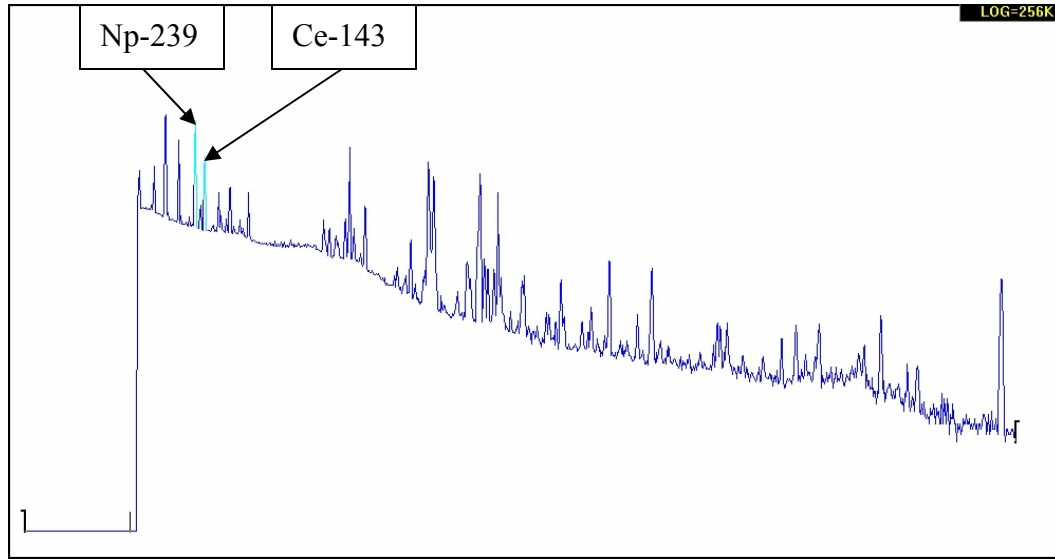
Figure 27: Gamma-ray spectrum for a UO$_2$ 3% irradiated fuel pin
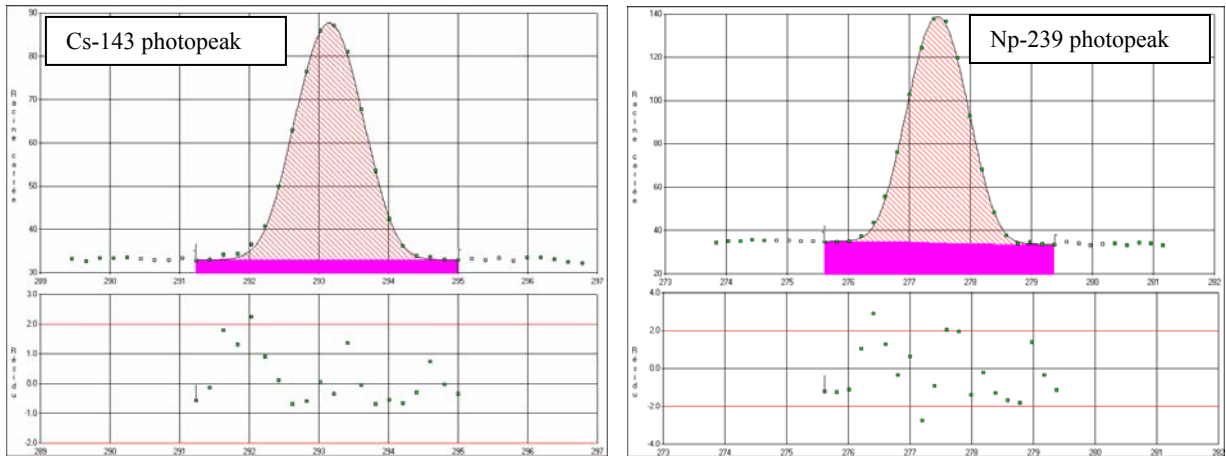
Figure 28: ^{143}Ce and ^{239}Np photopeaks for a UO$_2$ 3% irradiated fuel pin

The efficiency of the gamma spectroscopy device was measured using a ^{133}Ba calibration source. Results are shown in Table 14 for the energies of interest.

Table 14: Efficiency of the gamma spectroscopy device			
Isotope	Gamma-Ray Energy (keV)	Efficiency (%)	s.d. (%)
^{239}Np	277.60	38.51 %	0.24 %
^{143}Ce	293.27	35.71 %	0.21 %

The modified conversion ratios are determined using Equation 1 and the experimental technique described in reference [10] and are listed in Table 15 and Table 16 for the ENDF-B6.8 and JEF2.2 data libraries.

Table 15: Experimental modified conversion ratio (ENDF-B6.8)					
Conf.	Fuel Pin	C8/F	Δ(C8/F)/(C8/F) (nuclear data + calculations)	Δ(C8/F)/(C8/F) (reproducibility of the measurement)	Δ(C8/F)/(C8/F) (total)
R1-UO2	UOX0	0.495	2.09%	0.32%	2.11%
	UOX1	0.498	2.09%	0.32%	2.12%
	UOX4	0.498	2.10%	0.36%	2.13%
R1-MOX	UOX7	0.583	2.00 %	0.50 %	2.06 %
	UOX10	0.502	1.93 %	0.44 %	1.98 %

Table 16: Experimental modified conversion ratio (JEF2.2)					
Conf.	Fuel Pin	C8/F	Δ(C8/F)/(C8/F) (nuclear data + calculations)	Δ(C8/F)/(C8/F) (reproducibility of the measurement)	Δ(C8/F)/(C8/F) (total)
R1-MOX	UOX7	0.581	7.04 %	0.50 %	7.05 %
	UOX10	0.499	7.13 %	0.44 %	7.14 %

The modified conversion ratios of the UOX7 and UOX10 pins are almost the same when the effective fission yield and the gamma-ray shielding factors are calculated with the ENDFB-6.8 or the JEF2.2 data libraries. The uncertainty for the modified conversion ratio is increased when using JEF2.2 because of larger uncertainties on the thermal fission yield of ^{235}U.

The fundamental mode is established in the central zone of the R1-UO2 experimental lattice and the modified conversion ratio for the UOX0, UOX1 and UOX4 fuel pins agree within one standard deviation.

In the R1-MOX configuration, the modified conversion ratio of the UOX7 fuel pin is approximately 16% higher than for the UOX10 fuel pin. This is explained by the harder neutron spectrum at the interface between MOX and UOX pins that favors ^{238}U capture in the resonance. The modified conversion ratio of the UOX10 fuel pin for the R1-MOX configuration is in good agreement with the modified conversion ratio for the R1-UO2 configuration.

4.3 Measurements of safety parameters

4.3.1 Reactivity worth of the control rods

The reactivity worth of the control rods is derived in two steps. The reactivity worth of the rod from the critical position down to the fully inserted position is deduced from rod drop measurements and the reactivity worth from the critical position up to the fully withdrawn position is deduced from core excess reactivity measurements [10].

For the rod drop measurement, a ^{235}U fission chamber was used to follow the time dependent neutron population during the drop of the rod. The detector was located in the central oscillation channel for the R1-UO2 and R1-MOX configurations and also in the thermal column (Figure 3) for the R1-UO2 configuration.

The reactivity worth of the control rods obtained in the R1-UO2 and R1-MOX configurations are listed in Table 17 to Table 19. The rods are designated as R1, R2, R3 and R4 and are inserted in the east, south, west and north driver zone, respectively [7].

Table 17: Reactivity worth of the control rods for the R1-UO2 configuration (detector in the oscillation channel)		
Rod inserted	From critical positions ($)	Total ($)
R1	1.00 ± 0.06	1.18 ± 0.06
R2	1.14 ± 0.06	1.32 ± 0.06
R3	1.22 ± 0.07	1.40 ± 0.07
R4	1.14 ± 0.08	1.32 ± 0.08
4 rods*	5.44 ± 0.43	5.62 ± 0.43

*rod R3 in the critical position, all others fully withdrawn

Table 18: Reactivity worth of the control rods for the R1-UO2 configuration (detector in the thermal column)		
Rod inserted	From critical positions ($)	Total ($)
R1	1.14 ± 0.06	1.37 ± 0.06
R2	1.02 ± 0.06	1.25 ± 0.06
R3	1.29 ± 0.07	1.52 ± 0.07
R4	1.32 ± 0.08	1.55 ± 0.08
4 rods*	7.75 ± 0.43	7.98 ± 0.43

*rod R3 in the critical position, all others fully withdrawn

Table 19: Reactivity worth of the control rods for the R1-MOX configuration (detector in the oscillation channel)

Rod inserted	From critical positions ($)	Total ($)
R1	1.13 ± 0.06	1.34 ± 0.06
R2	1.30 ± 0.09	1.51 ± 0.09
R3	1.39 ± 0.08	1.60 ± 0.08
R4	1.06 ± 0.06	1.27 ± 0.06
4 rods*	7.04 ± 0.36	7.25 ± 0.36

*rod R3 in the critical position, all others fully withdrawn

The reactivity worth strongly depends on the position of the fission chamber during the rod drop measurement (Table 17 and Table 18). The difference between the two experiments range from 5% to 20% for individual rods and is approximately 40% for the four rods; advocating the need for spatial and energy corrections. To account for spatial and energetic effects at the exact location of the detector, MSM (Modified Source Multiplication) factors have to be calculated [10] [16].

The difference in the excess reactivity of the core between the different experiments is due to a variation of the water temperature in the core.

4.3.2   Axial fission rates and power distribution – Axial buckling

The axial power distribution was studied by integral gamma scanning [10] on irradiated fuel pins in the R1-UO2 and R1-MOX configurations. The location of the studied fuel pins (denoted MOX1 and MOX3 in the R1-MOX configuration, and UOX0, UOX1 and UOX4 in the R1-UO2 configuration) is shown in Figure 29 and Figure 30.

In parallel, the ^{237}Np and ^{235}U fission rate profiles were measured in the central oscillation channel with miniature fission chambers [10].

The oscillation basket, regrouping the 9 holes in the center of the experimental zone, has two plates of styrene at about $\pm$ 12-15 cm from the fuel center line [5]. Because styrene contains carbon and hydrogen, neutrons are locally slowed down enhancing the thermal neutron fission rate
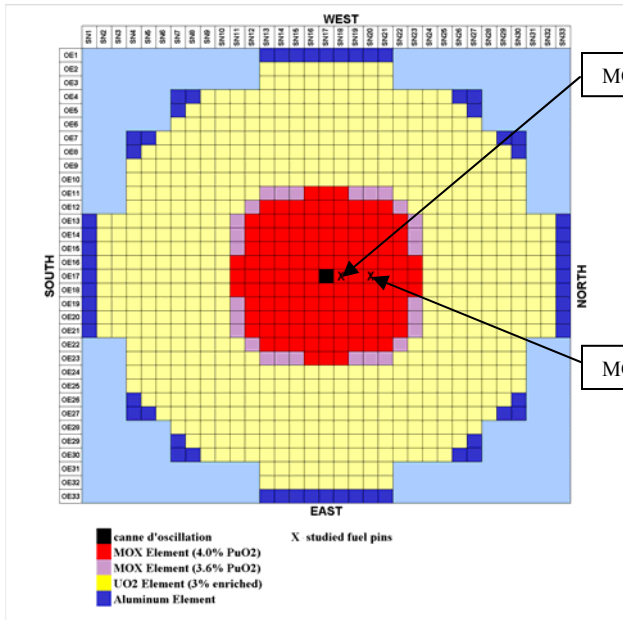
Figure 29: Locations of the studied fuel pins for axial profile measurements for the R1-MOX configuration
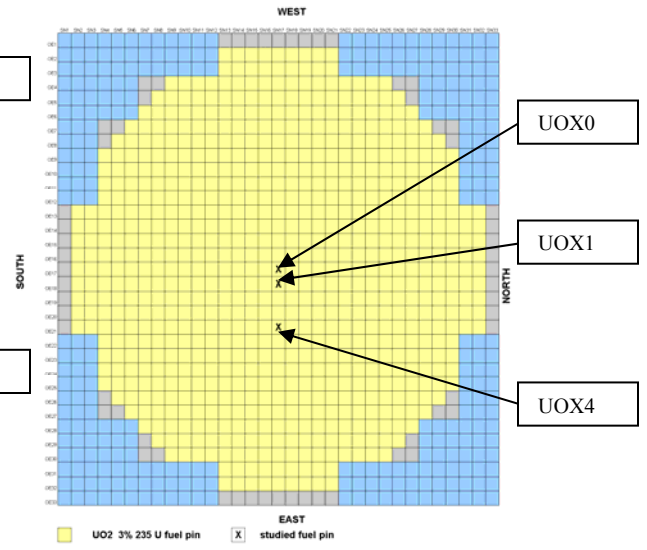
Figure 30: Locations of the studied fuel pins for axial profile measurements for the R1-UO2 configuration

4.3.2.1 The R1-UO2 configuration

The measured axial fission rate profile for the UOX0, UOX1 and UOX4 pins is shown in Figure 31. The fission rate distributions agree in the range ±20 cm from the fuel mid-plane.

The axial power profile measured by the ^{235}U and ^{237}Np fission chamber is shown in Figure 32. There is an overall agreement between fission rate distributions in the region of interest (between -20 cm and 20 cm). The neutron slowing down induced by the lower and upper Plexiglas spacer of the pins is starting to be observed at 20 cm from the core mid-plane for the ^{235}U fission chamber measurement. Similarly, the influence of the styrene spacers is shown in the ^{235}U fission chamber measurement at approximately -13 cm and 13 cm, but does not appear in the ^{237}Np fission chamber measurement because of the threshold for fission of ^{237}Np.
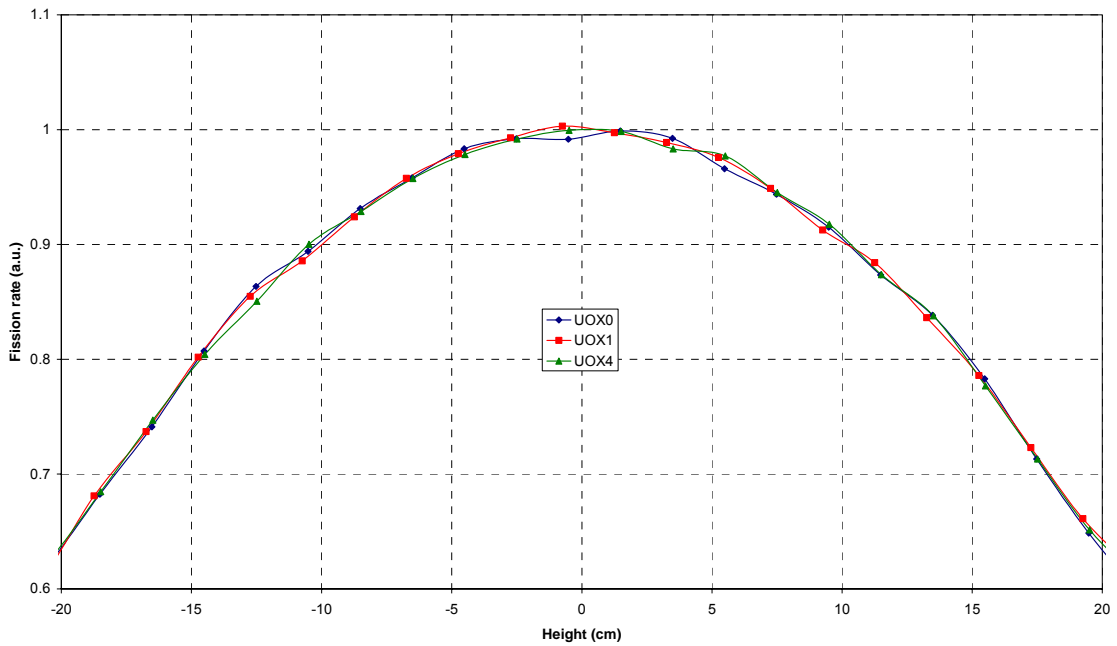
Figure 31: Axial fission rate distribution of the UOX0, UOX1 and UOX4 pins in the R1-UO2 configuration
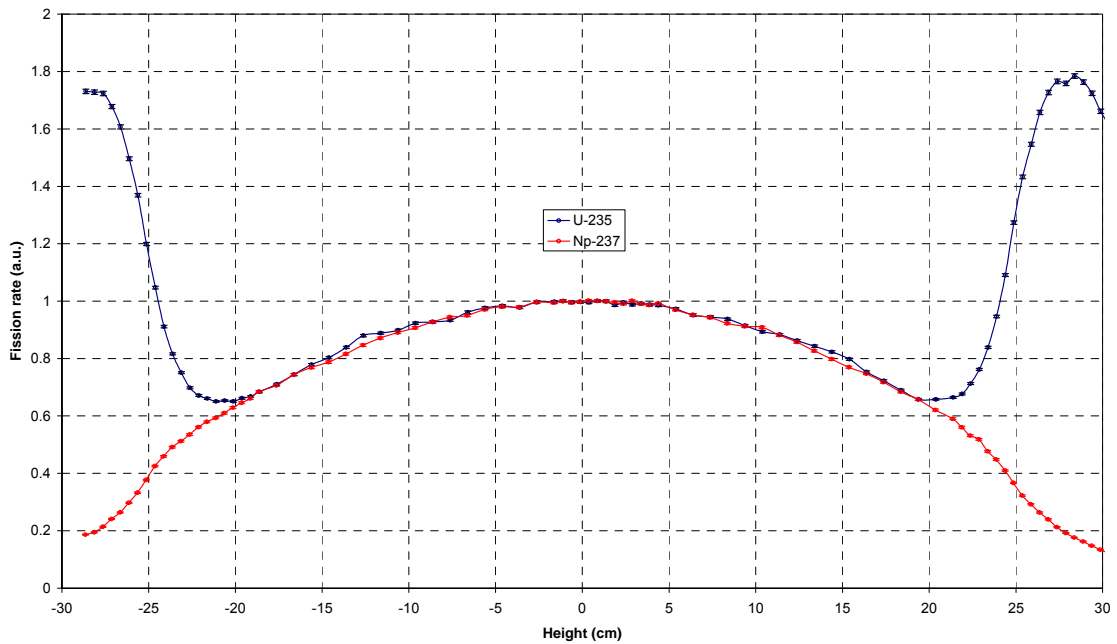
Figure 32: Axial fission rate profiles of ^{235}U and ^{237}Np fission chambers in the R1-UO2 configuration

Considering the fundamental mode established on an axial region centered on the core mid-plane, the axial fission rate distribution is a cosine function characterized by the axial buckling B^2. The fission rate distribution can be fitted by the function $f(z) = A \cos(B (z-z_0))$, where z_0 accounts for any offset.

Practically, the cosine function can be used in a region where the influence of the Plexiglas and Styrene spacer are negligible. The effect of the Plexiglas spacer can be neglected by narrowing the region around the core mid-plane. The influence of Styrene spacers are difficult to remove but are generally too small to significantly disturb the cosine shape.

To find the best value of the axial buckling from the measurements, parametric studies of the buckling versus the height of the axial region have been performed in [7]. Results of the buckling parametric study for the experimental power profiles concluded that the best fitting region is [-18 cm, 18 cm]. The axial bucklings determined experimentally are listed in Table 20.

Table 20: Experimental axial buckling ($\times 10^{-3}$ cm^{-2}) in the R1-UO2 configuration	
Source	Experiment
^{235}U	1.917 ± 0.011
^{237}Np	1.973 ± 0.011
UOX0	1.939 ± 0.013
UOX1	1.932 ± 0.013
UOX4	1.940 ± 0.013

The experimental bucklings agree within one standard deviation except for the buckling measured with the ^{237}Np fission chamber which agrees within two standard deviations.


4.3.2.2 The R1-MOX configuration

The measured axial fission rate profiles for the MOX1 and MOX3 pins are shown in Figure 33. The fission rate distributions agree in the range of ±20 cm from the fuel mid-plane. The axial power profile measured by the ^{235}U and ^{237}Np fission chamber is shown in Figure 34. The increase of the ^{235}U fission rate due to the neutron slowing down induced by the Plexiglas and styrene spacers is similar to the one observed in the R1-UO2 configuration.

To find the best value of the axial buckling from the measurements, parametric studies of the buckling versus the height of the axial region have been performed in [7]. Results of the buckling parametric study for the experimental power profiles concluded that the best fitting region is [-18 cm, 18 cm] and that the fitting region is hard to define for the ^{235}U and MOX1 measurements because of the influence of the styrene spacers. The axial bucklings determined experimentally are listed in Table 21 and agree within two standard deviations except for the ^{235}U and MOX1 measurements.
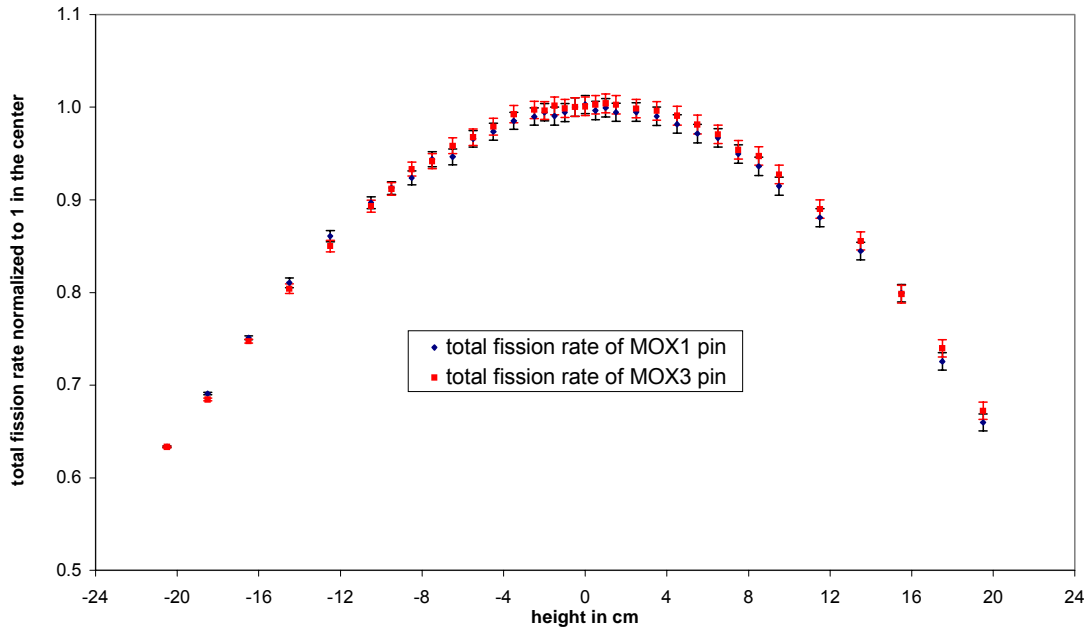
Figure 33: Axial fission rate distribution of the MOX1 and MOX3 pins in the R1-MOX configuration
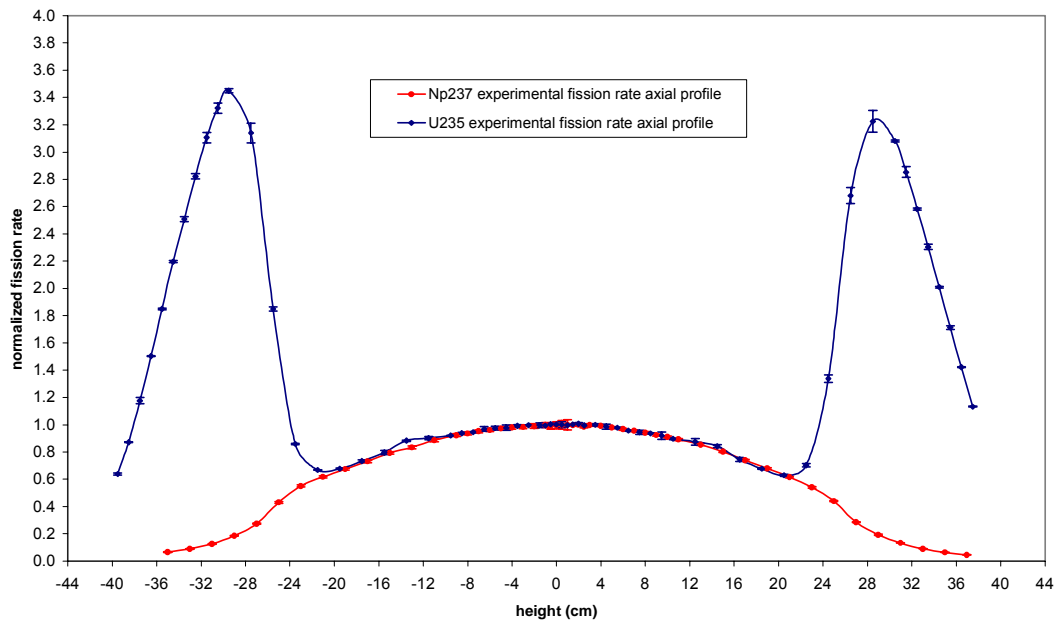
Figure 34: Axial fission rate profiles of ^{235}U and ^{237}Np fission chambers in the R1-MOX configuration

Table 21: Experimental axial buckling (*1e-3 cm^{-2}) in the R1-MOX configuration	
Source	Experiment
^{235}U	1.900 ± 0.010
^{237}Np	1.885 ± 0.012
MOX1	1.840 ± 0.009
MOX3	1.863 ± 0.009

4.3.3   Radial power distribution

The radial power distribution was measured in the R1-MOX configuration. The experimental technique is described in reference [10]. First, a radial fission rate distribution (see location of the fuel pins in Figure 35) was determined by integral gamma-scanning of each fuel-type zone of the core (e.g. on the MOX pins and on the UOX pins in the R1-MOX configuration). Then the two fission rate distributions were normalized using single peak gamma-spectroscopy of the ^{140}La gamma-ray at 1596.17 keV for pins of each fuel-type zone [16] (see fuel pins MOX3 and UOX10 in Figure 35).

The total fission rate inside a fuel pin calculated from the ^{140}La evolution equations is:

$$F = \frac{(\lambda_L - \lambda_B)\, N_L}{Y_B\; g_L\; \eta_L\; f_L \left(\frac{\lambda_L}{\lambda_B} e^{-\lambda_B T_o} \left(1 - e^{-\lambda_B T_i}\right)\left(1 - e^{-\lambda_B T_c}\right) - \frac{\lambda_B}{\lambda_L} e^{-\lambda_L T_o} \left(1 - e^{-\lambda_L T_i}\right)\left(1 - e^{-\lambda_L T_c}\right) \right)} \frac{T_c}{T_l}$$

Equation 2

where T_i is the irradiation time, T_0 is the cooling time, T_c is the counting time, T_l is the live time of the counting (i.e. $(T_c - T_m)$ where T_m is the dead time of the electronic chain), λ_i are the decay constants for isotope i, N_L is the total count of the studied gamma-ray of ^{140}La, f_L is the self-absorption coefficient of the ^{140}La gamma-ray at 1596.17 keV, g_L is the intensity of the gamma-ray of ^{140}La at 1596.17 keV and Y_B is the effective fission yield of ^{140}Ba.

The normalization factor between the MOX zone and the UOX zone is then defined as

$$r_{MOX} = \frac{\sum_i F_{MOX,i}}{\sum_i F_{UOX,i}}$$

Equation 3

For the R1-MOX configuration, the normalization factor is $r_{MOX} = F_{MOX3}/F_{UOX10}$.
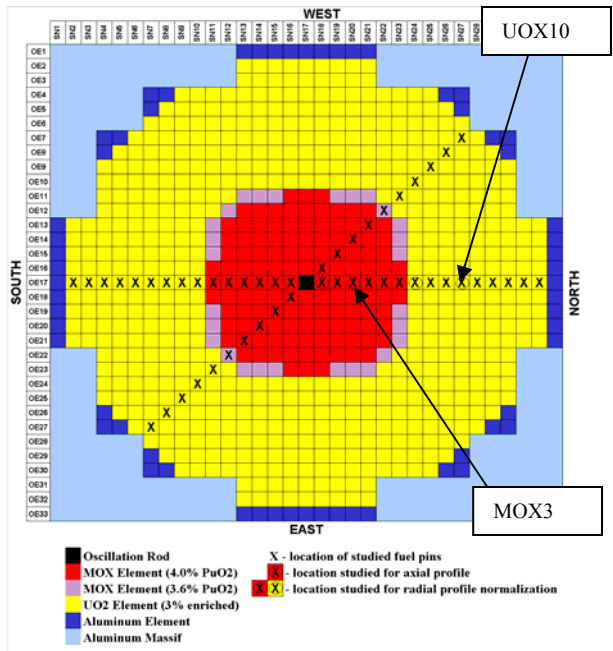
Figure 35: Location of the normalization fuel pins

Table 22 listed the shielding factors of the gamma-ray of ^{140}La at 1596.17 keV calculated for the 4 studied fuel pins. Results are the same with JEF2.2 and ENDF-B6.8 data libraries.

Table 22: Gamma-Ray Shielding Factors for the 1596 keV gamma-ray of ^{140}La		
Fuel Pin	f_L	s.d. (%)
MOX3	0.9363	1.56 %
UOX10	0.9354	1.02 %

Table 23 presents the values of the effective fission yields of ^{140}Ba calculated using the ENDF-B6.8 and the JEF2.2 data libraries. The difference between the calculated effective fission yield is a result of discrepancies between thermal fission yields of ^{239}Pu, ^{241}Pu, and ^{235}U in ENDF-B6.8 and JEF2.2.

Table 23: Effective Fission Yields of Ba-140 in the studied fuel pins		
Fuel Pin	Y_B with JEF2.2	Y_B with ENDF-B6.8
MOX3	0.0544	0.0549
UOX10	0.0624	0.0619

The standard deviation on the ratio Y_M/Y_U (where Y_M and Y_U are the effective fission yields of the MOX and UOX fuel pins [10]) in Equation 3 is 1.20% with JEF2.2 and 1.29% with ENDF-B6.8. Figure 36 shows an example of the measured gamma-ray of ^{140}La at 1596.17 keV for MOX3 fuel pin. For MOX pins, this peak is disturbed by the 2nd escape peak of ^{208}Tl at 2614.5 keV, coming from decays of ^{240}Pu. These two peaks have to be uncorrelated (gaussian uncorrelation) as shown in Figure 36.
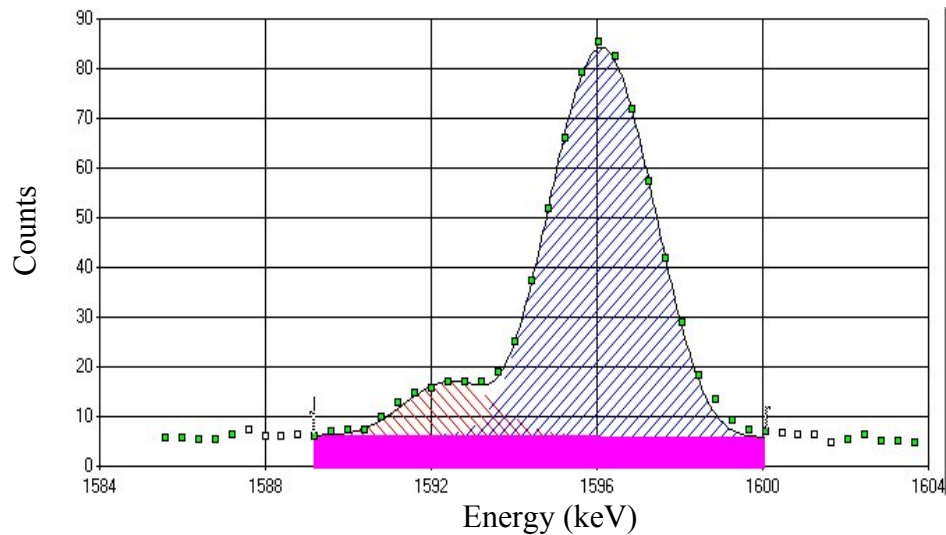
Figure 36: ^{140}La photopeak at 1596.17 keV and 2nd escape ^{208}Tl photopeak for the MOX3 fuel pin

Using the effective fission yields and shielding factors of Table 22 and Table 23, the derived power normalization factors are:

Table 24: Normalization factor r_{MOX} obtained with the JEF2.2 and the ENDF-B6.8 data libraries

Data library	r_{MOX}	$\Delta r_{MOX}/r_{MOX}$ (nuclear data + calculations)	$\Delta r_{MOX}/r_{MOX}$ (reproducibility of the measurement)	$\Delta r_{MOX}/r_{MOX}$ (total)
JEF2.2	1.017	1.59%	0.47%	1.66%
ENDF-B6.8	1.035	1.66%	0.47%	1.73%

The influence of the data library on the normalization factors is approximately 2%.

The horizontal and diagonal power profile distribution is shown in Figure 37 and Figure 38. Accuracies better than 3% were obtained for each point of the radial distributions. In every case, a slight asymmetry around the central cell is observed. It comes from the fact that the oscillation rod that was introduced in the central zone during the experiment was not perfectly centered which induces an asymmetry of the water blade around this rod.

The power profile at the interface between the MOX and UOX regions is also well reproduced. The strong gradient of total fission rate at the interface comes from the fact that the neutron spectrum is harder in MOX cells than in UO$_2$ cells due to resonances in the absorption cross sections for the plutonium isotopes.

42

Finally, the asymmetry of the power between the south region of the lattice and north region of the lattice is due to the asymmetry on the loading of the driver zone.
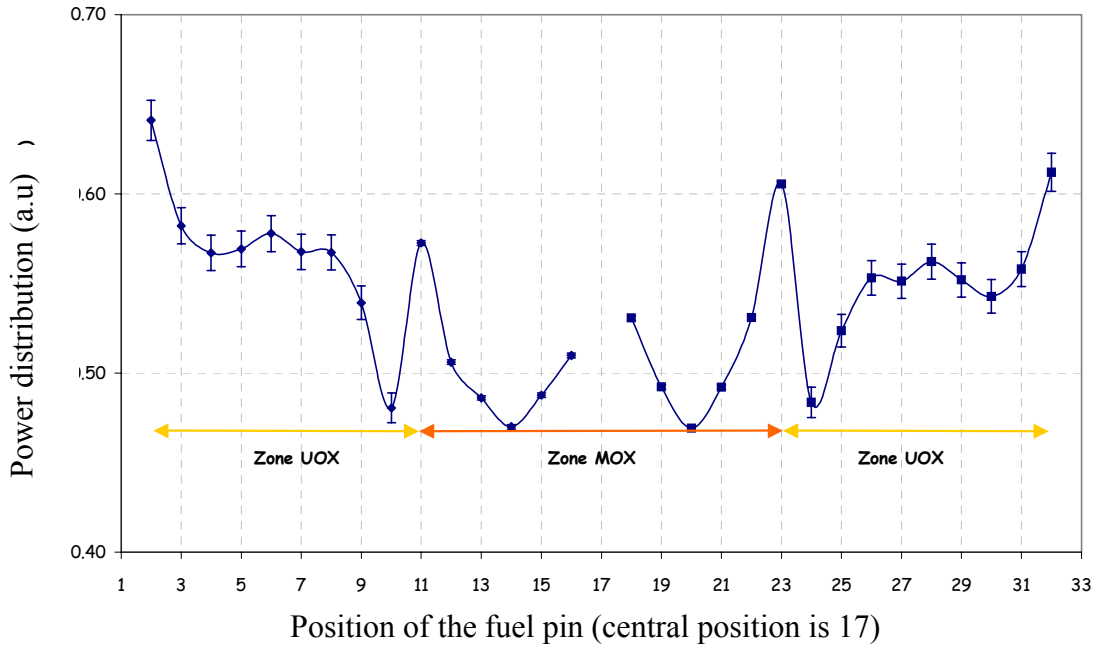
Figure 37: Horizontal radial power distribution for the R1-MOX configuration
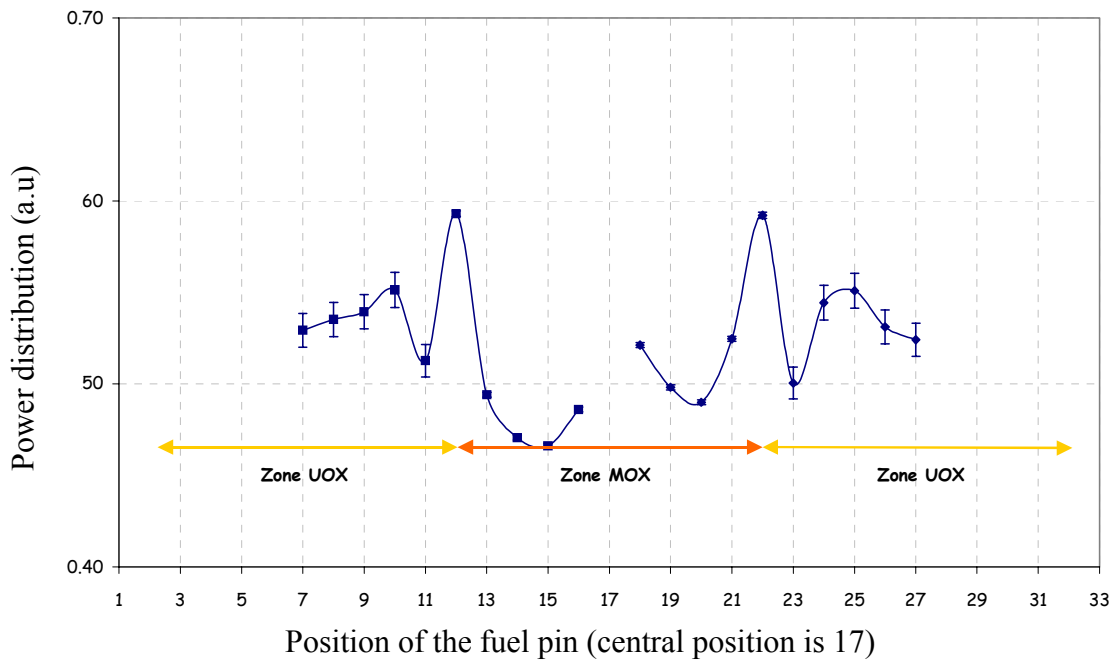
Figure 38: Diagonal radial power distribution for the R1-MOX configuration

43

5 TASK 5: DATA ANALYSIS

The MCNP and REBUS models have been used to predict safety and core parameters for the R1-UO2 and R1-MOX configurations. Results of the MCNP and REBUS calculations are compared with one another and also with the experimental results (see section 4) whenever possible. The safety and core parameters of interest are the reactivity worth of the control rods, the spectral indices in the oscillation channel at core mid-plane, the axial power profile, the radial power profile, and the conversion ratio.

The reactivity worths of the calibration samples calculated with the REBUS model are compared with the experimental values in the R1-UO2 and R1-MOX configuration.

5.1 The control rod reactivity worth

5.1.1 Experimental technique

Analysis of the rod-drop measurement is based on the point kinetic model. Considering that the investigated reactivity worth is greater than 700 pcm[1] (approximate value of the delayed neutron fraction), it is necessary to take into account spatial and energetic effects. One method is to calculate Modified Source Multiplication factors [10] and use these to adjust the values for the rod worths.

In the MCNP and REBUS models, the reactivity worths of the rods have been evaluated using two static calculations: one when all rods are withdrawn and the other when the rod of interest is fully inserted in the core.

5.1.2 Results and comparison

The reactivity worth determined experimentally is relative to the delayed neutron fraction and expressed in dollars (see section 4.3.1). MCNP and REBUS calculate multiplication factor. The conversion in relative reactivity uses a delayed neutron fraction of 716 pcm and 681 pcm for the R1-UO2 and R1-MOX configuration [17], respectively. The uncertainty on the reactivity worth of the rod determined by MCNP does not take into account the uncertainty on the delayed neutron fraction. A statistical uncertainty is not derived for the REBUS model.

Spatial and energy effects are a major problem to the interpretation of the rod-drop measurements (see section 4.3.1). However, the spatial and energy effects appear to be less critical when the ^{235}U fission chamber is located in the thermal column instead of the center of the core (Table 17 and Table 18 in section 4.3.1). Therefore, a primary comparison between experiment and calculation is reported in Table 25 when the fission chamber is located in the thermal column.

---

[1] 1pcm = 10^{-5}

Experiments and MCNP calculations agree within one standard deviation for all rods except R3. This agreement is still valid for the large reactivity worth of the four rods; suggesting small spatial and energy corrections. On the contrary, the difference between experiments and REBUS calculations increases with the reactivity worth. The REBUS calculations result in lower reactivity worth estimates than the MCNP calculations except for the rod R1. This might be explained because the pilot rod is modeled in MCNP and not in REBUS.

Table 25: Experimental and calculated rod worth in the R1-UO2 configuration						
Rods inserted	Exp. ($)	MCNP ($)	REBUS ($)	MCNP C/E	REBUS C/E	REBUS/MCNP
R1	1.37 ± 0.06	1.38 ± 0.03	1.45	1.010 ± 0.049	1.058	0.952
R2	1.25 ± 0.06	1.33 ± 0.03	1.29	1.060 ± 0.057	1.030	0.972
R3	1.52 ± 0.07	1.66 ± 0.03	1.35	1.094 ± 0.054	0.891	0.815
R4	1.55 ± 0.08	1.60 ± 0.03	1.38	1.030 ± 0.057	0.888	0.862
4 rods	7.98 ± 0.43	7.83 ± 0.03	6.81	0.981 ± 0.053	0.854	0.870

In the R1-MOX configuration, the rod-drop experiments have only been recorded with a U-235 fission chamber located in the central channel of the experimental lattice. The MCNP and REBUS rod worth are compared in Table 26. The trend between the MCNP and the REBUS calculations is the same as in the R1-UO2 configuration.

Table 26: Calculated rod worth reactivity in the R1-MOX configuration			
Rods inserted	MCNP ($)	REBUS ($)	REBUS/MCNP
R1	1.51 ± 0.03	1.77	1.173
R2	1.61 ± 0.03	1.61	0.998
R3	1.76 ± 0.03	1.58	0.896
R4	1.69 ± 0.03	1.62	0.958
4 rods	10.03 ± 0.03	9.43	0.940

Further investigations require calculation of spatial/energy correction factors such as Modified Source Multiplication factors to correct measurements in the thermal column or at least make sure that such corrections are negligible. Complementary REBUS models and experiments will be needed.

5.2   Spectral indices

The spectral indices have been determined in MCNP by using the track length estimate of the cell flux tally [6] on a 10 cm height and a 0.9 cm diameter void cylinder located in the center of the core. The height matches that of the oscillation samples and the diameter maximizes the statistic of the tally. Calculations are performed with all rods withdrawn, which should not influence the spectrum in the center of the core.

The spectral indices are reported in Table 27 and Table 28 for the R1-UO2 and R1-MOX configurations, respectively. Calculated and measured spectral indices agree within one standard deviation except for the ^{237}Np/^{239}Pu index in the R1-UO2 configuration which

agrees within two standard deviations. These conclusions are valid using either the ENDFB6 or the JEFF2.2 library for the MCNP calculations.

Table 27: Spectral indices for the R1-UO2 configuration					
Spectral Index	Experiment	MCNP		MCNP/Exp.	
		ENDFB6	JEFF2.2	ENDFB6	JEFF2.2
$^{239}Pu/^{235}U$	1.913 ± 0.023	1.918 ± 0.021	1.947 ± 0.047	1.003 ± 0.016	1.018 ± 0.027
$^{241}Pu/^{239}Pu$	1.133 ± 0.015	1.142 ± 0.012	1.137 ± 0.027	1.008 ± 0.017	1.004 ± 0.027
$^{237}Np/^{239}Pu$	0.00383 ± 0.00014	0.00361 ± 0.00003	0.00360 ± 0.00007	0.944 ± 0.035	0.940 ± 0.038

Table 28: Spectral indices for the R1-MOX configuration					
Spectral Index	Experiment	MCNP		MCNP/Exp.	
		ENDFB6	JEFF2.2	ENDFB6	JEFF2.2
$^{239}Pu/^{235}U$	1.941 ± 0.023	1.954 ± 0.035	1.968 ± 0.061	1.007 ± 0.022	1.014 ± 0.034
$^{241}Pu/^{239}Pu$	1.158 ± 0.015	1.147 ± 0.020	1.134 ± 0.035	0.991 ± 0.022	0.979 ± 0.033
$^{237}Np/^{239}Pu$	0.00742 ± 0.00027	0.00745 ±0.00010	0.00730 ± 0.00018	1.004 ± 0.039	0.984 ± 0.043

5.3 Axial power profile

5.3.1 Calculation technique

The REBUS model has been used to generate the axial power profile in the studied pins of the R1-UO2 and R1-MOX configurations. The fission rate is evaluated for each axial mesh; corresponding to at least one data point every centimeter.

Axial power profiles are also computed with the MCNP model for comparison with the fission chamber and integral gamma counting measurements. The power profile is calculated every 2 cm using the track length estimate of the cell flux tally [6]. This resolution is time consuming but necessary to have enough points for comparisons.

The oscillation basket, the 9 center holes of the experimental zone, has two plates of Styrene at about ± 12-15 cm of the fuel center line [7]. Because Styrene contains carbon and hydrogen, neutrons are locally slowed down enhancing the thermal neutron fission rate. The Styrene plates have not been included in the MCNP and REBUS models.

5.3.2 The R1-UO2 configuration

The measured and calculated axial power profile for the UOX0, UOX1 and UOX4 pins are shown in Figure 39 and Figure 40. For all pins, the REBUS and experimental power profiles match each other in the range of ±19 cm of the core mid-plane. MCNP power profiles exhibit fluctuations due to an insufficient number of particles in each tallied cell.

The axial power profiles derived from ^{235}U and ^{237}Np fission chamber measurements are compared with MCNP calculations in Figure 41. There is a very good overall agreement between calculation and experiment for the ^{235}U and ^{237}Np fission chamber profiles. The region of interest (between -20 cm and 20 cm) is shown in Figure 42. MCNP profiles oscillated near the core mid-plane. The influence of the styrene spacers is shown in the

[235]U fission chamber measurement at approximately -13 cm and 13 cm, but does not appear in the [237]Np fission chamber measurement because of the threshold for the [237]Np fission.

The fission rate distribution can be fitted by the function $f(z) = A \cos(B (z-z_0))$, where z_0 accounts for any offset (see section 4.2.1). To find the best value of the axial buckling, parametric studies of the buckling versus the height of the axial region have been performed in [7] for the measured and calculated data. For the MCNP and REBUS models, the best estimates of the buckling is for the range [-18 cm, 18 cm]. The measured and calculated bucklings are reported in Table 29.

	Experiment ($\times 10^{-3}$ cm^{-2})	MCNP ($\times 10^{-3}$ cm^{-2})	REBUS ($\times 10^{-3}$ cm^{-2})	MCNP/Exp.	REBUS/Exp.	REBUS/MCNP
Table 29: Experimental and calculated axial buckling in the R1-UO2 configuration						
Source	Experiment ($\times 10^{-3}$ cm^{-2})	MCNP ($\times 10^{-3}$ cm^{-2})	REBUS ($\times 10^{-3}$ cm^{-2})	MCNP/Exp.	REBUS/Exp.	REBUS/MCNP
[235]U	1.917 ± 0.011	1.901 ± 0.032	-	0.992 ± 0.018	-	-
[237]Np	1.973 ± 0.011	1.877 ± 0.020	-	0.951 ± 0.011	-	-
UOX0	1.939 ± 0.013	1.906 ± 0.030	1.944	0.983 ± 0.017	1.002	1.020
UOX1	1.932 ± 0.013	1.926 ± 0.030	1.942	0.997 ± 0.017	1.005	1.008
UOX4	1.940 ± 0.013	1.930 ± 0.031	1.921	0.995 ± 0.017	0.990	0.995

The experimental bucklings agree within one standard deviation except for the [237]Np fission chamber measurement. The bucklings calculated using MCNP all agree within one standard deviation. There is also a good agreement between the bucklings calculated using REBUS. The same conclusion can be drawn when comparing experimental and calculated results for a given pin. The only source of disagreement is observed for the [237]Np axial buckling. The reason can be an error in the measurement or an inaccuracy of the [237]Np cross section in ENDF-BVI as pointed out by the spectral indices (section 5.2).
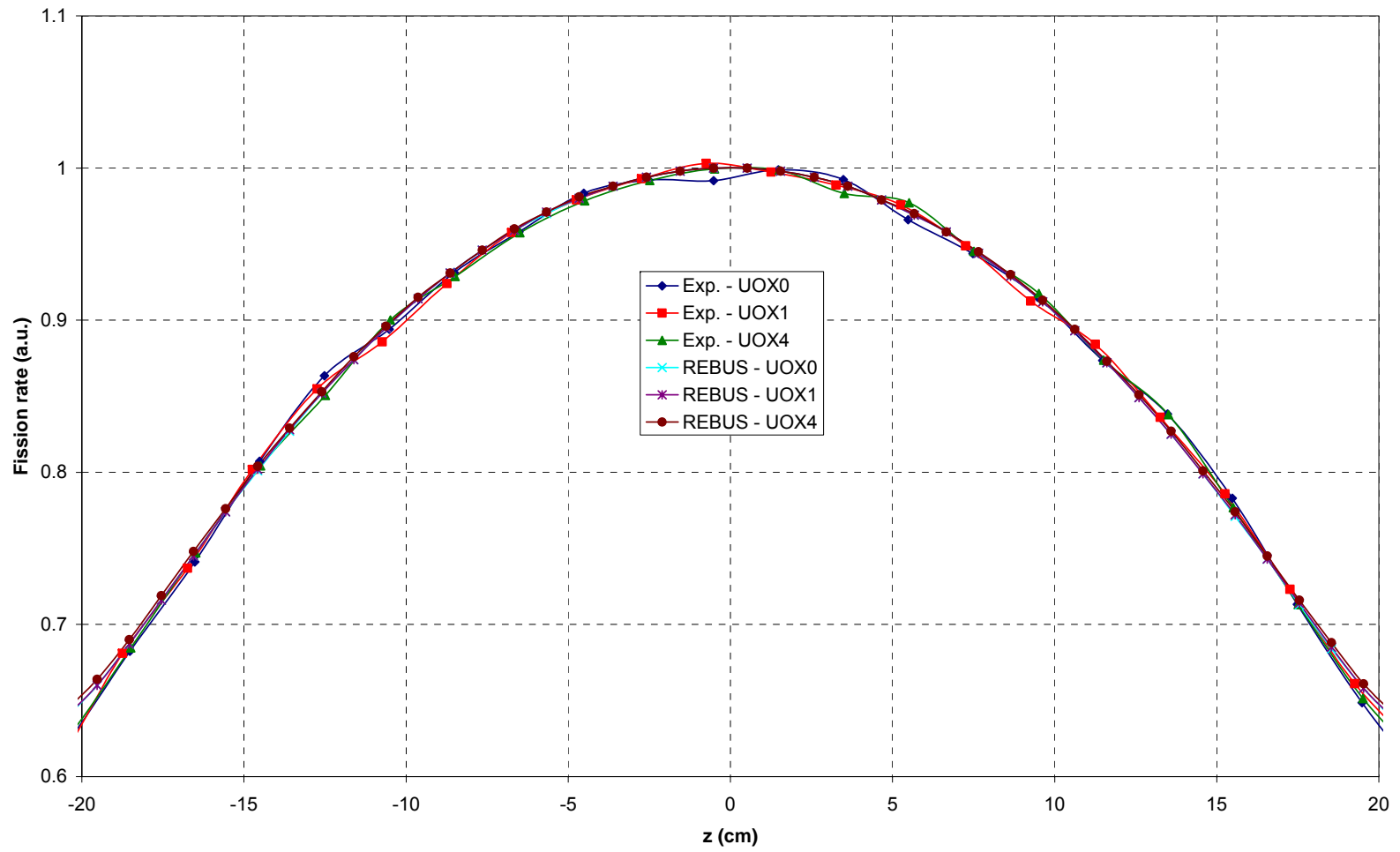
Figure 39: Axial power profile for specific pins in the R1-UO2 configuration – Comparison of REBUS results to measurements
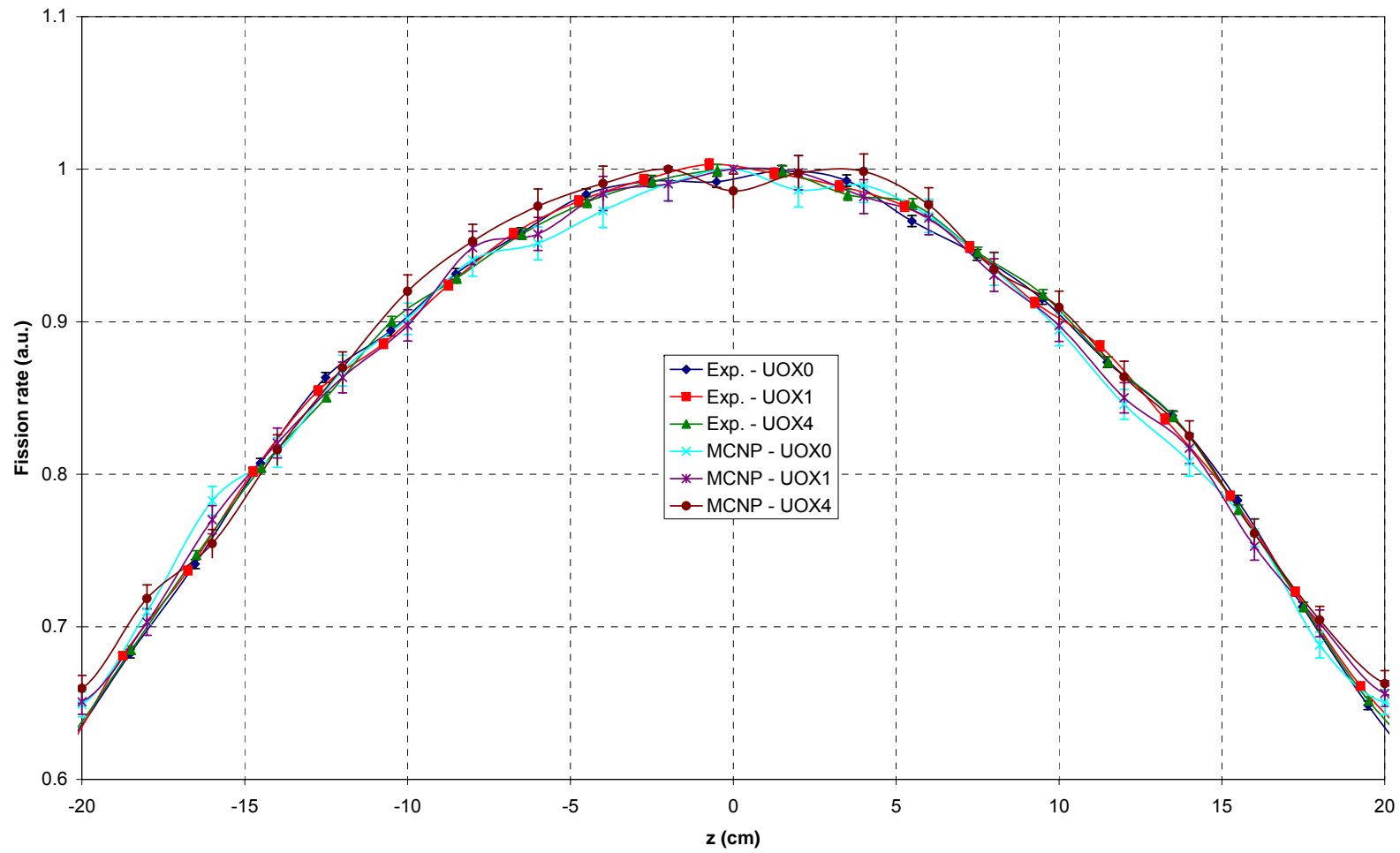
Figure 40: Axial power profile for specific pins in the R1-UO2 configuration – Comparison of MCNP results to measurements
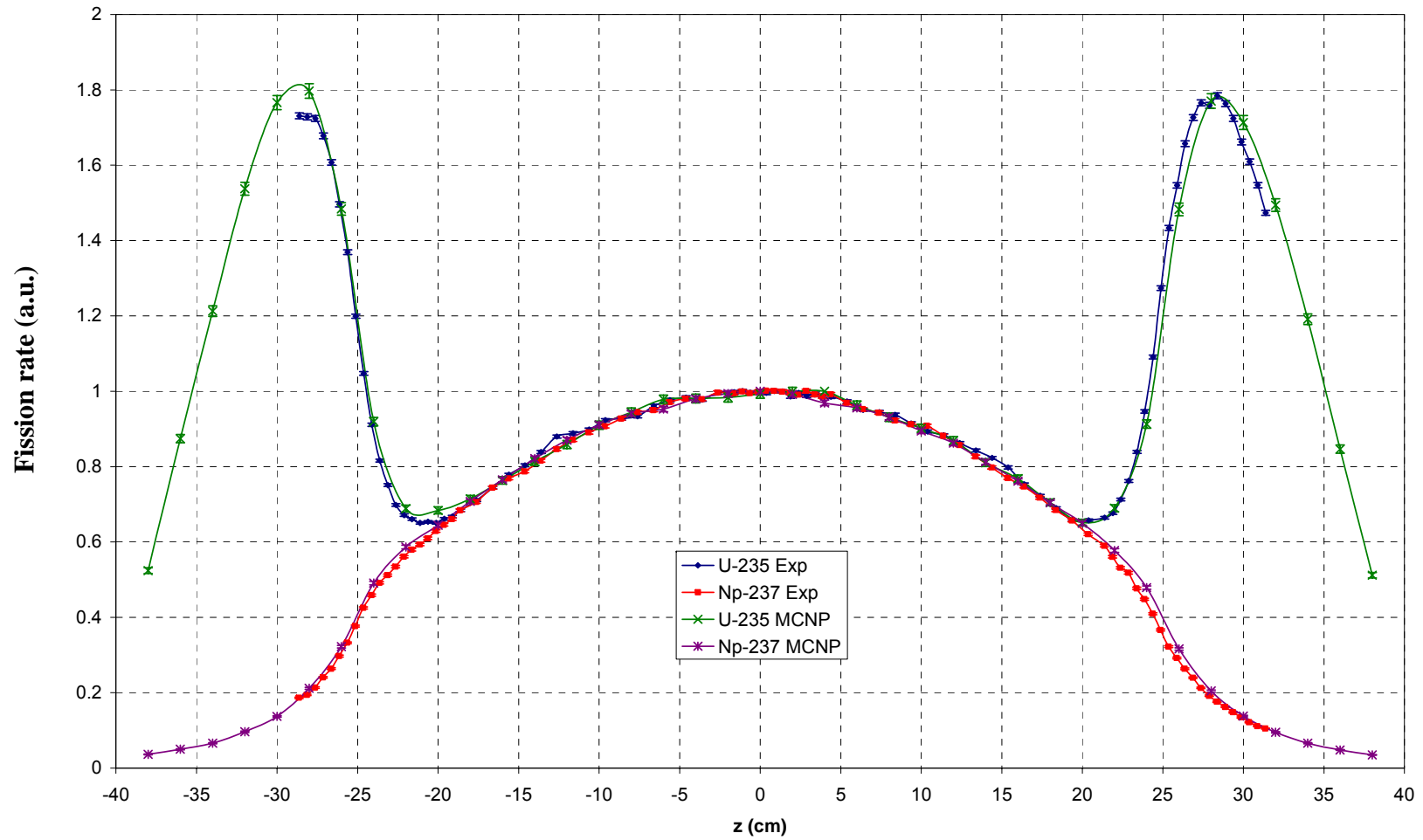
Figure 41: Axial fission rate profile of ^{235}U and ^{237}Np fission chambers in the R1-UO2 configuration – Comparison of MCNP results to measurements

Figure 42: Axial fission rate profile of ^{235}U and ^{237}Np fission chambers in the R1-UO2 configuration – Comparison of MCNP results to measurements over range of ±20 cm

5.3.3 The R1-MOX configuration

The axial power profile obtained by integral gamma scanning for the pins MOX1 and MOX3 are compared with the REBUS and MCNP calculations in Figure 43 and Figure 44. The uncertainty for the experimental data is not shown in the figures to ease comparison with the calculated values. REBUS profiles are in very good agreement with the experimental profiles whereas the MCNP profiles fluctuate because of poor statistics.

The experimental and MCNP axial power profiles are compared for the ^{235}U and ^{237}Np fission chambers in Figure 45. The ^{235}U fission profile calculated with MCNP overestimates the experimental profile by approximately 10 to 20% at ±30 cm from the core mid-plane. The increases are due to the Plexiglas spacers in the pins. The increase in fission rate occurs slightly closer (less than 1 cm) to the core mid-plane for the MCNP ^{235}U fission profile. This may be due to uncertainty in the exact location and composition of the Plexiglas spacers in the UO_2-PuO_2 pins. The region of interest [-20 cm, 20 cm] is shown in Figure 46. The MCNP profiles are not well converged and the effect of the Styrene spacers is readily observed in the experimental ^{235}U fission profile at around ±14 cm from the core mid-plane.

The evolution of the buckling as a function of the fitting range has also been investigated [7]. The range [-18 cm, 18 cm] is appropriate for all profile calculated with MCNP and REBUS. The final bucklings are reported in Table 30.

Table 30: Experimental and calculated axial buckling in the R1-MOX configuration						
Source	Experiment ($\times10^{-3}$ cm^{-2})	MCNP ($\times10^{-3}$ cm^{-2})	REBUS ($\times10^{-3}$ cm^{-2})	MCNP/Exp.	REBUS/Exp.	REBUS/MCNP
^{235}U	1.900 ± 0.010	1.830 ± 0.052	-	0.963 ± 0.028	-	-
^{237}Np	1.885 ± 0.012	1.778 ± 0.024	-	0.943 ± 0.014	-	-
MOX1	1.840 ± 0.009	1.753 ± 0.050	1.875	0.953 ± 0.027	1.019	1.069
MOX3	1.863 ± 0.009	1.836 ± 0.050	1.865	0.985 ± 0.027	1.001	1.016

The experimental bucklings agree within two standard deviations. The uncertainties on the bucklings from MCNP are 2 to 5 times larger than the experimental uncertainties. The bucklings from MCNP are in agreement within one standard deviation. The MCNP and experimental bucklings agree within two standard deviations (4 to 5%) for the pins MOX1 and MOX3 and for the ^{235}U fission chamber measurement. The bucklings from REBUS is well predicted (0.1%) for the MOX3 pin but not for the MOX1 pin (2%).

The use of MCNP to determine the axial buckling is strongly limited by the poor statistics on the power profile even for a huge number of particles (300 million). An experimental buckling is also hard to be derived for pin MOX1 and the ^{235}U fission chamber because of the influence of the Styrene spacers.
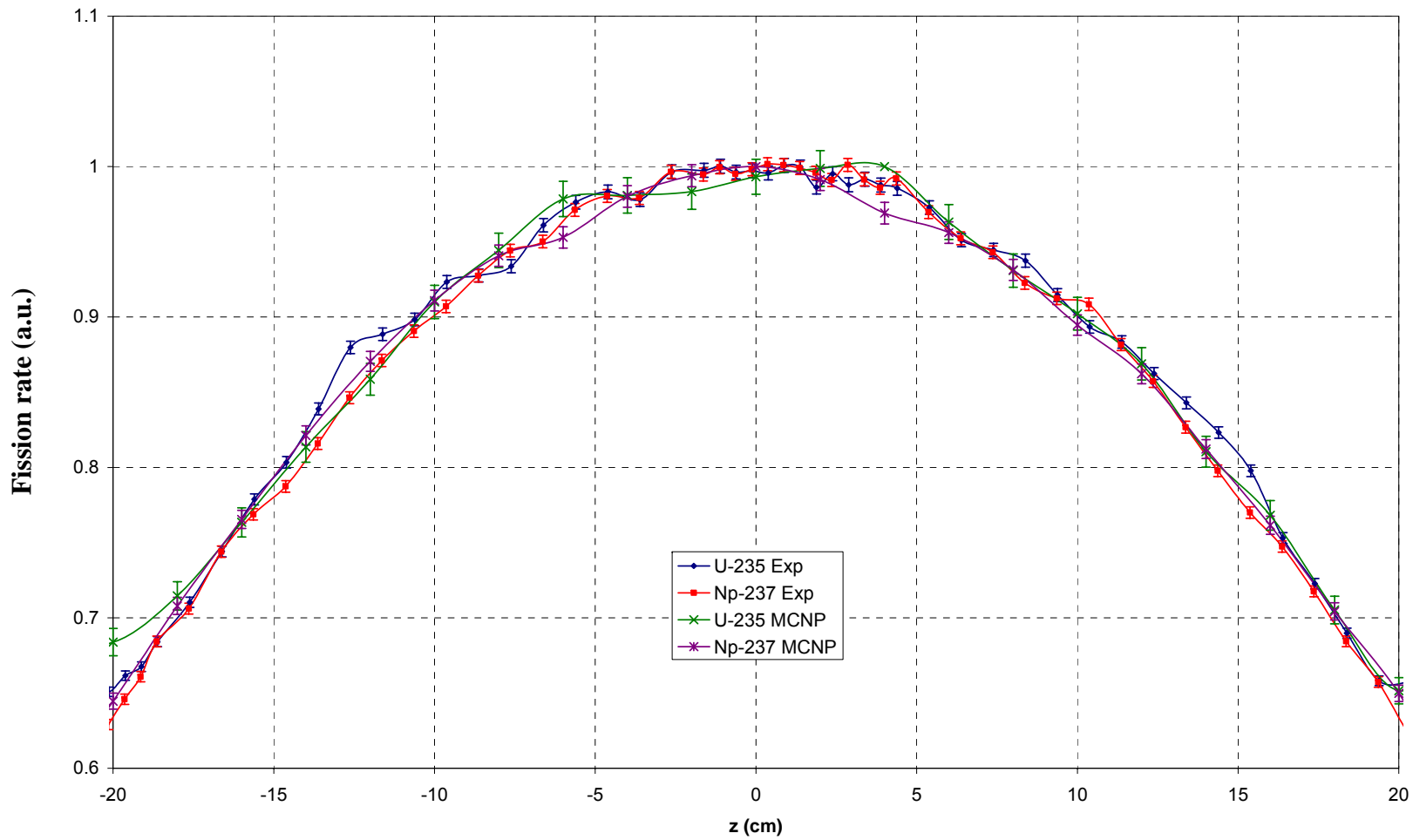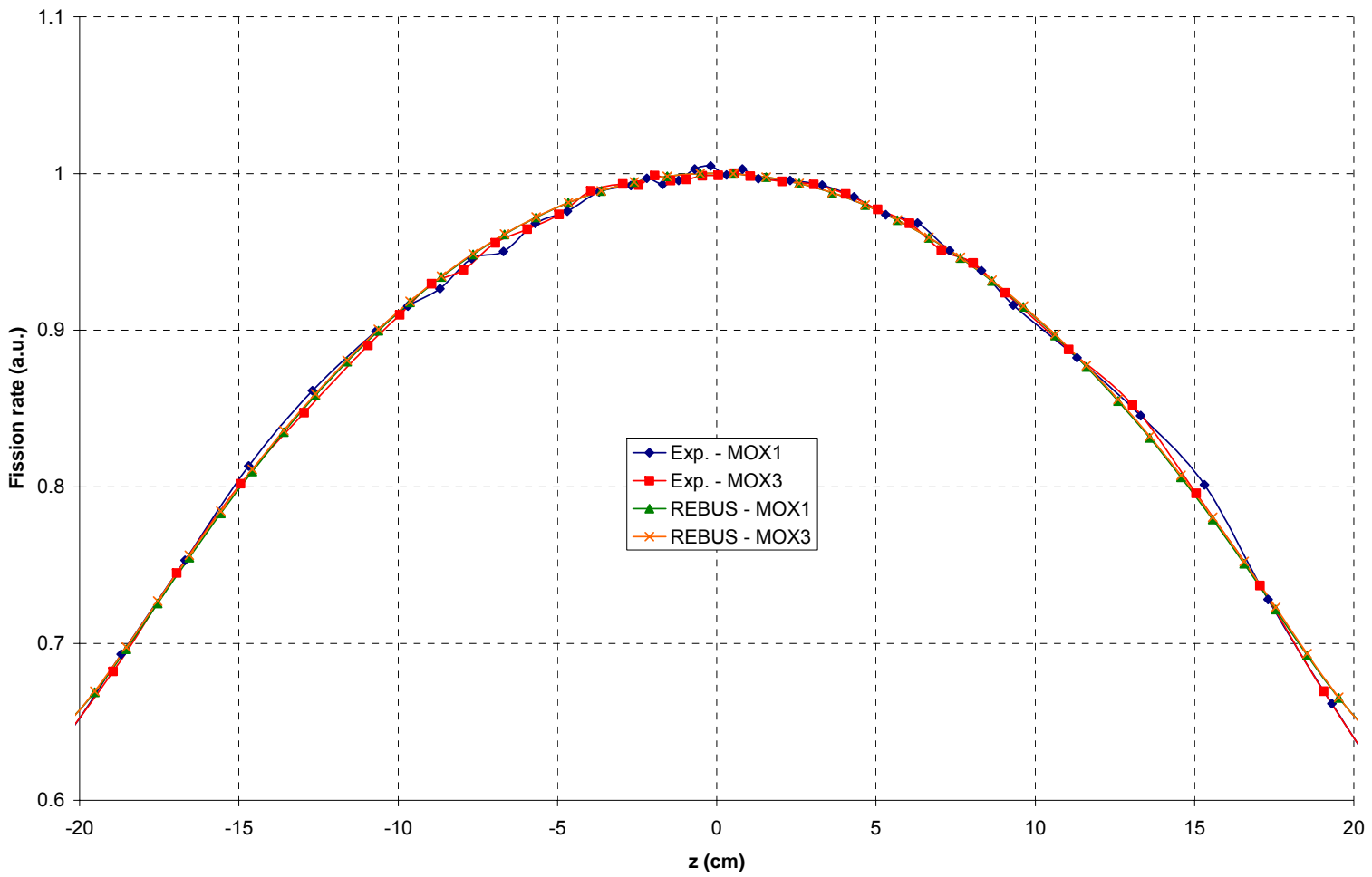
Figure 43: Axial power profile for specific pins in the R1-MOX configuration – Comparison of REBUS results to measurements
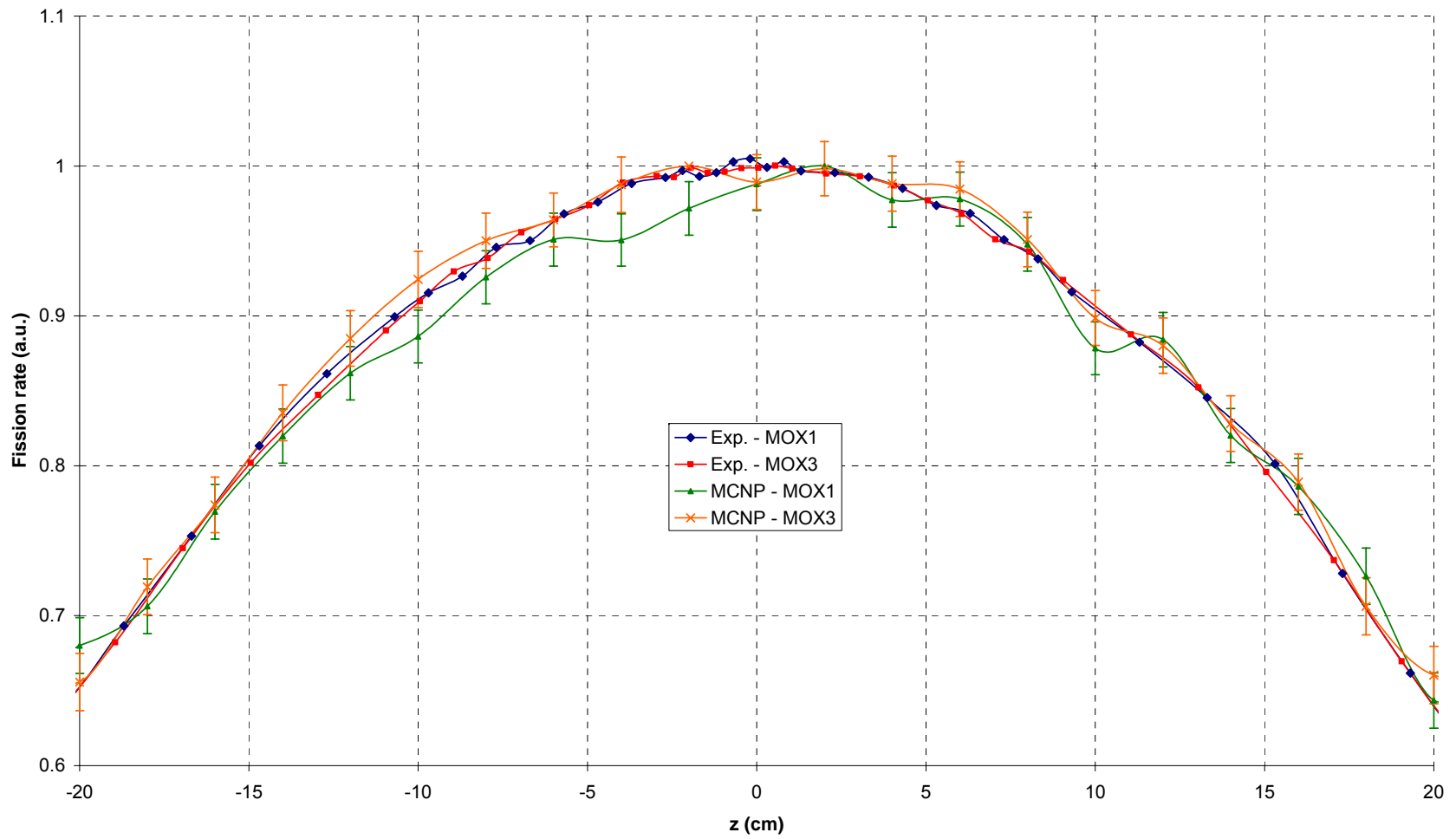
Figure 44: Axial power profile for specific pins in the R1-MOX configuration – Comparison of MCNP results to measurements
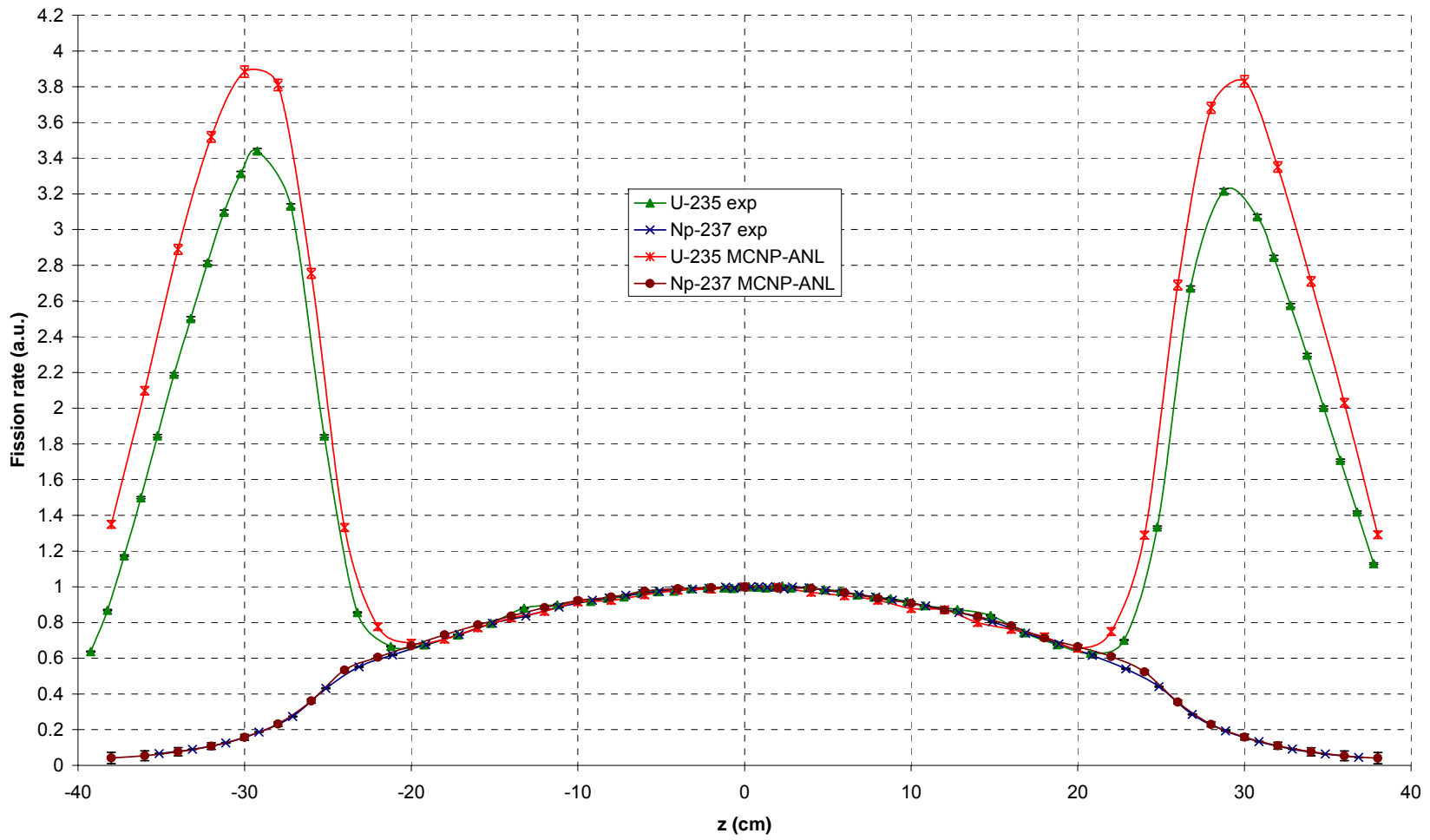
Figure 45: Axial fission rate profile of ^{235}U and ^{237}Np fission chambers in the R1-MOX configuration – Comparison of MCNP results to measurements
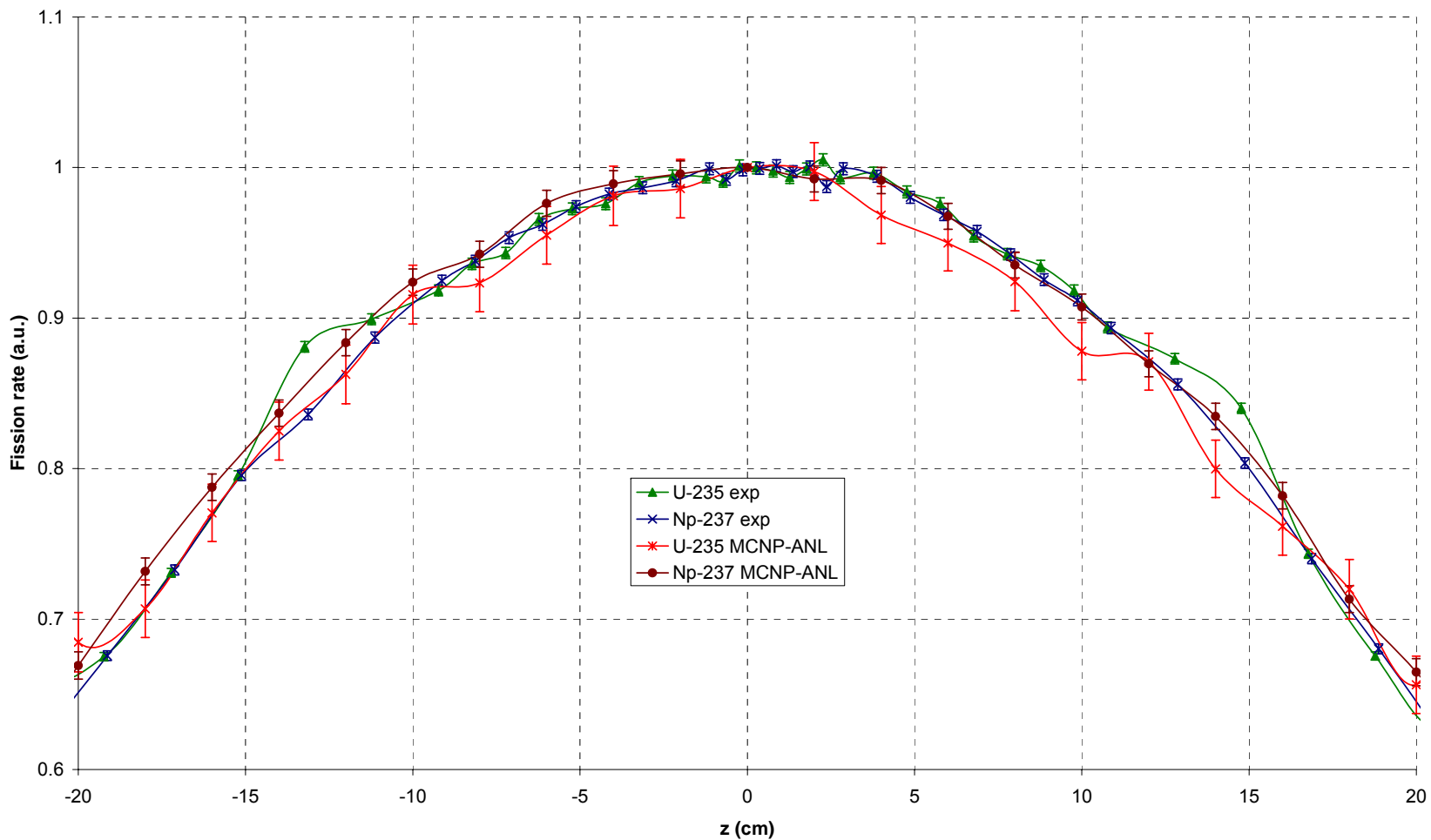
Figure 46: Axial fission rate profile of ^{235}U and ^{237}Np fission chambers in the R1-MOX configuration – Comparison of MCNP results to measurements over range of ±20 cm

5.4 Radial power profile

The radial power profiles have been determined experimentally on a horizontal and a diagonal traverse in the R1-MOX configuration (see section 4.3.3).

The horizontal and diagonal radial power profiles have been calculated in both configurations by MCNP and REBUS. The MCNP fission rates are calculated using the track length estimate of the cell flux tally [6] on the fuel meat of the studied pins. The REBUS fission rates were calculated on regions accounting for individual pins $(1.26 \times 1.26 \text{ cm}^2)$ composed of homogenized materials.

5.4.1 The R1-UO2 configuration

The horizontal and the diagonal radial power profiles are compared for the MCNP and REBUS models in Figure 47 and Figure 48. The power profiles are normalized to the total power of the traverse. In both cases, there is a slight disagreement between REBUS and MCNP. Further investigation is underway to determine the source of the difference. The absence of specific self-shielding for the UO_2 pins close to the AG-3 buffer in the REBUS model might be a source of error.

5.4.2 The R1-MOX configuration

The measured horizontal power profile is compared to the calculated values from REBUS and MCNP in Figure 49. The power of each pin is normalized to the total power of the traverse. The pin numbers are centered on the oscillation channel (pin 0). The interface between the UO_2-PuO_2 (4%) and UO_2 pins is observed for pins [-6, -7, 6, 7]. The pins [-15, 15] are adjacent to AG-3 pins.

The MCNP power profile matches the experimental values on the North side of the traverse, especially the interface between UO_2-PuO_2 (4%) and UO_2 pins. On the South side, the change of power between the adjacent UO_2 and UO_2-PuO_2 pins predicted by MCNP is 50% higher than the change of power obtained experimentally. The power of the UO_2-PuO_2 (4%) pins is well predicted with MCNP and the power of the UO_2 pins agrees within nearly one standard deviation.

The power of the UO_2 pins calculated with REBUS underestimates the experimental power on both sides of the traverse. On the contrary, the power of the UO_2-PuO_2 (4%) pins calculated with REBUS, overestimates the experimental values. The power at the interface between the UO_2-PuO_2 (4%) and UO_2 pins is similar to the MCNP values.

The REBUS model uses slightly different cross sections for pins # 1, 5, 6 and 15 to account for self-shielding due to an adjacent buffer region [7]. The change of cross sections has improved the agreement between the experimental and calculated power of the pins next to the POLINE overclad (cell # 0) but no significant change is seen for the power of the pins next to the Aluminum buffer [7].

To improve the REBUS power profile, the cross sections of the UO_2-PuO_2 (4%) and the UO_2 pins might have to be self-shielded by taking into account more than the 8 adjacent pins.

The South East – North West traverse calculated with MCNP and REBUS is compared with the experimental value in Figure 50. The MCNP model well predicts the fission rates in the UO_2 pins and the change of fission rate at the interface between the UO_2 and UO_2-PuO_2 fuel pins (nearly within one standard deviation). The fission rates of the UO_2-PuO_2 fuel pins calculated with MCNP agree with the experimental values within two standard deviations. The REBUS model has similar problems to estimate the fission rate of the pins in the South-North traverse and the South East – North West traverse. The REBUS model underestimates the power of the pins near the aluminum buffer and tends to overestimate the UO_2-PuO_2 (4%) power on the South East side of the traverse.
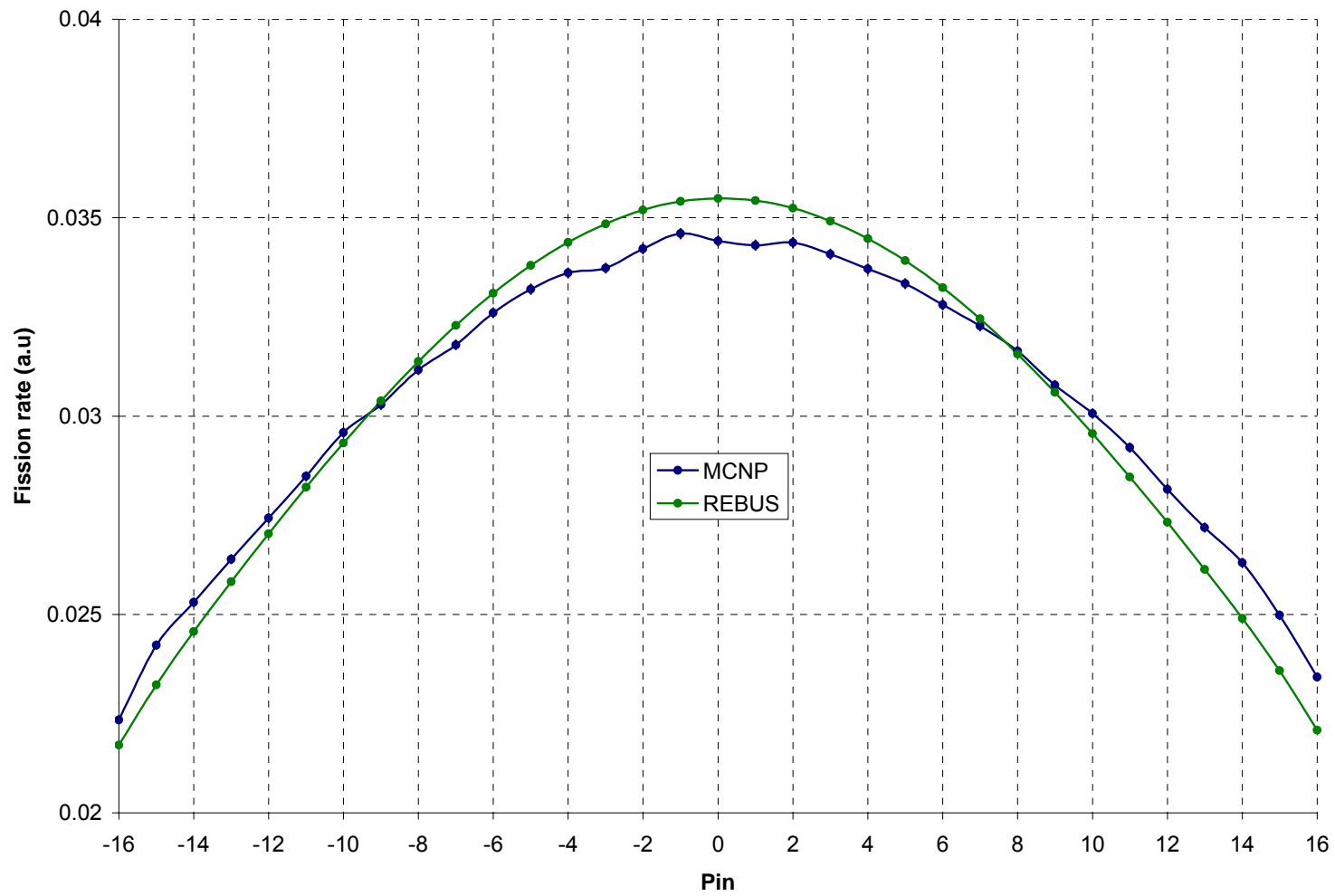
Figure 47: Fission rate distribution in the R1-UO2 configuration for the S-N traverse
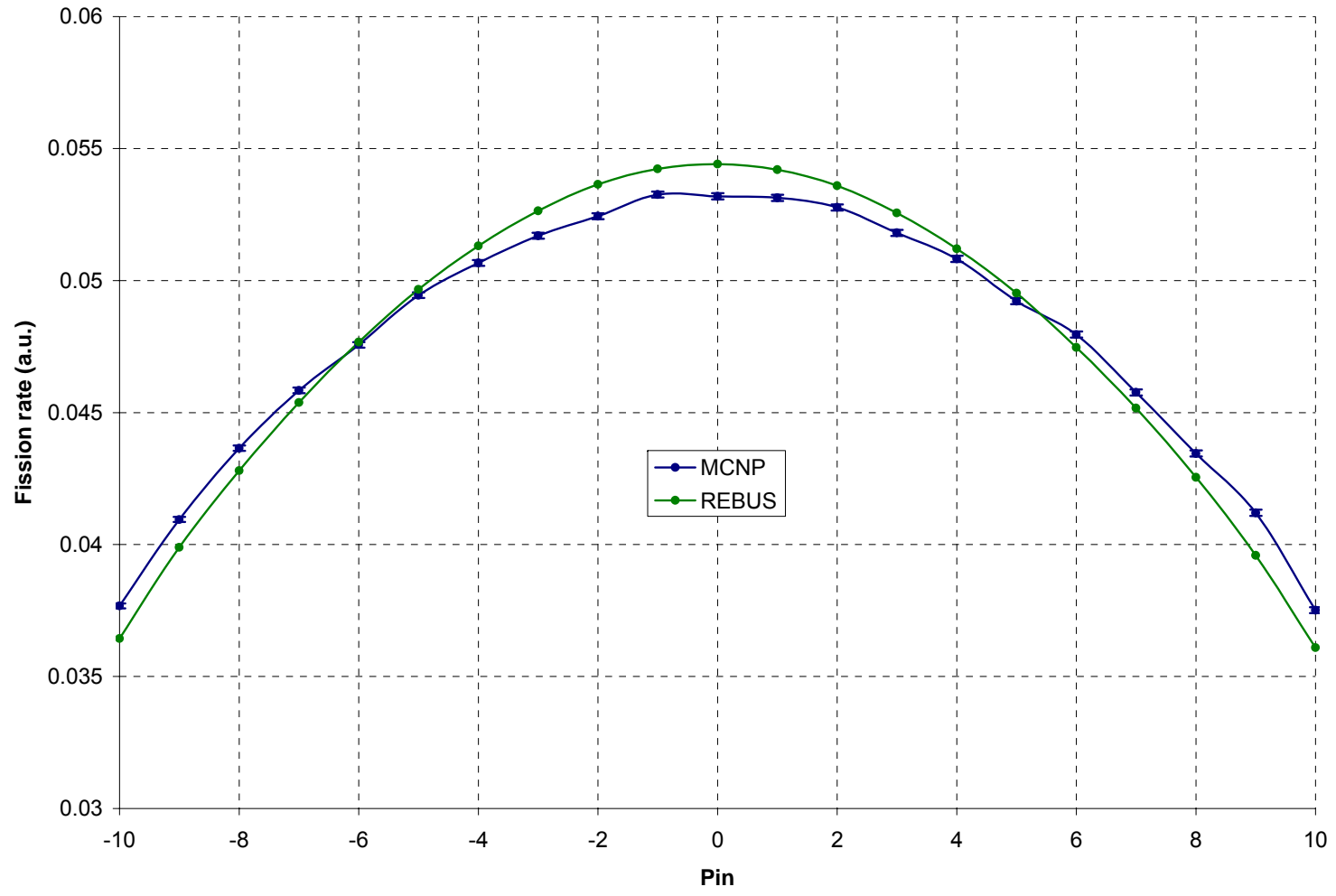
Figure 48: Fission rate distribution in the R1-UO2 configuration for the SE-NW traverse

Figure 49: Fission rate distribution in the R1-MOX configuration for the S-N traverse

Figure 50: Fission rate distribution in the R1-MOX configuration for the SE-NW traverse

5.5 Modified conversion ratio

The modified conversion ratio is defined as the ratio of neutron capture in ^{238}U to the total fission rate. The conversion ratios of the pins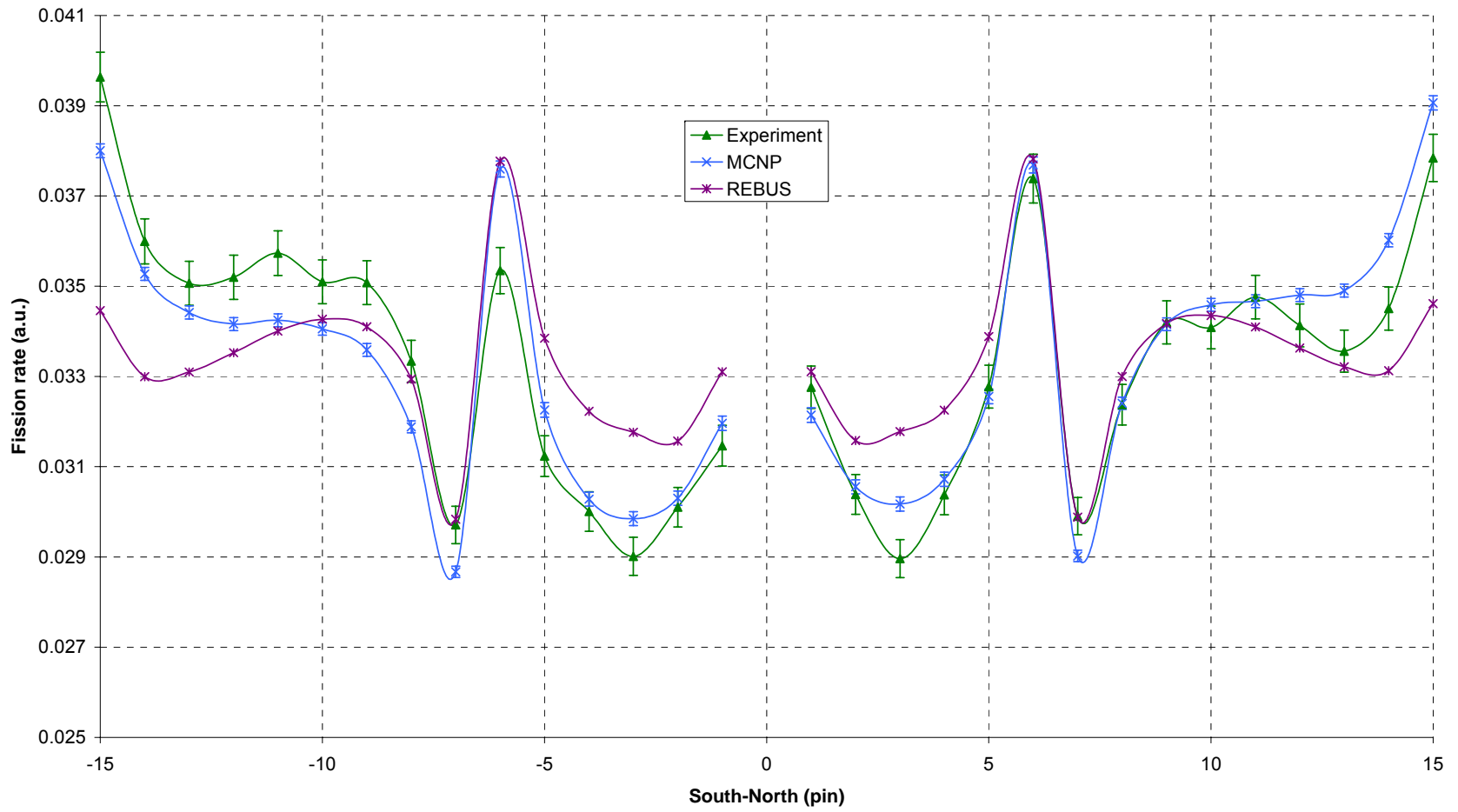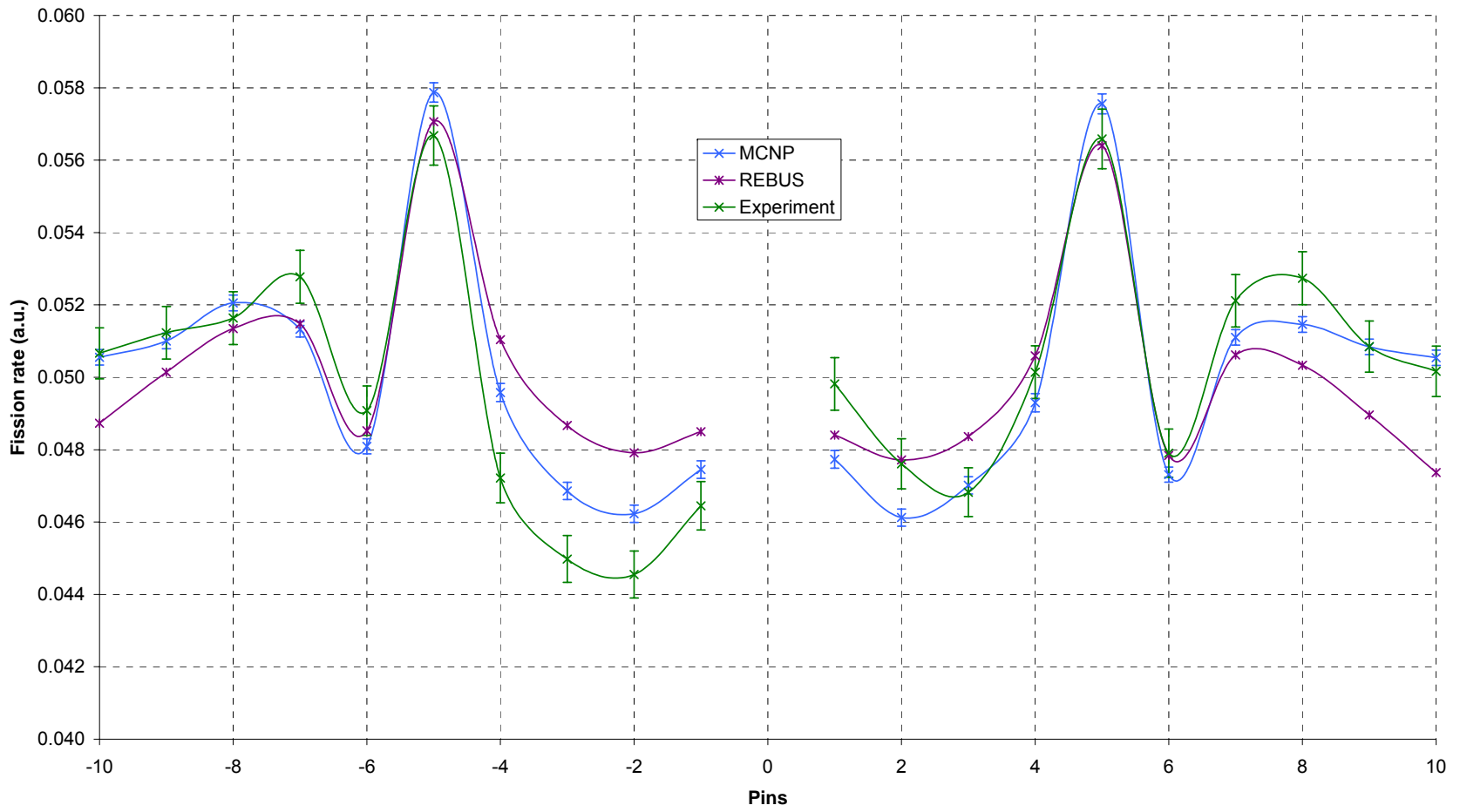 UOX7 and UOX10 have been measured in the R1-MOX configuration (see section 4.2.2). The two conversion ratios have been calculated with MCNP and are compared with the experimental values in Table 31. The measured and calculated conversion ratios agree within one standard deviation for the pin UOX7 and within two standard deviations for the pin UOX10. The overestimation of the calculated conversion ratio for the pin UOX10 implies an overestimation of the ^{238}U capture because the total fission rate is in good agreement with the experimental value as shown in Figure 49 for pin #10.

Table 31: Modified conversion ratio in the R1-MOX configuration			
Pin	Experiment	MCNP	MCNP/Exp.
UOX7	0.583 ± 0.012	0.592 ± 0.009	1.016 ± 0.026
UOX10	0.502 ± 0.010	0.527 ± 0.008	1.050 ± 0.026

5.6 Calibration sample reactivity worth

Experimentally, the oscillation of two calibration samples induces a change in position of the pilot rod to sustain criticality. The mean change of the pilot rod, noted $\Delta\theta$, is expressed in an arbitrary unit (pilot units) and is proportional to the change in reactivity of the core. The value $\Delta\theta$ is characteristic of the studied calibration samples and the reference sample used. The reference sample is the borated sample #8 (Table 8). The values $\Delta\theta$ and their uncertainties are listed in Table 9 and Table 10 for the R1-UO2 and R1-MOX configurations, respectively.

In the REBUS model, a multiplication factor is calculated when each calibration sample is inserted in the core (the other sample not being modeled). A reactivity value ρ is deduced for each calibration sample. The variation of reactivity $\Delta\rho$ between the calibrated sample and the reference sample (sample #8) is then derived. The relation $\Delta\theta = f(\Delta\rho)$ should be linear and the slope should only be dependant on the configuration. The measured pilot rod angle variation $\Delta\theta$ and the calculated reactivity variation $\Delta\rho$ are listed in Table 32 for the UO$_2$ calibration samples oscillated in the R1-UO2 configuration. The linear fit of the points $(\Delta\rho,\Delta\theta)$ is shown in Figure 51 and the results of the fit, that is the slope $\Delta\theta/\Delta\rho$ and the χ^2 are listed in Table 32.

Table 32: UO$_2$ calibration sample in the R1-UO2 configuration								
Sample	H1	H2	H3	H4	H5	H6	H7	H8
^{235}U enrichment (%)	0.25	0.49	0.71	1.00	2.01	3.01	4.00	4.93
Measured $\Delta\theta$ (pilot unit)	11528	42000	73467	104953	219321	313875	403243	475926
Calculated $\Delta\rho$ (pcm)	1.315	1.945	2.479	3.195	5.434	7.421	9.178	10.71
Linear fit	$\Delta\theta/\Delta\rho = 49491 \pm 234$ pilot unit / pcm $\quad \chi^2 = 1.0$							

The measured pilot rod angle variation, the calculated reactivity and the results of the linear fit for the borated oscillation sample oscillated in the R1-UO2 configuration are listed in Table 33 and shown in Figure 51.

Table 33: Borated UO$_2$ calibration sample in the R1-UO2 configuration					
Sample	#7	#9	#10	#32	#33
Boron fraction (ppm)	0	150	419	0	333
^{235}U enrichment (%)	0.25	0.25	0.25	0.53	0.53
Measured $\Delta\theta$ (pilot unit)	22299	-124638	-428772	34973	-316500
Calculated $\Delta\rho$ (pcm)	1.411	-1.524	-6.355	2.085	-4.424
Linear fit	$\Delta\theta/\Delta\rho = 55535 \pm 322$ pilot unit / pcm $\quad \chi^2=30.3$				

For the R1-UO2 configuration, the value of the χ^2 confirm the linear trend of $\Delta\theta = f(\Delta\rho)$ for the UO$_2$ calibration samples. The relation $\Delta\theta = f(\Delta\rho)$ obtained with the borated calibration samples is clearly not linear ($\chi^2 = 30.3 \gg 1$) and the slope $\Delta\theta/\Delta\rho$ does not agree with that of the UO$_2$ calibration sample.

The same study is performed for the R1-MOX configuration and the results are listed in Table 34 and Table 35 for the UO$_2$ and borated calibration samples. The linear fits are shown in Figure 52.

Table 34: UO$_2$ calibration sample in the R1-MOX configuration								
Sample	H1	H2	H3	H4	H5	H6	H7	H8
^{235}U enrichment (%)	0.25	0.49	0.71	1.00	2.01	3.01	4.00	4.93
Measured $\Delta\theta$ (pilot unit)	-11907	-5157	-67	6856	36727	61321	85974	104687
Calculated $\Delta\rho$ (pcm)	0.3857	0.5760	0.7402	0.9591	1.656	2.273	2.833	3.327
Linear fit	$\Delta\theta/\Delta\rho = 40379 \pm 151$ pilot unit / pcm $\quad \chi^2=0.6$							

Table 35: Borated UO$_2$ calibration sample in the R1-MOX configuration							
Sample	#7	#9	#10	#32	#33	#34	#35
Boron fraction (ppm)	0	150	419	0	333	1062	2360
^{235}U enrichment (%)	0.25	0.25	0.25	0.53	0.53	0.53	0.53
Measured $\Delta\theta$ (pilot unit)	-10964	-41613	-104193	-7551	-72967	-216175	-389847
Calculated $\Delta\rho$ (pcm)	0.4172	-0.4523	-1.898	0.6317	-1.311	-4.883	-9.628
Linear fit	$\Delta\theta/\Delta\rho = 37650 \pm 189$ pilot unit / pcm $\quad \chi^2=2.8$						

For the R1-MOX configuration, the same conclusion as for the R1-UO2 configuration can be drawn for the UO$_2$ and borated calibration samples.

The bad agreement between the experimental signal issued from the oscillations of the borated calibration samples and their calculated reactivity is thought to come from uncertainties in the composition of the borated samples and a possible migration of the boron to the periphery of the sample during the sintering of the fabrication process inducing self shielding effects. New borated calibration samples with a well known composition are under fabrication and will allow the confirmation of these conclusions.

The UO$_2$ calibration samples have been recently fabricated and the uncertainty on their compositions is well known [18]. As expected, the linear trend is excellent for the R1-UO2 and R1-MOX configurations.

Because the predictions of the reactivity worth of the UO$_2$ calibration samples are well behaved compared to the experimental measurements, the REBUS model can be used to calculate the reactivity worth of the OSMOSE samples with a high degree of confidence for the R1-UO2 and R1-MOX configurations. If a difference is observed between measurements and calculations for an OSMOSE sample, it will most likely be the result of an error in the isotopic cross section.

UO$_2$ calibration sample

Borated calibration sample
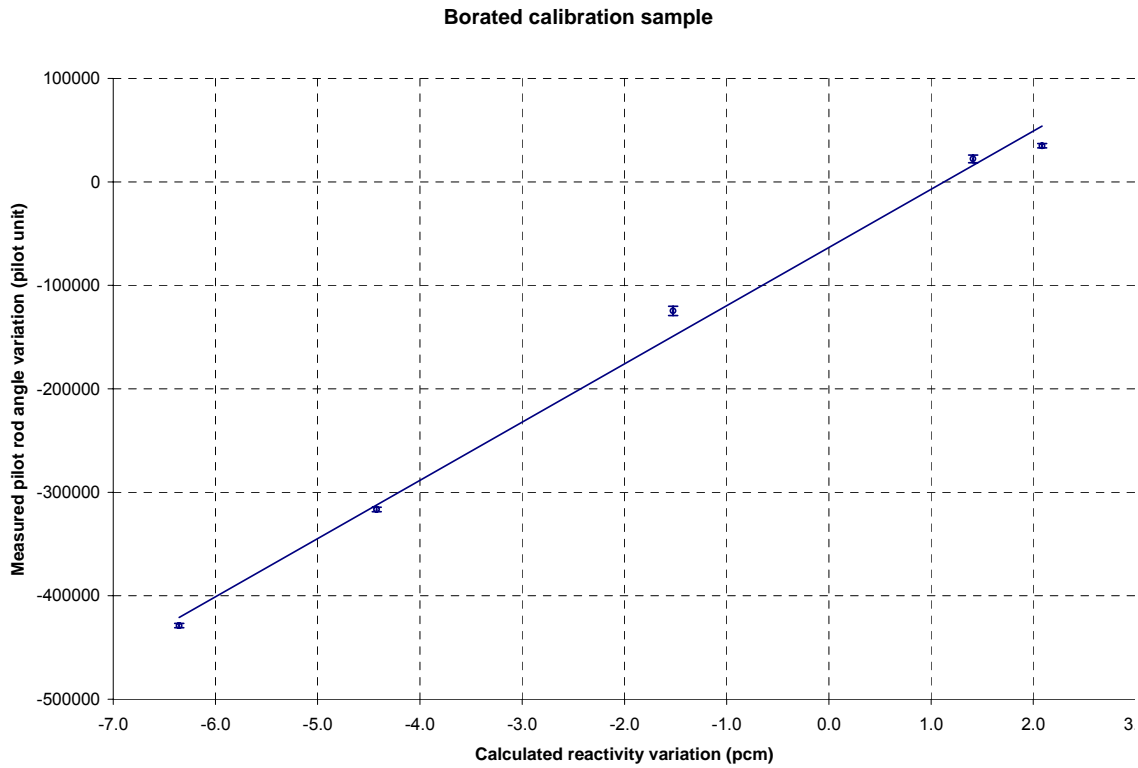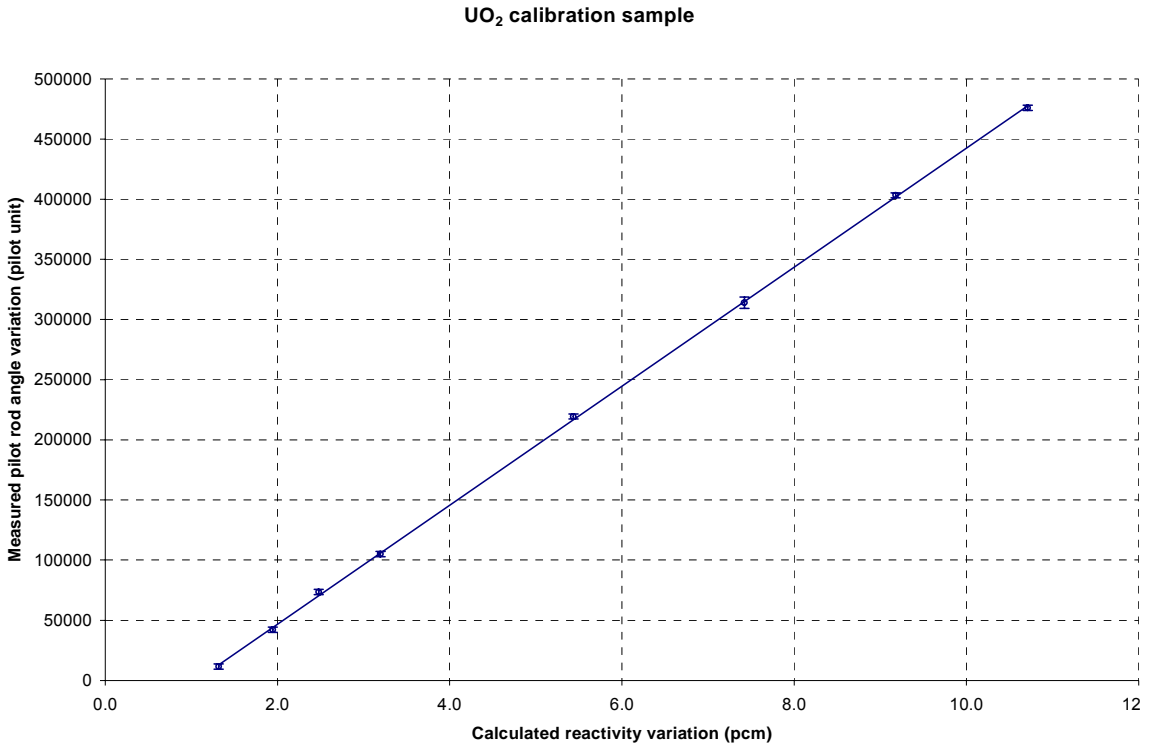
Figure 51: Experimental and calculated reactivity worth of the calibration samples in the R1-UO2 configuration

UO₂ calibration sample
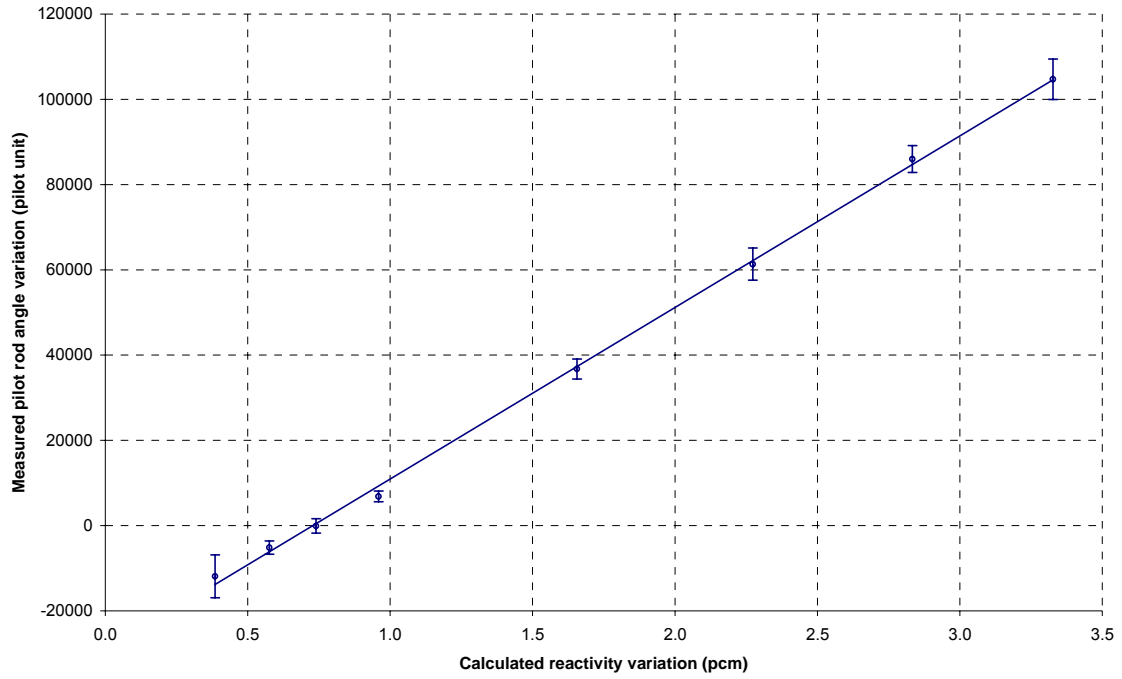
Borated calibration sample

Figure 52: Experimental and calculated reactivity worth of the calibration samples in the R1-MOX configuration

6 STUDENT ACTIVITIES

In addition to the critical objectives of the project, one of the primary objectives was to involve as many young scientists and students in all aspects of the experimental and analytical program. By introducing young experimentalists to the project through key involvement in tasks, expertise is developed within the United States and France. This is vital since there are very few remaining experimentalists in this area.

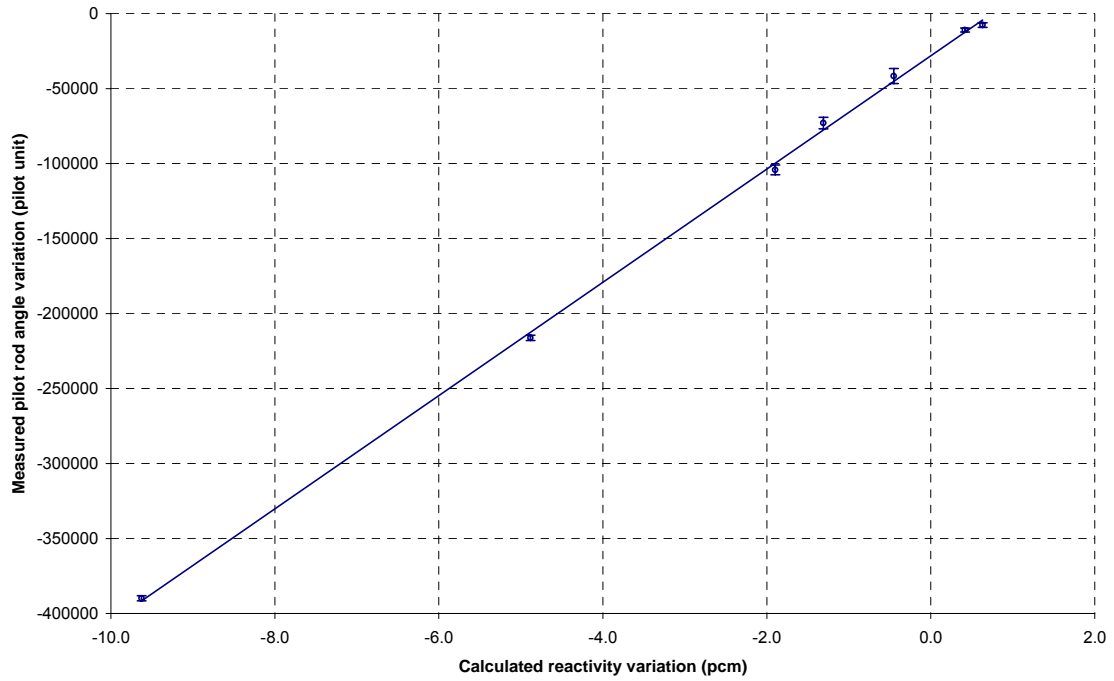In the United States, student involvement was accomplished by collaborating with Dr. John Lee at the University of Michigan. Involvement from the University of Michigan during the three-year project period supported four different areas: (a) survey of the capabilities of university research reactors (URRs) in the United States for performing reactivity sample oscillation tests as part of the OSMOSE project, (b) testing of fast Fourier transform (FFT) techniques for the determination of the sample worths through power oscillation tests, (c) simulation of the MINERVE reactor core with the MCNP code, and (d) use of deterministic reactor physics codes for the simulation of the MINERVE reactor. Two graduate students, Gregory O'Donnell and Yan Cao, and one undergraduate student, Keith Drudy, worked on various phases of the project.

A report of the student activities at the University of Michigan during the three-year period is included as Attachment 1 to this report.

In France, Pierre Leconte, a PhD student, has been involved in the OMOSE project. Pierre has participated in the gamma spectroscopy measurements and analyzed the experimental data for the radial power profile in the R1-MOX configuration and for the modified conversion ratio in the R1-UO2 configuration. He worked on the assessment and propagation of uncertainties, the gamma self-shielding factor calculated with MCNP, the effective fission yields, the influence of nuclear data and the equations to obtain the uncertainties, the renewal of the electronics of the gamma spectroscopy devices and the reduction of the uncertainty due to dead time losses, and the treatment of photopeaks.

7 CONCLUSIONS

The need for better nuclear data has been stressed by various organizations throughout the world, and results of studies have been published which demonstrate that current data are inadequate for designing the projects under consideration [1] [2]. In particular, a Working Party of the OECD has been concerned with identifying these needs [3] and has produced a detailed High Priority Request List for Nuclear Data.

The French Atomic Energy Commissariat (CEA) has also recognized the need for better data and launched an ambitious program aimed at measuring the integral absorption rate parameters at the CEA-Cadarache Research Center. A complete analytical program is associated with the experimental program and aims at understanding and resolving potential discrepancies between calculated and measured values. The final objective of the program is to reduce the uncertainties in predictive capabilities to a level acceptable to core designers and government regulators.

Argonne National Laboratory has expertise in these areas. In the past, ANL teams have developed very accurate experimental techniques and strongly enhanced the development of several French experimental and analytical programs, and have contributed to the computational tools used at CEA-Cadarache.

CEA recognized the expertise that ANL has in these areas and was interested in collaborating with ANL in the experimental design, measurements, and analysis tasks of the OSMOSE program. The development and execution of the first phase of the OSMOSE program within the DOE I-NERI Program was a resounding success. Both parties saw improved performance in the conduct of the program because of the contribution from both parties.

The collaboration included several key aspects:
1. DOE supplied specific minor actinide isotopes to CEA that were not easily obtainable in France,
2. ANL staff participated and supported the experimental program,
3. ANL and CEA personnel performed analysis for the characterization of the reactor using separate suites of reactor analysis codes,
4. comparisons of the analysis results and analytical techniques have enhanced the experimental program, and
5. all of the analytical and experimental data was available to the U.S. and France as part of this collaboration.

8 FUTURE ACTIVITIES AND CONTINUED COLLABORATION

The OSMOSE program aims at improving neutronic predictions of advanced nuclear fuels through measurements in the MINERVE facility on samples containing the following separated actinides : ^{232}Th, ^{233}U, ^{234}U, ^{235}U, ^{236}U, ^{238}U, ^{237}Np, ^{238}Pu, ^{239}Pu, ^{240}Pu, ^{241}Pu, ^{242}Pu, ^{241}Am, ^{243}Am, ^{244}Cm and ^{245}Cm.

During the period covered by the I-NERI program, samples were prepared, the reactor was upgraded and characterized, and calibration measurements were performed for two core configurations. The goal of the OSMOSE program can now begin to be realized by conducting measurements with the separated actinide samples. Measurements with the samples begin in 2005 and continue through 2012 for different neutron spectra.

The continuation of the DOE/CEA collaboration on the OSMOSE program includes the participation of DOE in the conduct of the experiments and the development and comparison of analytic tools and models of CEA and DOE based on Monte Carlo and deterministic methods. CEA continues to support and fund the experimental and analytical programs at the CEA Cadarache Research Center. The U.S. involvement in the program is being supported in 2005 as part of the ANL-Model Improvement work package within the Generation-IV program. The project is also continuing as a CEA/DOE collaboration within the guidelines of the new I-NERI program.

The OSMOSE experimental program will produce very accurate sample worth measurements for a series of actinides in various spectra, from very thermalized to very fast. The objective of the analytical program is to make use of this experimental data to establish deficiencies in the basic nuclear data libraries, identify their origins, and propose paths towards correcting them, in coordination with international nuclear data programs.

A fundamental property of the oscillation experiments performed in the OSMOSE program is that the neutron flux at the sample location has reached the asymptotic fundamental mode of the MINERVE lattice (note that this is the replaceable central part of MINERVE, which establishes the spectrum at the sample location). This property allows for the use of simple spatial analysis methods (e.g. a lattice code with axial buckling representing the leakage) without loss of accuracy. The computational challenge is then reduced to the need for correct representation of cross-sections and for accurate resonance shielding algorithms. Modern codes (commercial lattice codes, Monte Carlo codes, etc.) have such high quality algorithms that cross-comparisons between codes will be used to eliminate potential algorithmic deficiencies. Thus the comparison of calculated to experimental values (C/E) will yield direct information on cross-section weaknesses.

Sensitivity calculations will be run using information from the measurements in several spectra, in order to pinpoint the origin of observed discrepancies and propose possible solutions. This work will be performed in collaboration with CEA Cadarache, the

European Nuclear Data Project JEFF, and the OECD Working Party on Evaluation Cooperation.

9   MILESTONES

The milestones identified for the first phase of the OSMOSE Program (within the INERI program) are shown in Table 36 along with the completion dates or current status level. Almost all of the tasks and deliverables were completed within the timeframe of the INERI program (FY02-FY04). Because of external constraints on the schedule of the MINERVE Reactor, some of the tasks were not completed by the planned completion dates. The delay of these tasks did not impact the schedule of the measurement program at the MINERVE facility as many of these delays were a result of priority scheduling conflicts.

A few of the sample fabrication tasks have not been completed as of the end of FY2004. These tasks include the isotope purification and qualification of the welding process. As identified in the report, the welding qualification is pending based on company availability. The isotope purification has not been completed on several of the samples as these samples require processing as close to fabrication as possible to limit the amount of contaminant isotopes in the samples from radioactive decay of the sample isotope. These delays have not impacted the schedule of the project, however, these items are now on the critical path for beginning sample measurements during the summer of 2005.

Table 36: OSMOSE Project Milestones		
Milestone/Task Description	Planned Completion Date	Actual Completion Date
Task 1: Reactor modifications		
Subtask 1.1: Completion of Reactor Modifications	1/31/03	1/10/03
Subtask 1.2: Characterization of new control and oscillator	2/15/03	2/1/03
Subtask 1.3: Calibration of the pilot rod	2/15/03	2/15/03
Subtask 1.4: Change of the control system of the pilot rod	12/31/04	3/31/04
Task 2: Reactor modelling		
Subtask 2.1: MCNP model of R1-UO2 configuration	2/28/03	2/28/03
Subtask 2.2: Deterministic model of R1-UO2 configuration	12/01/03	3/1/04
Subtask 2.3: Reactivity worth estimates for calibration samples in R1-UO2 configuration	2/01/04	3/31/04
Subtask 2.4: Spectral indices and power distribution estimates in R1-UO2 configuration	3/01/04	3/01/04
Subtask 2.5: Reactor models and reactivity-worth estimates for R1-MOX configuration	10/13/03	5/31/04
a. MCNP model		6/30/03
b. REBUS model		12/20/03
c. Reactivity-worth estimates of calibration samples		5/31/04
Subtask 2.6: Reactivity-worth estimates of OSMOSE samples in R1-UO2 and R1-MOX core configurations	4/30/05	
a. Estimates in R1-UO2 configuration		
b. Estimates in R1-MOX configuration		
Task 3 : Sample fabrication		
Subtask 3.1: OSMOSE oven qualification and tests	4/25/03	12/17/03
Subtask 3.2: Pellet fabrication for 5 samples	12/19/03	6/30/04
a. Nat UO2 pellets		6/30/03
b. Np237 pellets for 2 samples		6/30/04

Milestone/Task Description	Planned Completion Date	Actual Completion Date
Table 36: OSMOSE Project Milestones		
c. Th232 pellets for 2 samples		3/30/04
Subtask 3.3: Analysis of the fabricated pellets	12/31/04	10/31/04
Subtask 3.4: Isotope supply : purification and analytical control	12/19/03	75%
Subtask 3.5: Qualification of welding process	12/19/03	75%
Subtask 3.6: Pellet fabrication of 8 additional samples in 2004	12/18/04	
Task 4 : Experiments		
Subtask 4.1: Calibration measurements in R1-UO2 lattice	1/30/04	1/30/04
Subtask 4.2: Calibration measurements in R1-MOX lattice	11/11/03	11/11/03
Subtask 4.3: Oscillation measurements of VALMONT samples	2/28/04	2/28/04
Subtask 4.4: Spectral indices and flux measurements in R1-UO2	3/15/04	2/28/04
Subtask 4.5: Spectral indices and flux measurements in R1MOX	11/11/03	11/11/03
Task 5: Data Analysis		
Subtask 5.1: Data analysis of R1-UO2 and R1-MOX calibration measurements	1/31/04	5/31/04
a. R1-UO2 Calibration samples data treatment		3/15/04
b. R1-UO2 Calibration samples data interpretation		5/31/04
c. R1-MOX Calibration samples data treatment		5/31/04
d. R1-MOX Calibration samples data interpretation		5/31/04
Subtask 5.2: Analysis of R1UO2 spectral indices measurements	9/30/03	12/20/03

Acknowledgment

10 REFERENCES

[1]   M. Salvatores, Experimental Facilities, Training and Expertise in the Nuclear Data Field: Needs and Gaps for Reactor Physics Applications, Conference Proceedings, Vol. 59, Nuclear Data for Science and Technology, G. Reffo, A. Ventura and C. Grandi (eds.), SIF, Bologna, 1997.

[2]   G. Palmiotti, et al., Uncertainty Assessment for Accelerator Driven Systems, Proceedings of GLOBAL99, Jackson Hole, WY, September, 1999.

[3]   P. Finck, et al., Activities of the OECD NEANSC Working Party on International Evaluation Cooperation, Conference Proceedings, Vol. 59, Nuclear Data for Science and Technology, G. Reffo, A. Ventura and C. Grandi (eds.), SIF, Bologna, 1997.

[4]   JP. Chauvin, et al., "The MINERVE facility and the OSMOSE program", ANS- San Diego June 2000, USA.

[5]   G. Perret et al., Geometry and material specification of the MINERVE facility with the MELODIE IV experimental, ANL – 04/17, Dec. 2004.

[6]   J.F. Briesmeister, MCNP^{TM} – A General Monte Carlo N-Particle Transport Code (Version 4C), LA-13709-M.

[7]   G. Perret, et al., Modeling report of the CEA Cadarache MINERVE reactor for the OSMOSE project, ANL – 04/18, Dec. 2004.

[8]   A.P. Olson, A users guide for the REBUS-PC code, Version 1.4, ANL/RERTR/TM02-32, Dec. 2001.

[9]   J.R. Deen and L.Woodruff, WIMS-ANL user manual Rev.4, ANL/RERTR/TM-23, Jan. 2001.

[10]   JP. Hudelot, Experimental Techniques in Support to the OSMOSE I-NERI Project on the MINERVE Facility, Technical Report, CEA/DER/SPEx/LPE/04-125.

[11]   JP. Hudelot at al., OSMOSE: An Experimental Program for the Qualification of Integral Cross Sections of Actinides, Proceedings of the PHYSOR-2004 Topical Meeting, April 2004.

[12]   R.T. Klann et al., MINERVE Reactor Characterization in Support of the OSMOSE Program: Spectral Indices, Proceedings of the PHYSOR-2004 Topical Meeting, April, 2004.

[13] JP. Hudelot et al., Measurement of the modified conversion ratio of ^{238}U by gamma-ray spectrometry on an irradiated fuel pin, CGS11 Conference, 11th international symposium on capture gamma-ray spectroscopy, Prague, September 2002.

[14] JP Hudelot et al. , Mesures d'indices de spectre dans les configurations R1-UO2 et R1-MOX du réacteur MINERVE, Technical Report CEA/DEN/DER/SPEx/LPE/04-077.

[15] JP. Hudelot et al., Calibration des chambres à fission EOLE/MINERVE et MASURCA dans les spectres de référence du réacteur BR1 du CEN Mol, Technical Report CEA/DEN/DER/SPEx/LPE/02-037.

[16] JP. Hudelot, et al., MINERVE Reactor Characterization in Support of the OSMOSE Program: Safety Parameters, Proceedings of the PHYSOR-2004 Topical Meeting, April, 2004.

[17] M. Darrouzet et al., Mesures de distributions de puissance et d'effets en réactivité dans les configurations UO2 et UO2-PuO2 réalisées dans MINERVE, Rapport final CEA/EDF, Note B04, March, 1980.

[18] C. Döderlein, Bilan matière des échantillons de calibration des programmes OSMOSE et VALMONT, NT SPRC/LPN 03-1367, 2003.

Final Report for the OSMOSE Project
November 2001 – October 2004

John C. Lee
Department of Nuclear Engineering and Radiological Sciences
University of Michigan

October 31, 2004

Our effort during the three-year project period covered four different areas: (a) survey of the capabilities of university research reactors (URRs) in the United States for performing reactivity sample oscillation tests as part of the OSMOSE project, (b) testing of fast Fourier transform (FFT) techniques for the determination of the sample worths through power oscillation tests, (c) simulation of the MINERVE reactor core with the MCNP code, and (d) use of deterministic reactor physics codes for the simulation of the MINERVE reactor.   Two graduate students, Gregory O'Donnell and Yan Cao, and one undergraduate student, Keith Drudy, have worked on various phases of the project.   In this report, we present only highlights of our activities in the first three areas and concentrate on the recent effort in the fourth area simulating the MINVERVE reactor with the WIMS and DIF3D deterministic codes.

1. Highlights of Activities during the Period 2001-2003

1.1 Survey of URR capabilities for power oscillation tests

To assess the feasibility of performing power oscillation tests at URRs in the United States, contacts were made with reactor operations staff at nine key URRs and effort was made to collect key reactor parameters including the minimum reactor period allowed for routine operations. With the understanding that incore irradiation locations would render high flux levels and high reactivity worth for oscillating samples, we also solicited additional information, including the core layout, incore irradiation locations, and fuel burnup. We summarized in October 2002 the relevant data for five URRs with a rated power of 1.0 MW or higher and noted that the proposed power oscillation tests could be performed at anyone of the five URRs, although no reactor is currently equipped to perform such tests.

1.2 Testing of FFT techniques for analysis of power oscillation test data

In an effort to evaluate the adequacy of FFT techniques for the determination of reactivity worths of small samples from the power oscillation tests proposed for the OSMOSE project, we performed a numerical study using the point kinetics equations with six groups of delayed neutron precursors. In the first part of the study, using a noise-free sinusoidal sample reactivity input $K(t)$, we obtained time-domain solutions for power $n(t)$, which is transformed via FFT to yield the reactor transfer function $G(s)$. In the second part of our study, we considered noisy power signals and generated the sample reactivity transforms $K(s)$ for several oscillation frequencies that allow for a minimum reactor period $T \geq 10$ s for a sample worth $K_0 = \$0.01$. Our numerical study demonstrated that the use of standard FFT routines, at a sufficient sampling frequency and with a sufficient number of cycles sampled, provides accurate solutions for $G(s)$ in the first part and for K_0 in the second part of our study. A summary report was submitted in August 2003.

1.3 MCNP Simulation of the MINERVE Reactor

Effort was initiated in July 2003 to review and continue MCNP calculations performed both at CEA and ANL for the simulation of the MINERVE reactor core. The effort led to MCNP4C and MCNP5 simulations at the University of Michigan of both the R1-MOX and R1-UO2 configurations. Through consultations with ANL, several enhancements to the MCNP5 input decks have been made during the past year and a number of parametric studies have been performed in a continuing effort. One particular issue still under study is the MCNP overprediction of the fission rate peaks, observed in the ^{235}U detector signals, at the core-reflector interfaces in the R1-MOX configuration. The MCNP models have served as the basis for our effort to simulate the MINERVE core with the WIMS and DIF3D deterministic codes[1,2] summarized below.

2. Development of the WIMS-DIF3D Model for the MINERVE Reactor

In parallel with the MCNP modeling of the MINERVE core, effort was initiated in early 2004 to develop deterministic reactor physics models for the core with a plan to perform the prediction and simulation of reactivity worth measurements for the OSMOSE project. A paper[3] summarizing our combined WIMS-DIF3D results was submitted in July 2004 for presentation at the American Nuclear Society meeting. Subsequently, a number of improvements to the WIMS-DIF3D models have been made and additional calculations performed. The recent calculations will be included in our

November ANS presentation. We plan to continue our deterministic core modeling effort, concentrating on the sample reactivity worth calculations.

3. Description of the WIMS-DIF3D Modeling of the MINERVE Core

In our effort to simulate the rather complex configuration of the MINERVE core, we have concentrated on pin-cell models in Figure 1(a), described in our ANS summary,[3] to represent the central MOX and UO_2 regions, coupled with one-dimensional slab models in Figure 1(b) for the fuel plates of the driver region. Although our basic model employed pin-cell geometry, we have used varying compositions of buffer regions to represent the surrounding fuel and non-fuel materials. We have developed one super-cell model associated with a total of 34 buffer configurations for the fuel rods, and 10 one-dimensional slab models related to another super-cell model for the fuel plates, control rods and reflector materials to generate four-group macroscopic cross sections.
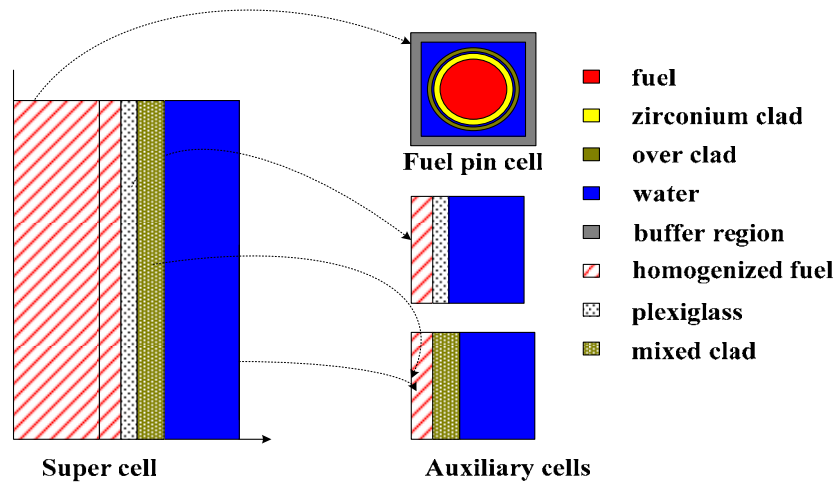
(a) Super-cell model for fuel rod
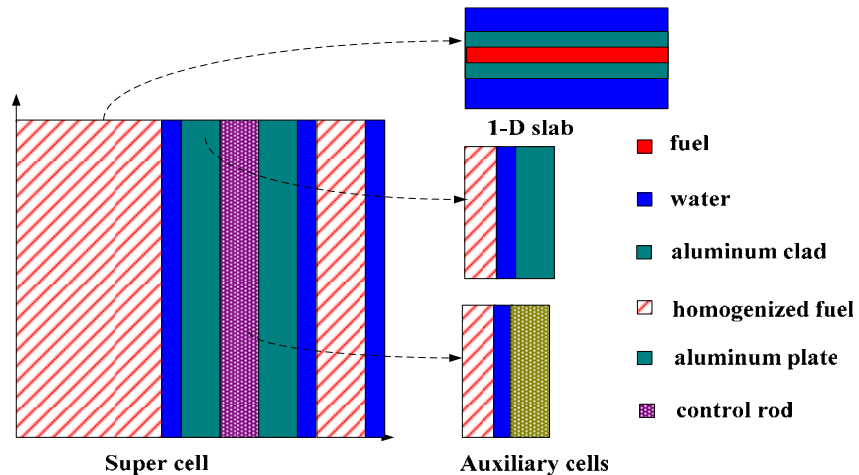
(b) Super-cell model for fuel plate

Figure 1. WIMS super-cell models for the MINERVE reactor.

As illustrated in a side view in Figure 2(a), the MINERVE core is modeled as a cube 1.1 m on a side, submerged under 0.4 m of water, with vacuum boundary conditions applied at the core boundary. We have used a total of 174 meshes in the x-direction, 176 meshes in the y-direction, and 218 meshes in the z-direction for four-group full-core calculations. Figure 2(a) also illustrates a stainless steel layer added to represent the cover plate above the experimental zone. In addition, compared with our earlier quarter-core model,[3] we have implemented a number of modifications in fuel configurations, including the composition and density of the fuel rods and fuel plates, reflecting the updated data of Ref. 4.


4. WIMS-DIF3D Calculations for Core Eigenvalue and Rod Worths

For our DIF3D full-core model with control rods withdrawn, we obtained effective multiplication factor k_{eff} = 0.997329, indicating a discrepancy of less than 0.5% $\Delta k/k$ from the measured value of 1.00143. Eigenvalue calculations with the 2004 version of the MCNP deck provided by G. Perret and the 2003 version from R. Klann, together with previous quarter-core calculation, are compared in Table I. The eigenvalue from our full-core DIF3D model was larger than the previous quarter-core result[3] as expected because of the modifications we made to the fuel configurations and the asymmetry of the driver zones not fully represented in the quarter-core model.


Table I. Effective Multiplication Factor Comparison

Experimental Data[5]	DIF3D-ANL[5]	DIF3D-UM		MCNP	
		Quarter[3]	Full	2003 version	2004 version
1.00143	0.99941	0.99312	0.99733	0.9947 ± 0.0003	1.0011 ± 0.0002

We have also performed integral control-rod worth calculations using the full-core model, and the results are compared with preliminary experiment data[6] in Table II, with an effective delayed neutron fraction β_{eff} = 0.0068. The DIF3D results are generally in agreement with the preliminary experimental data within one standard deviation of the experimental data, but with large deviations from the experimental data for control rod B1 located at the east driver zone.
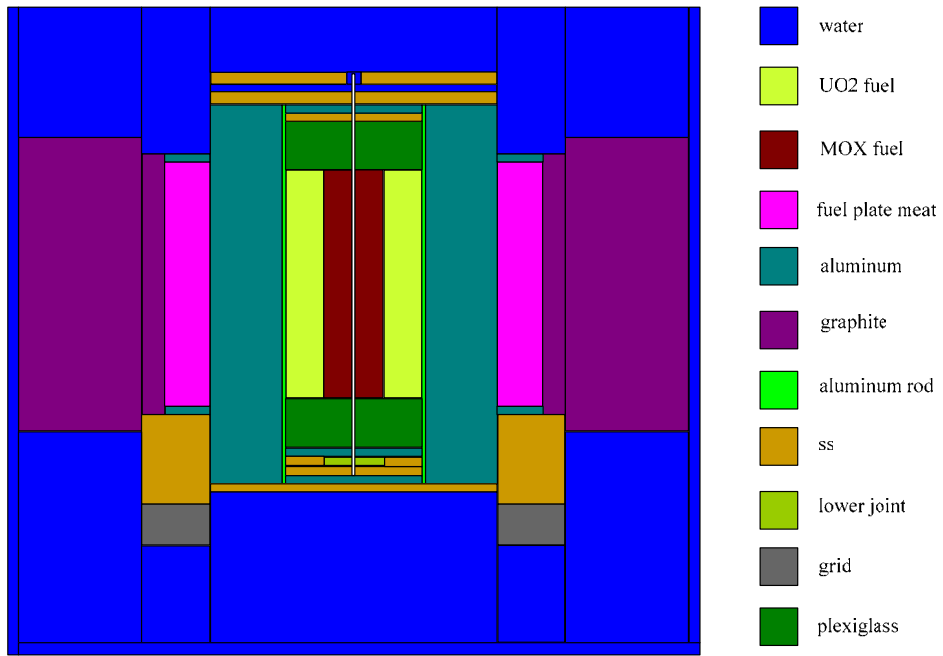
(a) Side view of the full core
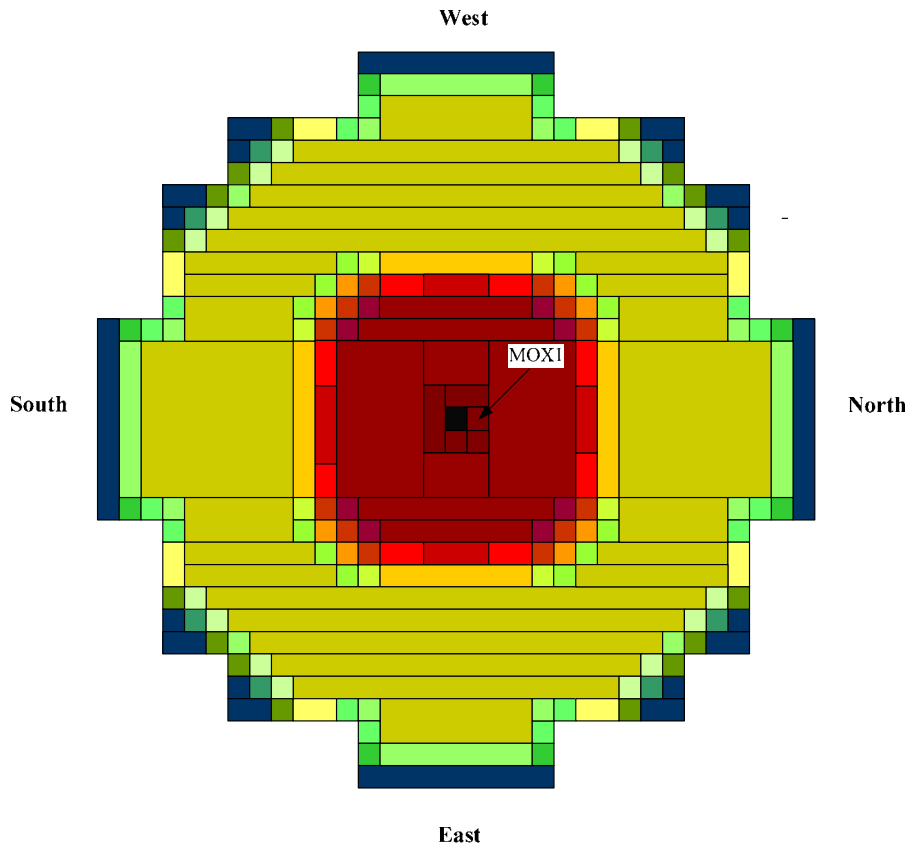
(b) Top view of the experimental zone

Figure 2. DIF3D full-core model for the MINERVE reactor.

Table II. Control Rod Worth Calculations (β_{eff} = 0.0068)

Control Rod		B1	B2	B3	B4
Experiment ($)		1.34 ± 0.103	1.51 ± 0.103	1.61 ± 0.103	1.26 ± 0.102
DIF3D	C/E	1.22	1.08	0.938	1.02
	σ(%)	7.7	6.8	6.4	8.1

5. Spectral Index Comparison

We performed DIF3D calculations for key spectral indices by modelling a small amount of fuel sample placed in the oscillation channel. Four-group macroscopic cross sections for isotopes ^{239}Pu, ^{235}U, ^{241}Pu and ^{237}Np were obtained through a WIMS super-cell model, with mass of 226.2 µg for ^{235}U , 162 µg for ^{239}Pu, 75.8 µg for ^{241}Pu and 368 µg for ^{237}Np distributed in a cylinder with a volume of 1.005 cm^3, centered at the midplane of the oscillation channel. The fission rate was then integrated over each sample volume to generate the total fission rate of the sample. A comparison between experimental data, MCNP simulations, and DIF3D calculations for fission spectral indices in the R1-MOX core is given in table III.

Table III. Fission Spectral Indices in the R1-MOX core

	^{239}Pu/^{235}U	^{241}Pu/^{239}Pu	^{237}Np/^{239}Pu
Experimental Data[5]	1.952 ± 0.049	1.123 ± 0.0303	0.00729 ± 0.00023
MCNP-ANL[5]	1.935 ± 0.050	1.142 ± 0.0281	0.00749 ± 0.00015
DIF3D-UM	2.161	1.056	0.00830

The MCNP results[5] are in good agreement with the experimental data, with discrepancies less than 3%.   In contrast, the DIF3D calculations show large discrepancies: up to 15% for the ^{237}Np/^{239}Pu index and 10% for the ^{239}Pu/^{235}U and ^{241}Pu/^{239}Pu indices. To improve the spectral index results, we will perform fine-group DIF3D calculations and develop alternate representations of the fuel samples. We will also use MCNP cross sections to benchmark the DIF3D results.

6. Calculations for Flux and Fission Rate Distributions

An axial profile of the thermal flux fraction of the total flux at the oscillation channel, plotted in Figure 3, agrees well with the profile obtained with the 2004 MCNP version, both in the central fuel region (–0.22 m ~ 0.22 m) and deep in the plexiglass region. However, at the upper interface of the plexiglass and fuel rods regions, the DIF3D model indicates a softer neutron spectrum than the MCNP simulation, similar to our previous quarter-core model.[3]
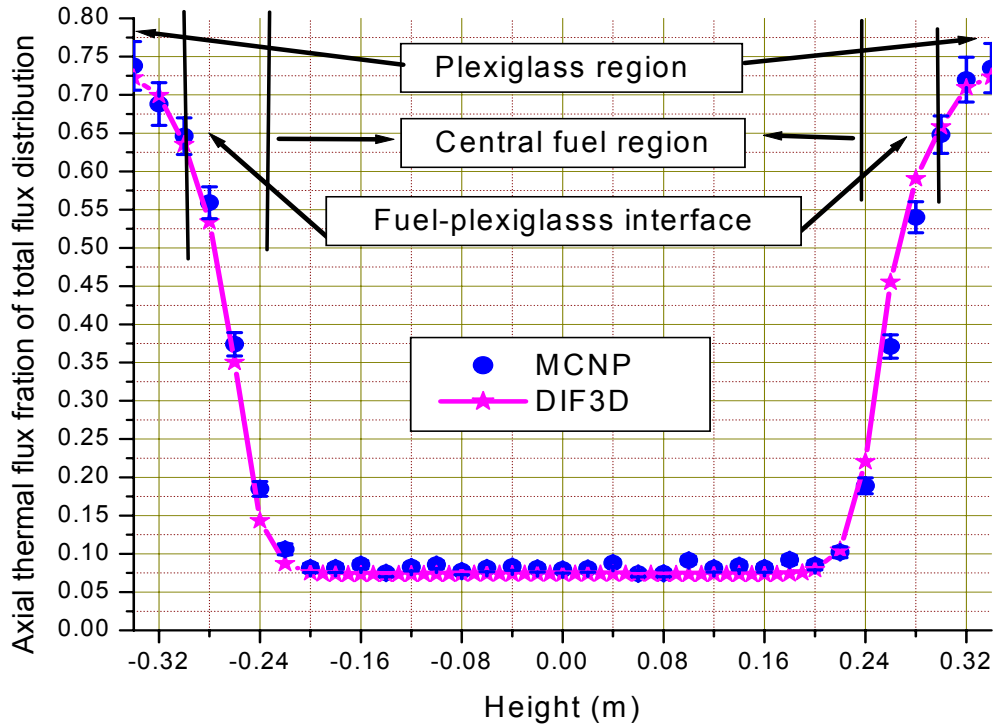

Figure 3. Axial profile of thermal flux fraction of total flux in the oscillation channel.

Furthermore, we obtained four-group microscopic cross sections for ^{235}U either by extracting flux-weighted cross sections from our WIMS super-cell model for the MOX fuel rod, or through MCNP fission rate tallies along the oscillation channel as we presented in the ANS summary.[3] We then combined the cross sections with DIF3D fluxes to calculate the fission rates for ^{235}U detector at different axial positions, which are compared with the experimental fission rate profile in Figure 4. Both the DIF3D and MCNP calculations show good agreement with the experimental data in the central fuel

region. However, there exist large discrepancies of about 15% for the MCNP simulation and of more than 20% for the DIF3D calculations at the fuel rod and plexiglass interface. In addition, both sets of DIF3D calculations yield nearly the same results, indicating that the disagreement between DIF3D and experiment data are primarily due to errors in the flux distribution calculations.
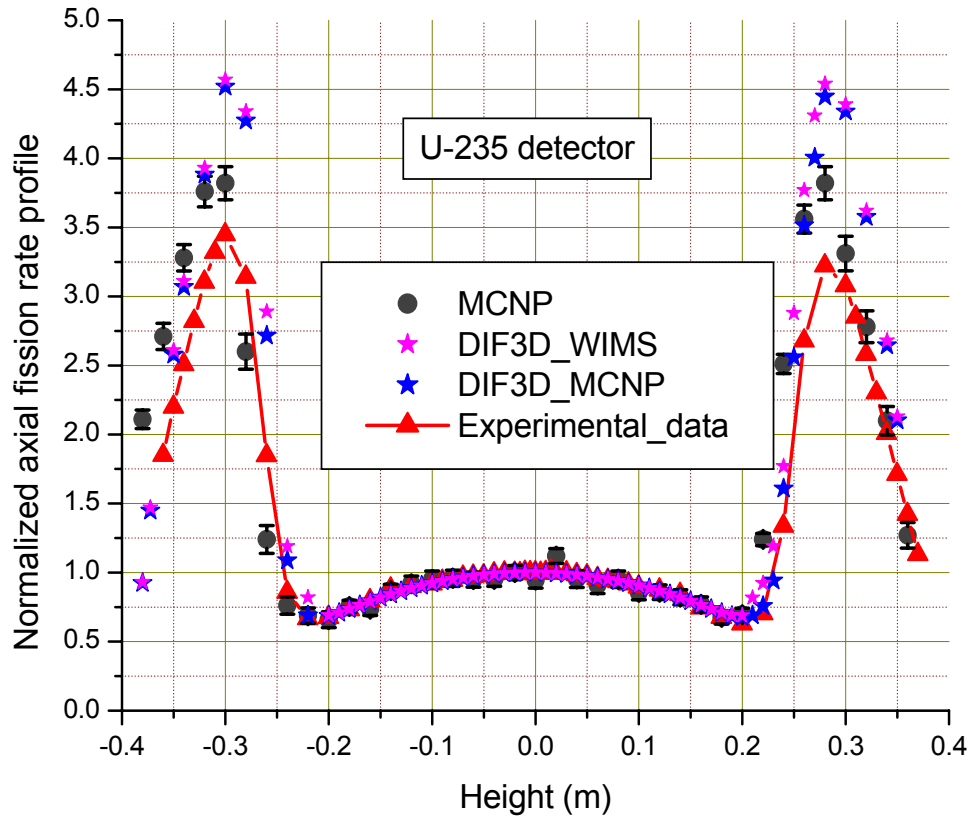

Figure 4. Axial fission rate profile for ^{235}U detector in the oscillation channel.

We have also calculated the radial fission rates traverse across the UO$_2$ to MOX zones along the south-north direction at the core configuration of dry oscillation channel without a sample represented. The result is compared in Figure 5 with the experimental data and MCNP simulation, where the average of each data set is normalized to unity. In the UO$_2$ zones as indicated in the figure, both the MCNP and DIF3D simulation results give the right overall variations but with 10% and 5% under-predictions for the DIF3D calculation and MCNP simulations, respectively, at the outermost fuel pin 2, and larger than 5% error in opposite direction at fuel pin 32. We note, in this regard, that the

accuracy of the measured fission rate at pin 11 was questioned.[6] A tilt which we noted in our quarter-core calculation[3] has now disappeared, thanks to improved and complete representations in both the WIMS and DIF3D full-core models. In the central MOX zone, both the MCNP simulation and DIF3D calculation agrees with the experiment data within one standard deviation.
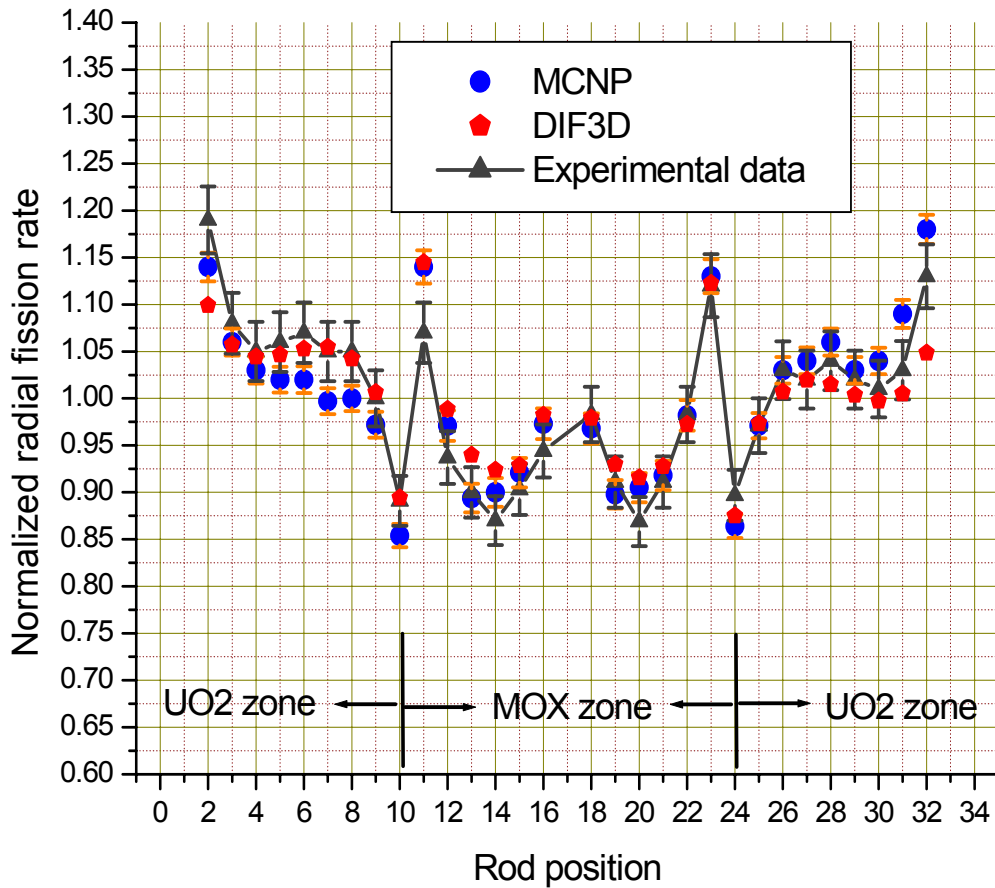

Figure 5. Radial profiles of fission rate along the south-north direction.

7. Reactivity Worth Calculations for UO$_2$ Samples

Using our WIMS-DIF3D model that has been extensively compared with the MCNP simulations and experimental data, we calculated the reactivity worths of a series of UO$_2$ calibration samples with enrichments of 0.25, 0.49, 0.71, 1.0, 2.01, 3.01, 4.0, and 4.93 wt% ^{235}U in the R1-MOX core. We have modeled each fuel sample as a cylinder with a radius of 4 mm and a height of 0.1 m, representing a fuel mass of approximately 0.32 kg.

Four-group macroscopic cross sections were obtained with the WIMS super-cell model representing a homogenized mixture of the fuel sample, zirconium alloy cladding, overclad and water outside the overclad in the oscillation channel. DIF3D eigenvalues calculated with samples located at the center of the reactor are listed in Table IV. The sample reactivity worths are determined from the eigenvalues and compared both with the experimental data and ANL calculations also in Table IV.

Table IV. UO$_2$ Sample Reactivity Calculations in the R1-MOX Core

Enrichment (wt% ^{235}U)	Mass (kg)	k_{eff} (DIF3D/UM)	Experiment (p.u.)	DIF3D (pcm)	
				UM	ANL
0.00	0.000	0.997269	---	---	---
0.25	0.316	0.997270	0	0.17	0.00
0.49	0.317	0.997254	6.75E03	−1.49	0.19
0.71	0.318	0.997255	1.18E04	−1.35	0.35
1.00	0.321	0.997257	1.88E04	−1.17	0.57
2.01	0.321	0.997263	4.86E04	−0.55	1.27
3.01	0.321	0.997269	7.32E04	0.02	1.89
4.00	0.322	0.997274	9.79E04	0.55	2.45
4.93	0.322	0.997279	1.17E05	1.01	2.94

The first case of Table IV, with eigenvalue k_{eff} = 0.997269, is our base case for a core configuration including zirconium cladding in the oscillation channel but without any fuel sample. This indicates a decrease of 6 pcm due to the zirconium cladding, compared with our reference k_{eff} = 0.997329 in Section 4. Starting with an essentially zero reactivity worth of the 0.25-wt% sample, four of the low-enrichment samples, up to 2.01 wt%, yield negative reactivity worths in our DIF3D calculations. Eventually, as the enrichment increases further, the reactivity worth turns positive. A comparison of our reactivity worths with ANL results in Figure 6 shows that our DIF3D reactivity worths increase linearly as the fuel enrichment increases similar to the ANL results. In fact, the

calibration curve indicates a reactivity worth of 2.24×10^{-5} pcm per pilot unit (p.u.) with our DIF3D calculation, which is 9% less than the ANL calculation of 2.46×10^{-5} pcm per p.u. The essentially zero reactivity worth for the 0.25-wt% sample is excluded in Figure 6. Fission and absorption rates of the UO_2 samples in our DIF3D calculations indicate negative net contributions for the samples with enrichment from 0.25 to 3.01 wt%, which may explain the negative reactivity worths calculated for these samples. Further investigation will be performed, including MCNP calculations, to explain what appears to be an overall bias in our DIF3D reactivity worths.
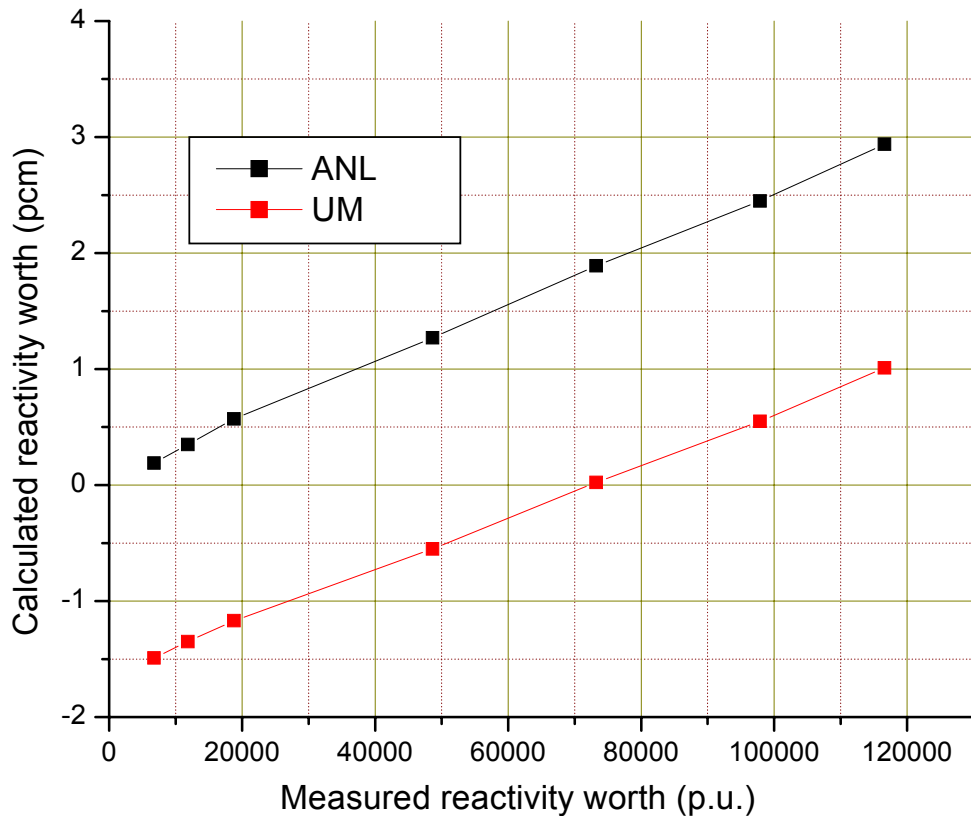

Figure 6. UO_2 sample reactivity worth calculations.

8. Summary and Conclusions

A full-core WIMS-DIF3D model has been developed for the MINERVE R1-MOX core, providing generally acceptable agreement with the experimental data and MCNP simulations. Among the items that still need further analysis and improvement are the discrepancies of radial fission rate at fuel pin 32 and significant discrepancies in the [235]U detector fission rate profile and spectral indices. Parametric studies will be performed

with the full-core WIMS-DIF3D model to investigate the effects of uncertainties in the composition and density of various materials in the MINERVE core. Further effort will also be made to improve our reactivity worth calculations for UO_2 calibration samples. In this effort we will make full use of MCNP simulations as reference calculations, whenever meaningful.

References

1. J. R. Deen, W. L. Woodruff, C. I. Costescu, and L. S. Leopando, "WIMS-ANL User Manual Rev. 5," ANL/TD/TM99-07, Argonne National Laboratory (2003).
2. K. L. Derstine, "DIF3D: A Code to Solve One, Twom abd Three-dimensional Finite Difference Diffusion Theory Problems," ANL-82-64, Argonne National Laboratory (1982).
3. Y. Cao, G. Perret, R. T. Klann, and J. C. Lee, "Reactor Physics Analysis of the MINERVE Reactor for the OSMOSE Program," to be presented at the American Nuclear Society Meeting, November 2004.
4. "Translation of the Technical Note of CEA: NT-SPEx/LPE-03/005," Argonne National Laboratory, draft report (June 2004).
5. G. Perret and R. T. Klann, "I-NERI OSMOSE Project Progress Report," Presentation at the University of Michigan, July 2004.
6. R. T. Klann and J. P. Hudelot, "I-NERI Annual Technical Progress Report," Argonne National Laboratory (October 2003).